A TECHNIQUE FOR ESTIMATING THE RESILIENT MODULUS OF UNSATURATED SOILS FROM MODIFIED CALIFORNIA BEARING RATIO TESTS

Kenneth Onyekachi Omenogor

Thesis submitted in partial fulfillment of the requirements for the degree of

MASTER OF APPLIED SCIENCE

in Civil Engineering

Department of Civil Engineering

Faculty of Engineering

University of Ottawa

Ottawa, Canada

June 2022

Dedicated to my parents,

Andy B. Omenogor, and Judith O. Irozueh.

Isaiah 30:15 In repentance and rest is your salvation, in quietness and trust is your strength.

ABSTRACT

The Mechanistic-Empirical Pavement Design Guide (MEPDG) which is widely used for the rational design of pavements has three different design levels (i.e., Level 1, Level 2, and Level 3) that are typically based on the resources and the level of risk associated for a given project. Specifically, Level 2 design requires the estimation of the resilient modulus, M_R (which is the key parameter in the mechanistic design procedures) from simple experiments such as the California Bearing Ratio (*CBR*), Unconfined Compressive Strength (UCS) and *R*-value tests. In this study, a technique is proposed for estimation of M_R from *CBR* that can be used in Level 2 designs of pavements.

The California Bearing Ratio (*CBR*) is a relatively inexpensive laboratory test which provides a measure of the strength of a soil. The *CBR* test can easily be performed as the experimental procedure is relatively straightforward to execute. The *CBR* test procedure widely used and is simple, however the fundamental engineering principles governing *CBR* tests do not realistically describe the mechanical behavior of pavements. Due to this reason, there has been a significant interest to design pavements using a mechanistic approach such as the resilient modulus (M_R). The M_R test method provides an indication of the stiffness of pavement materials under cyclic loads, which closely represents the typical loading conditions that are experienced by pavements. M_R is a reliable method as it considers the cyclic loading (i.e., resilient response) of pavements. However, it has one major drawback as the triaxial testing equipment used for measurement of the M_R is relatively costly, testing is complex and requires trained professional to perform them.

The *CBR* and M_R are both used in present day practice to evaluate the strength of pavement materials. However, the *CBR* is widely used because of its relatively low cost and the vast experience with its use in the design of pavements. The common trend in today's practice is to estimate the M_R from *CBR* as evident in most pavement design procedures used around the world. For instance, the Mechanistic-Empirical Pavement Design Guide (AASHTO 2008) suggests that the M_R may be estimated from standard tests like the *CBR* for design of Level 2 pavements. Numerous studies in the literature propose relationships between *CBR* and M_R, but only a hand full of these studies takes account of the effect of matric suction, ψ which is a key stress state variable that describes the rational behavior of unsaturated soils. This thesis document includes the explanation of a modified *CBR* test equipment capable of measuring unsaturated properties (ψ and

water content) of specimens subjected to wetting and drying. In addition, some correlations were developed using the measured *CBR* data and the data of M_R from other studies. The results provide useful information for Level 2 mechanistic-empirical design of pavement structures for various soils in the province of Ontario.

ACKNOWLEDGEMENTS

I would like to express my deepest appreciation to Dr. Sai K. Vanapalli for his mentorship and guidance throughout my master's program. I would also like to acknowledge the contributions of Jean Claude, Leo Denner, Sada Haruna, Junping Ren, Yu "Toby" Bai and Michael Merhi. Jean Claude, Leo Denner and Sada Haruna played a vital role in acquisition of the testing equipment as well as set-up, maintenance and trouble shooting. Junping Ren provided guidance and assistance in organising the soils and data used for the research study. Yu "Toby" Bai and Michael Merhi assisted with specimen preparation and performing some of the experiments presented in this manuscript. Special appreciation to the Ministry of Transportation Ontario (MTO) for the funding provided to facilitate this research program.

TABLE OF CONTENTS

LIST OF FIGURES

LIST OF TABLES

LIST OF ACRONYMS

AASHO	American Association of State Highway Officials
AASHTO	American Association of State Highway and Transportation
AC	Asphalt Concrete
AI	Asphalt Institute
ASTM	American Society for Testing and Materials
ATB	Asphalt Treated Base
CISR	Council for Scientific and Industrial Research
C-SHRP	Canadian Strategic Highway Research Program
CRCP	Continuously Reinforced Concrete Pavement
CTB	Cement Treated Base
DARWin	Design Analysis and Rehabilitation for Windows
EICM	Enhanced Integrated Climatic Model
FHWA	Federal Highway Administration
HIIFP	Highway Infrastructure Innovation Fund Program
HRB	Highway Research Board
JPCP	Jointed Plain Concrete Pavement
JRCP	Jointed Reinforced Concrete Pavement
JTFP	Joint Task Force on Pavements
KLC	Kincardine Lean Clay
KSC	Kingston Silty Clay
LVDT	Linear Variable Differential Transducer
M-E	Mechanistic Empirical

MEPDG	Mechanistic Empirical Pavement Design Guide
MTO	Ministry of Transportation, Ontario
NCHRP	National Cooperative Highway Research Program
OLC	Ottawa Leda Clay
PCC	Portland Cement Concrete
PCP	Prestressed Concrete Pavement
PR	Public Roads
PSI	Present Serviceability Index
SWCC	Soil Water Characteristic Curve
TCS	Thermal Conductivity Sensors
TDR	Time Domain Reflectometry
TLC	Toronto Lean Clay
TSC	Toronto Silty Clay
UCS	Unconfined Compression Strength
USACE	United States Army Corps of Engineers
USCS	Unified Soil Classification System
WASHO	Western Association of State Highway Officials

LIST OF SYMBOLS

a_b, b_b	Parameters for estimating the SWCC using Brutsaert (1967) model.
a_f, b_f, c_f	Parameters for estimating the SWCC using Fredlund and Xing (1994) model.
a_g, b_g	Parameters for estimating the SWCC using Gardner (1956) model.
a_m, b_m	Parameters for estimating the SWCC using McKee and Bumb (1987) model.
a_v, b_v, c_v	Parameters for estimating the SWCC using Van Genuchten (1980) model.
CBR_s	*CBR* under soaked or saturated condition.
CBR_u	*CBR* under unsoaked or unsaturated condition.
G_s	Specific gravity.
M_{Ropt}	Resilient modulus at optimum water content.
M_{Rsat}	Resilient modulus at saturation state.
P_a	Atmospheric pressure (i.e., 1 atm or 100 kPa).
S_{opt}	Degree of saturation at optimum water content.
S_r	Residual degree of saturation.
V	Volume of *CBR* mold, measured from its actual dimensions.
V_v	Volume of voids.
V_w	Volume of water.
w_{opt}	Optimum water content.
w_r	Residual gravimetric water content.
w_{sat}	Saturated gravimetric water content.
γ_d	Dry unit weight.
γ_w	Specific unit weight of water (i.e., 9.81 kN/m^3).
ε_r	Recoverable strain.

$\boldsymbol{\theta_b}$	Bulk stress.
$\boldsymbol{\Theta_n}$	Normalised water content.
$\boldsymbol{\theta_r}$	Residual volumetric water content.
$\boldsymbol{\theta_{sat}}$	Saturated volumetric water content.
$\boldsymbol{\theta_w}$	Volumetric water content.
$\boldsymbol{\rho_{bulk}}$	Bulk density.
$\boldsymbol{\rho_{d,max}}$	Maximum dry density.
$\boldsymbol{\rho_d}$	Dry density.
$\boldsymbol{\rho_w}$	Density of water (i.e., 1000 kg/m^3).
$\boldsymbol{\sigma_1}$	Axial stress.
$\boldsymbol{\sigma_3}$	Confining stress.
$\boldsymbol{\sigma_d}$	Deviatoric stress.
$\boldsymbol{\tau_{oct}}$	Octahedral shear stress.
$\boldsymbol{\lambda_{bc}}$	Pore-size distribution index for the Brutsaert (1967) model to estimate the SWCC.
$\boldsymbol{\psi}$	Matric suction.
$\boldsymbol{\psi_b}$	Matric suction at air entry value.
$\boldsymbol{\psi_{opt}}$	Matric suction at optimum water content condition.
$\boldsymbol{\psi_T}$	Total suction.
$\boldsymbol{\psi_\pi}$	Osmotic suction.
$\boldsymbol{C(\psi)}$	Correction factor, which is primarily a function of the suction at which residual water content occurs.
$\boldsymbol{CBR}$	California Bearing Ratio.
$\boldsymbol{D_{60}}$	The effective grainsize corresponding to 60 percent passing by weight on the grain-size distribution curve.

e	Void ratio.
I_P	Plasticity index.
M_R	Resilient modulus.
P_{200}	Percent passing No. 200 sieve or 0.075 mm on the grain-size distribution curve.
***R*-value**	A measure of the response of a compacted sample of soil or aggregate to a vertically applied pressure.
S	Degree of saturation.
w	Gravimetric water content.
w_L	Liquid limit.
w_P	Plastic limit.

CHAPTER 1
INTRODUCTION

Pavement structural capacity can be characterized based on the mechanical properties (strength and stiffness) of the base, subbase, and subgrade layers. The mechanical properties of pavement materials are affected by environmental factors associated with the moisture and temperature changes which occur due to seasonal weather fluctuations. The influence of water content and temperature changes with climate factors on the mechanical properties of pavement materials have been highlighted by several researchers (e.g., Winterkorn and Fang 1972; Han 2016; Ren 2020). Winterkorn and Fang (1972) discussed the influence of these parameters on the engineering properties of subgrade soils. For example, Han (2016) highlighted the importance of considering moisture variation in the rational design of pavements. Along similar lines, Ren (2020) discussed the effect of freeze-thaw cycles on subgrade material properties. The conclusions derived by Han (2016) and Ren (2020) were based on extensive studies using widely used soils in Ontario province of Canada extending principles of unsaturated soil mechanics. The results of their studies are consistent with the research of Winterkorn and Fang (1972) that highlight the importance of temperature and moisture on the performance of pavements.

1.1 Pavement behavior in unsaturated soils

Pavements are typically constructed at elevations well above the ground water table to reduce deterioration associated with excess moisture in the pavement system. Nonetheless, influx of moisture in pavements can arise due to several reasons, resulting in fluctuation (i.e., rising and lowering) of the ground water table. A typical moisture profile pertaining to a pavement system can be divided into three regions: namely, the saturated zone, the capillary zone (or capillary fringe), and the vadose (or unsaturated) zone. Figure 1-1 shows a conceptual schematic of a typical moisture profile in a pavement structure.

The saturated zone is situated below the groundwater table. In this zone, pores in the soil are filled with water, and the pore-water pressures are hydrostatic. Above the ground water table is the vadose zone in which the soil pores are partially filled with air and water. In other words, the soil in the vadose zone is in an unsaturated state. The moisture profile within the vadose zone varies from the saturated state at its base, where the capillary fringe is situated, to the natural soil or material moisture content at the upper extent (Salour 2015).

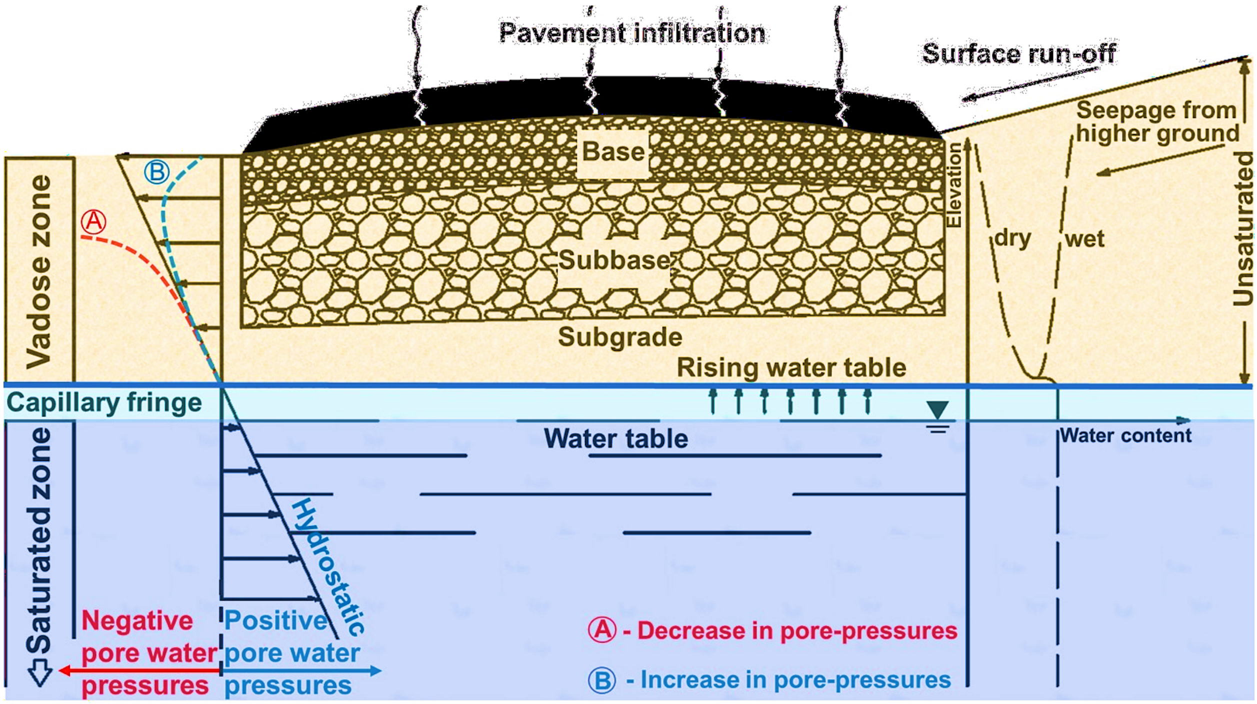

Figure 1-1 A typical pavement system along with moisture profile

In the capillary fringe, water from the groundwater table is pulled upwards due to capillary forces. The material pores in this zone are almost filled with water that may contain some occluded air bubbles. In other words, the air phase in the capillary fringe is discontinuous. The thickness of the capillary fringe can vary depending on the grain-size distribution and other material properties.

In the vadose zone, the pore-water is held in place by the potential energy of the tensile forces created due to capillary and surface adsorptive forces (matric suction, ψ), and potential differences due to solute concentrations (osmotic suction, ψ_π). Soil suction (i.e., total suction, ψ_T) is defined as the summation of ψ and ψ_π. In most engineering problems ψ component largely governs the mechanical behavior of unsaturated soils; the ψ_π is not commonly determined because its contribution in several geotechnical applications is not relevant (Fredlund 2006).

The moisture content and ψ in the pavement layers above the ground water table (i.e., layers that are in an unsaturated state) can vary in response to influx or efflux of moisture that occurs in the pavement system. It is important to note that the moisture boundary zones change with influx or efflux of moisture. Moisture influx in pavements can be associated to events such as flooding, precipitation or other anthropogenic activities that can lead to excess run off and percolation. Efflux can be associated with extended periods of droughts or periods of extremely high atmospheric temperatures.

Pavements are typically situated in the vadose zone, which is above the ground water table. As a result, these layers are typically in an unsaturated state. Furthermore, the materials used for the construction of pavement base, subbase and subgrade layers widely constitute of compacted soils that are typically in a state of unsaturated condition. ψ is a key stress state variable used in the interpretation of the behaviour of unsaturated soils. Thus, the hydro-mechanical behavior of pavement materials should be interpreted taking account of the influence of ψ and the degree of saturation (Mirzaii and Negahban 2016).

1.2 Pavement design methods practiced in Canada

There are different pavement design procedures used around the world, and the theoretical background for these design procedures varies from one transportation agency to another. Generally, these design procedures are grouped into 3 categories, namely: (i) empirical methods, (ii) mechanistic methods, and (iii) mechanistic-empirical (M-E) methods. Empirical methods used in pavement design are solely based on the results of limited experimental studies or engineering experience (i.e., observations from past performance). These methods rely on a specific set of environmental factors, material properties, and loading conditions. For example, the AASHTO-1993 design guide (which is practised globally because of its simplified and straightforward design procedure) is purely empirical as the design guide is based on field performance data that was measured from the American Association of State Highway Officials (AASHO) road test conducted in Ottawa, Illinois during the late 1960s. Empirical based approach are often referred to as "state-of-the-practice" as these methods are relatively simple to interpret and frequently used in practice.

Mechanistic principles are "state-of-the-art" methods which are based on the precise evaluation of the key factors that may possibly have an influence on the performance of the pavement. Some of these factors include: the loading type, material properties, and environmental factors such as temperature and moisture changes that occur due to weather fluctuations. The mechanistic approach can prove advantageous as it allows for pavements to be designed with increased performance and reliability. However, this method is costly, and it is time consuming to model or interpret all key factors precisely. The mechanistic-empirical (M-E) methods involve the use of mechanistic principles in conjunction with empirical based procedures for prediction of pavement strength and performance. The M-E method is perceived to bridge the gap between "state-of-the-art" and "state-of-the-practice" in pavement design as it incorporates an element of both the mechanistic and empirical based approaches. Of all three methods, the empirical based and the M-E based pavement structural design approaches are the two principal methods widely studied and used around the world today.

Unlike the Federal Highway Administration (FHWA) in the United States of America, there is no single entity responsible for funding pavement construction and rehabilitation or for developing pavement design standards in Canada (C-SHRP 2002). Most Canadian provincial transportation agencies (for example, Alberta, British Columbia, Manitoba, New Brunswick, Nova Scotia, Ontario, and Québec) design pavements based on the American Association of State Highway and Transportation Official design guide (AASHTO 1993) except Prince Edward Island and Saskatchewan, whose pavements design methods are based on Asphalt Institute (AI 1991) method (Saha 2011). The AASHTO-1993 design guide is commonly practiced because of its simplified and straightforward design procedure. However, the method is purely empirical as the design guide is based on field performance data measured at the AASHO road test conducted in 1958-60 (Christopher et al. 2006). The AASHO road test was conducted for materials, traffic loading and environmental conditions experienced in Ottawa, Illinois. Empirical methods are disadvantageous as it only applies to a specific set conditions, and if these conditions are changed, the design is no longer valid (Huang 2004).

A more sophisticated pavement design method which alleviates the limitations of the AASHTO-1993 guide is the Mechanistic-Empirical Pavement Design Guide (AASHTO 2008), commonly known as MEPDG. The MEPDG is a more rigorous design tool that considers the M-E design of pavements which takes account of the resilient response as well as the effects of environmental factors on the pavement material properties.

1.3 Mechanistic-Empirical Pavement Design Guide (MEPDG)

The MEPDG and associated software DARWin-ME was first released in 2004. The software design tool was given the name DARWin-ME to differentiate it from the computer version of the

AASHTO-1993 design guide called DARWin (design, analysis, and rehabilitation for Windows) (Kim et al. 2011). DARWin-ME is an advanced tool that utilizes M-E approach to simulate incremental damage taking into account the temperature and moisture variations experienced over the life cycle of the pavement. The design and analysis procedure estimates pavement responses (stresses, strains, and deflections) and applies those responses to calculate incremental damage over time (Coelho 2016). These responses are computed using detailed inputs attained from data, including traffic loading, material properties, and environmental conditions. The latest version of the MEPDG software is presently developed under the name AASHTOWare® Pavement ME (AASHTOWare®). The software is presently used by several transportation agencies in the United States, and currently being implemented for use in some provinces in Canada.

The MEPDG offers a unique hierarchical approach that provides users with flexibility in selecting project design inputs based on the size, importance, and available resources for a particular project (Kim et al. 2011). This hierarchical approach divides the input parameters (traffic, materials, and environmental) required for AASHTOWare® software into three levels (i.e., Level 1, 2 and 3) depending on project size and available resources. Level 1 is recommended for projects with high costs and criticality. Level 2 is recommended for projects with moderate cost and criticality, while Level 3 is suggested for projects with low risks and limited resources.

1.4 MEPDG Implementation in Ontario

Ontario Ministry of Transportation (MTO) is amongst the leading transportation agencies in Canada that is gradually mandating to implement the MEPDG in the design of pavements. The implementation of MEPDG in Ontario require the gathering of region-specific data related to traffic loading, material properties, and climate (i.e., temperature and moisture changes) for use as input parameters in the AASHTOWare® software. The region-specific data is collected following the MEPDG hierarchical approach which divides the input parameters for traffic loading, material properties and climate into three levels (i.e., Level 1, 2 and 3) depending on project size and available resources. Climatic data can be obtained using weather stations, while the traffic loading can be estimated from traffic volume analysis. In addition, the material properties are determined from carrying out extensive laboratory tests on the standard materials used in construction of pavements (i.e., asphalt or concrete, granular fill, and subgrade).

M_R is the key material property used in the MEPDG for design and analysis of flexible pavements (Ba et al. 2013). The AASHTOWare® software input parameters for Level 1 design requires the direct determination of M_R using elaborate testing equipment. Level 2 design permits the use of relationships between the M_R and other material properties such as the *CBR*, *R*-value, and Unconfined Compression Strength (UCS) tests for estimation of the M_R. For Level 3 design, M_R can be estimated from material classification and index properties.

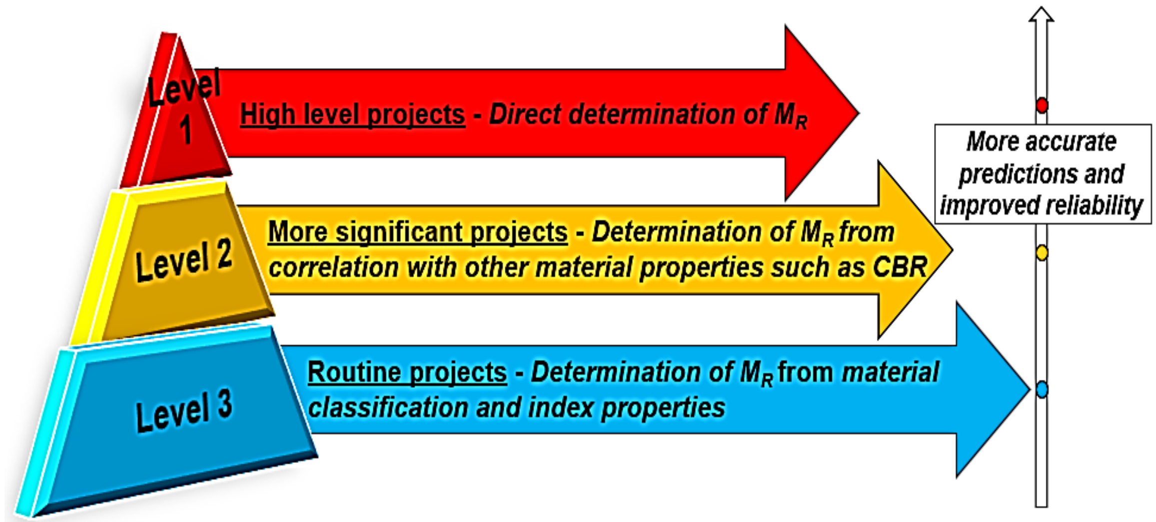

Figure 1-2 The MEPDG hierarchical approach for determination of M_R

It is evident that extensive research study needs to be carried out to determine M_R of the typical materials used in Ontario as pavement subgrades and geo-materials. Specifically, the subgrade characterization requires extensive research and laboratory experimentation to determine M_R of Ontario subgrade soils considering the typical environmental conditions experienced in Ontario. To facilitate the subgrade characterization study, six natural subgrade soils were collected from various locations in Ontario (one soil each from Kincardine, Sudbury, Kingston, Ottawa and two soils from Toronto). All soils were sampled at shallow depths of approximately 3 m, which is the typical depth subgrade soils are encountered. The collected soils are tested considering the hierarchal classification proposed in the MEPDG (i.e., direct measurement of M_R for Level 1, estimation of M_R from other material properties such as the *CBR* for Level 2, and approximation of M_R from material classification and index properties for Level 3).

The laboratory tests carried out to obtain the input parameters for Level 1 involved the direct measurement of M_R considering the typical temperature and moisture changes experienced in Ontario. In other words, the collected soils were tested for M_R under wetting-drying and freezing-thawing conditions. Detailed discussions on the experimental methods and findings for the studies carried out for Level 1 input parameters can be found in work published by Vanapalli and Han (2017) and Ren (2020).

Vanapalli and Han (2017) carried out extensive studies to measure the M_R of the collected soils at varying water content (i.e., wetting and drying). While the research study completed by Ren (2020) was carried out to measure the M_R of the same soils under freeze-thaw conditions, taking account of the typical sub-zero temperatures that typically occur in Ontario. In the study carried out by Vanapalli and Han (2017), experiments were conducted on specimens that were initially compacted at optimum water content (w_{opt}) and then wetted or dried prior to M_R testing.

Further research and laboratory studies need to be conducted to gather the necessary data of M_R for Level 2 and 3 input parameters. The study for Level 2 is primarily focused on laboratory *CBR* tests which are to be conducted considering freezing-thawing and wetting-drying behavior of the soils.

1.5 Objective of study

The objective of this research study is to develop correlations for estimation of M_R from *CBR* considering the variations in moisture content. As such, the soils collected are to be subjected to wetting or drying prior to *CBR* testing. For this study, *CBR* tests are performed on the same soils tested by Vanapalli and Han (2017) and Ren (2020). Furthermore, the specimens made for each soil are replicated to have a similar soil fabric as the soils tested by Vanapalli and Han (2017) and Ren (2020). The specimens were then either saturated, wetted, or dried to achieve similar moisture contents as measured in Vanapalli and Han (2017). Finally, the data from the present study are analyzed together with the M_R values measured from Vanapalli and Han (2017) to develop correlations between *CBR*, M_R and properties of unsaturated soils. The results provide useful information for Level 2 mechanistic-empirical design of pavement structures in Ontario.

1.6 Structure of Thesis

This thesis document is summarized in six Chapters. Chapter 1 provides the introduction of the research problem. Chapter 2 entails a literature review which includes a background on pavements and pavement design methods and a summary of the advances made towards the evolution of modern pavement design. Chapter 2 also provides succinct details on two commonly accepted methods used in practice to determine strength and stiffness of pavement materials, a synopsis of studies available in literature that describe the relationship between *CBR* and M_R for design of pavements extending unsaturated soil mechanics, and the SWCC and methods to measure ψ and model the SWCC. Chapter 3 summarizes the research background and methodology and includes a discussion on the research studies published in literature that has provided inspiration for the concepts and instrumentation fabricated to measure unsaturated soil properties for the present study. Chapter 4 contains a detailed description of the experimental program, which includes: sample preparation, specimen compaction, specimen wetting-drying or saturation, *CBR* tests and suction measurements using the filter paper technique. Chapter 5 summarizes the research findings alongside comparison of measured test data to trends observed in literature. Finally, Chapter 6 provides a brief conclusion and recommendations for future research.

CHAPTER 2

LITERATURE REVIEW

2.1 Historical background on pavements

Pavements can be dated back to the Bronze Age, roughly between 3000 BC and 2500 BC. This timeline is linked to two main historical events. Firstly, the domestication of horses in Southern Russia by the late third millennium BC, and soon after that, the utilization of horses and carts as a mode of transportation around 3500 BC. Some historians credit the Carthaginians as the first to construct and maintain a road system. However, there are others who argue that Romans were the first to construct real roads which are similar in terms of layout and structure to the pavement systems used today (Cekerevac et al. 2009). The Carthaginian city was in Carthage, currently known as the City of Tunis, Tunisia. Presently, Rome stands in the core of Italy. For the Roman road construction purposes, the designer (architectus) was operationally helped by a surveyor (agrimensor) and a leveler (librator), while the soldiers worked as builders (Garilli et al. 2017). The road structure constructed by the Romans typically consisted of four layers: Summa crusta, Nucleus, Rudus and Statumen. An illustration of the Roman road structure is shown in Figure 2-1. The Summa crusta is similar to a surface layer in today's pavement structure. It is comprised of lime-grouted smooth polygonal blocks, artfully cut to the advantage of the closest fitting.

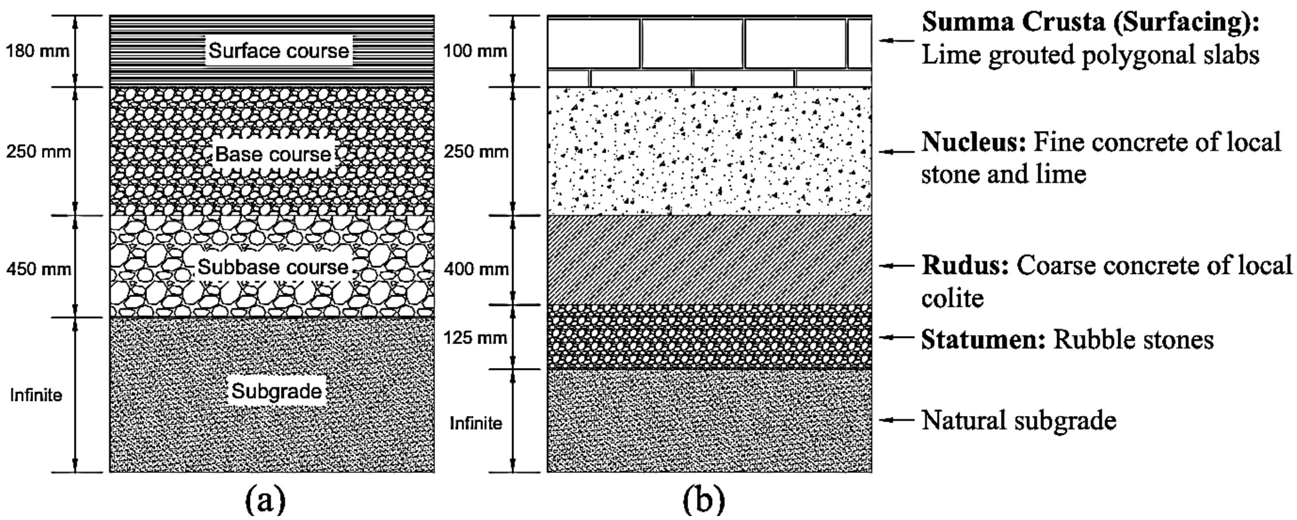

Figure 2-1 (a) Typical pavement structure used in present time, (b) Roman pavement structure used in Bronze Age

The nucleus layer is a base layer, composed of gravel and sand grouted with lime cement. The third layer, named Rudus was designed to have a water drainage function and constituted of crushed stones or rubbles grouted with lime. Statumen is the last layer which was made of two or three courses of flat stone oriented either horizontally or vertically and bounded with lime mortar or clay. Domestication of horses in Southern Russia by the late third millennium BC, which was followed not long afterward by development of carts in Ukraine highlights pavement existence around the fourth millennium. At this time, stone slabs made an excellent and long-lasting pavement surface suitable for both pedestrian, donkeys, camels, horses, and carts (Tillson and Thomson 1900). However, neither concrete nor asphalt was used by pavement engineers during this era. Today, pavements constitute a major component of the transportation industry and national economies around the world; they provide access to basic services as well as underpinning the economic wellbeing of a country (Pearson 2011).

Roman roads were approximately 900 mm deep, and could range up to 2 m in depth or, in any case, until a more compact soil is achieved (Garilli et al. 2017). The Roman road system is expensive to construct compared to current-day pavement systems. Nevertheless, the pavement structure presently used in practice share similarities with the Roman pavements constructed during the Bronze Age. The key difference is the substitution of the statumen layer with the natural subgrade. This replacement can be accredited to advancements in geotechnical engineering which provides means for engineers to design pavements considering the effect of stresses on subgrade soils.

2.2 Pavement structure

Pavements are layered materials which have been engineered and structured to adequately distribute applied vehicle loads to the natural subgrade soil. There are three conventional types of pavements, namely: flexible, rigid, and composite pavements. The term flexible and rigid pavement refer to the way asphalt and Portland Cement Concrete (PCC) pavements respectively transmit stress and deflection to underlying layers (Papagiannakis and Masad 2012). Pavements layers are often also referred as courses. The generic pavement courses are surface course, base course, subbase course and subgrade. Each pavement layer is designed to resist specific distresses, which are dependent on the pavement type in consideration. The surface course is usually made of asphalt or PCC, the base and subbase courses are often constructed using geo-materials (i.e., crushed aggregate or engineered fill), and the subgrade material is typically compacted or natural depending on its strength and conditions.

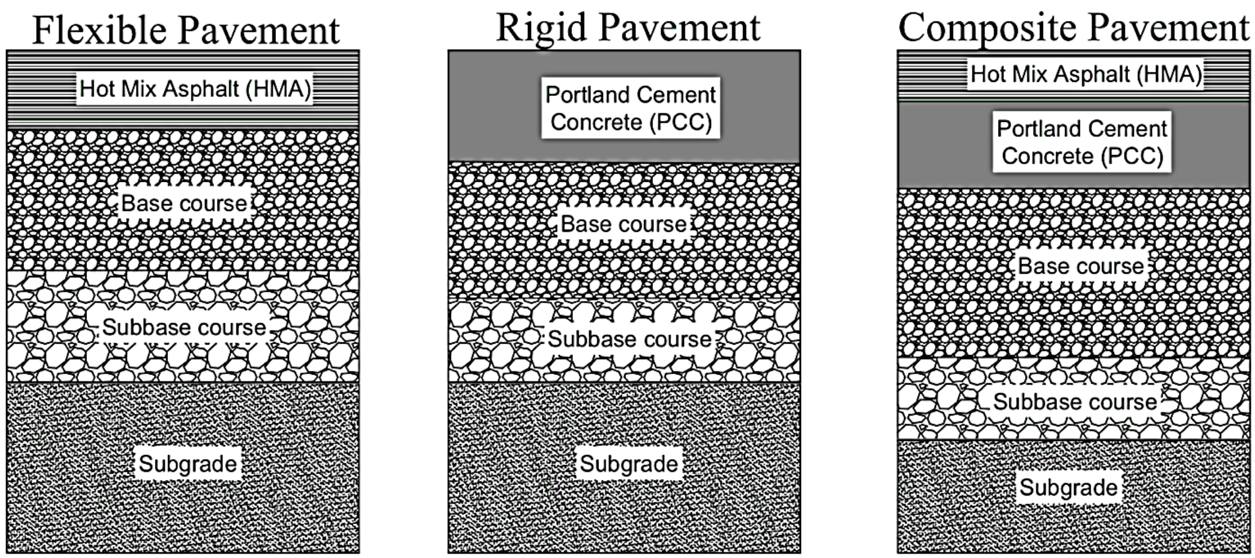

Figure 2-2 Typical pavement structure for flexible, rigid and composite pavements

2.2.1 Flexible pavements

Flexible pavements are also referred to as asphalt pavements. This type of pavement consists of an asphalt surface built over a base and subbase course which is supported by compacted or natural subgrade soil. Figure 2-2 shows a typical cross-section of a flexible pavement. The surface course material is made of asphalt, which is often protected using a thin layer of seal coat. There are three types of coats used in asphalt pavements: namely, seal coat, tack coat and prime coat. These coats are made up of liquid bitumen. The seal coat is a thin bituminous liquid applied on the pavement wearing surface (Myer 2011). It serves as a surface barrier to prevent water penetration into pavement structure and improve skid resistance of surface course. The tack coat is a water-based asphalt emulsion sealer, which can be applied on top of stabilized base layers and between lifts in thick asphalt surface layers (Yoder and Witczak 1975). Prime coats serve as a good interface bond and are often used to stabilize the surface of the base course to serve as a support for paving construction activities.

Adequate compaction of the asphalt layer during construction is essential for satisfactory pavement performance. It is common in practice to use field compaction requirement between 92 and 96 % of the laboratory maximum Marshall density of the asphalt mixture (Holt et al. 2011).

The base course and subbase course are generally comprised of compacted granular materials, and subgrade layer may be compacted to improve soil conditions. Typical construction requirements specify field compaction levels of 98 % or more of the in-situ maximum dry density of the soil or material (Kodikara et al. 2018). A fabric or geotextile is often used to demarcate the natural subgrade from overlying layers (Papagiannakis and Masad 2012). This helps reduce migration of fines from overlying layers and maintain the integrity of the natural subgrade soil.

Flexible pavements in Ontario typically consist of asphalt laid over a granular base and subbase layers. The asphalt materials used in Ontario municipalities typically consist of Superpave asphalt mix designs. The asphalt mix used for municipal roadways in Ontario is based on specifications provided by the Ontario Ministry of Transportation as detailed in OPSS 1511 (MTO 2016). This specification provides guidance on the mix design and placement of the different types of mixes commonly used for Ontario roadways. The mixes commonly used as a surface course for collector and arterial roadways are Superpave 12.5, Superpave 12.5 FC1, and Superpave 12.5 FC2. Superpave 12.5 is commonly used for lower traffic volume roadways, Superpave 12.5 FC1 is typically used for most collector and minor arterial roadways, while Superpave 12.5 FC2 is used for the high volume, major arterial roadway classification (Holt et al. 2011). The most commonly available aggregates used in pavement construction in Ontario consist of Granular "A" for the base course, and Granular "B" for the subbase course. These materials are described in OPSS 1010 (MTO 2013).

2.2.2 Rigid pavements

Rigid pavements, also referred to as PCC pavements are layered systems which consist of a PCC surface course underlain by a base course and the natural subgrade below. Rigid pavements may or may not be constructed to have a base layer between the PCC and natural subgrade (Myer 2011). Figure 2-2 shows a typical cross-section of a rigid pavement. These pavements are designed to have stiffer layers, undergo little deflection, and have longer service life compared to flexible pavements. PCC pavements can further be divided into four types: jointed plain-concrete pavement (JPCP), jointed reinforced-concrete pavement (JRCP), continuous reinforced-concrete pavement (CRCP), and prestressed-concrete pavement (PCP). The three types of concrete pavements commonly used are JPCP, JRCP and CRCP (Hall 2000).

JPCP are the most common type of rigid pavements due to their cost and simplicity (Mallick and El-Korchi 2011). JPCP pavements are not reinforced, as the name implies. Loads imposed on JPCP are transferred via dowels or aggregate interlock. JRCP are similar to JPCP, except the slabs are longer and constructed with reinforcement steel. A typical illustration of the reinforcement steel orientation for JPCP, JRCP and CRCP is shown in Figure 2-3. CRCP are characterized by the absence of transverse joints (Alao 2014). They are heavily reinforced to increase flexural capacity and control cracks that may develop due to temperature changes. However, the cost of CRCP is much higher than that of JPCP or JRCP because of the heavy reinforcement steel used (Mallick and El-Korchi 2011). Rigid pavements in Ontario typically consist of a JPCP over a granular base which provides uniform support for the concrete slabs.

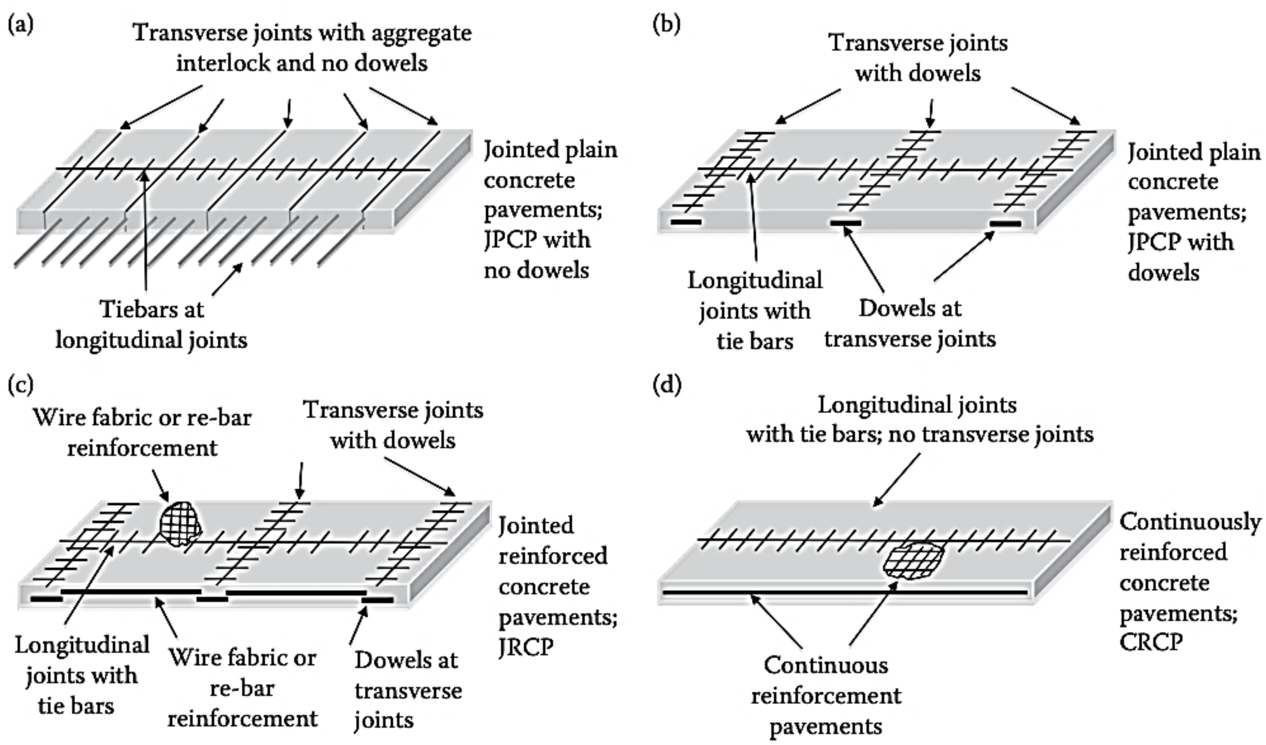

Figure 2-3 Jointed plain concrete pavement (JPCP) with tie bars and (a) no dowels, (b) with dowels, (c) jointed reinforced concrete pavements (JRCP) with tie bars and dowels, and (d) continuously reinforced concrete pavements (CRCP) (from Mallick and El-Korchi 2011)

It is important to note that flexible pavements may possess stiffness as much as rigid pavement. This is true when stabilized materials are used in any of the pavement components or if, for example, a relatively thick asphalt layer is used (Yoder and Witczak 1975). Conversely, the pavement can be considered flexible if the surface layer is relatively thin. Hence it is necessary to bear in mind that these pavement definitions are arbitrary and may or may not be strictly true, but rather dependent on the behavior of the pavement materials.

2.2.3 Composite pavements

A composite pavement structure is defined as a structure comprising two or more layers that combine different characteristics and that act as one composite material (Flintsch et al. 2013). These pavements are mostly designed for rehabilitation projects. Composite pavements consist of asphalt surface course placed over PCC or treated bases (asphalt-treated base (ATB) or cement-treated base (CTB)) as shown in Figure 2-4. These types of composite pavements are identified as AC overlays. AC overlay on top of a PCC rigid pavement system is a widely used rehabilitation scenario (Christopher et al. 2006).

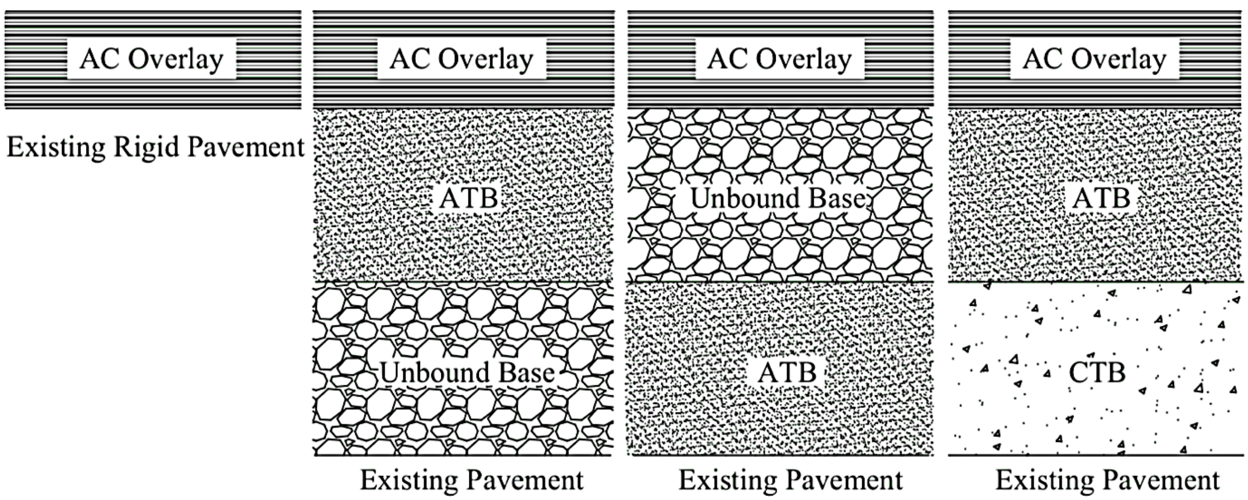

Figure 2-4 Typical composite pavement sections (from Christopher et al. 2006)

2.3 Pavement design methods

There are different methods of pavement design practiced around the world. These methods can be classified into three groups based on the methodology employed to characterize material strength, response, and performance of pavements. They are: (i) empirical methods, (ii) mechanistic methods, and (iii) mechanistic-empirical (M-E) methods.

2.3.1 Empirical methods

Empirical methods used in pavement design procedures are solely based on the results of limited experimental studies or engineering experience (i.e., observations from past performance). These procedures use models which are extrapolated from real world experimental data to relate design inputs (i.e., materials, loads, and environmental factors) to outputs such as pavement response and performance. Empirical design procedures prove advantageous as the analysis is often simplified. Nonetheless, these methods have several shortcomings as the validity of empirical relationships are constrained to the conditions in which the underlying experimental data was inferred (Christopher et al. 2006). For example, the AASHTO-1993 design guide (which is practised globally because of its simplified and straightforward design procedure) is purely empirical as the design guide is based on field performance data that was measured from the American Association of State Highway Officials (AASHO) road test conducted in Ottawa, Illinois during the late 1960s. As such, the validity of this data is constrained to the traffic loading and environmental conditions experienced in Ottawa, Illinois at the time of the tests.

2.3.2 Mechanistic methods

Mechanistic methods are the group of design procedures which use analytical models that are based on fundamental engineering mechanics to evaluate the state of stress in a pavement and predict its response, behavior, and performance (Seeds 2000). Mechanistic design procedures provide more reliable predictions as they consider the resilient response as well as the effects of environmental factors (moisture and temperature) on the rheological properties of pavement materials. Mechanistic methods are based on the assumptions that the pavement can be modelled as a multi-layered elastic or visco-elastic structure on an elastic or visco-elastic foundation, and assuming that pavements can be modelled in this manner, it is possible to calculate the stress, strain, or defection due to traffic loadings or environmental factors (AASHTO 1993). Mechanics is the action of motion and forces on bodies (Vujičić and He 2004). Thus, a mechanistic approach seeks to describe a material's rheological behavior by direct reference to a physical cause. Pavements typically undergo cyclic loading, as such rational design is one that considers the resilient properties of the pavement materials. Visco-elastic models such as the resilient modulus, M_R provides a framework for understanding the capability of a strained material to recover its size and shape after deformation (i.e., cyclic response).

Mechanistic methods provide the most accurate predictions for pavement performance and strength compared to empirical methods. Nonetheless, this method has some drawbacks as pavement performance may also be influenced by several other factors which are too complex and expensive to be completely modelled. Empirical methods are commonly accepted compared to mechanistic methods because of their simplicity. Nonetheless, both methods have their respective limitations; the mechanistic approach is expensive and sophisticated to fully implement, while the empirical approach does not consider the effect of seasonal weather fluctuations and cyclic loads, which is the actual type of loading experienced in pavements. The limitations of both solely empirical methods and solely mechanistic methods are evident and combining both methods allow for the realization of a reliable, yet economical method known as the M-E method.

2.3.3 Mechanistic-empirical (M-E) design methods

M-E methods fall into the category of design procedures which use an approach wherein classical mechanics of solids are combined in conjunction with empirically derived relationships to accomplish the design objectives (Christopher et al. 2006). For example, the *Mechanistic-Empirical Pavement Design Guide* (AASHTO 2008) commonly known as MEPDG is an advanced tool that utilizes M-E approach to simulate incremental damage of the pavement, taking into account the temperature and moisture variations experienced over its life cycle. The mechanistic component of the MEPDG associates to the mechanistic models used for predicting pavement responses (deflections, strains, and stresses), while the empirical component relates to the dependence on experimental results for development of these mechanistic models. The MEPDG approach fully considers the changes of temperature and moisture profiles in the pavement structure and subgrade over the design life of a pavement through the incorporation of the Enhanced Integrated Climate Model (EICM) into the MEPDG design software (Li et al. 2011).

EICM is a one-dimensional coupled heat and moisture flow program that predicts changes in the material properties of the base, subbase, and subgrade layers in conjunction with environmental variations over the pavement service life (ARA Inc. ERES Division 2004). The program uses an adjustment factor (F_{env}) to account for the effect of conditions such as ground water movements, freezing, thawing, and recovery from thawing on the pavement strength. F_{env} is modelled to vary with position within the pavement structure and with time throughout the pavement lifecycle.

The EICM can predict changes in moisture and ψ of pavement layers in response to climate and environmental variations over the pavement life based on unsaturated soil mechanics using the Soil Water Characteristic Curve (SWCC) as a tool. SWCC can be defined as the variation of water storage capacity within the micro- and macro pores of a soil (Fredlund et al. 1995). Experimental data of SWCC that can be determined from various techniques is usually plotted as the variation of water content (volumetric, gravimetric, or degree of saturation) with ψ. There are several models proposed in literature to model the SWCC. However, the equation proposed by Fredlund and Xing (1994) is used to fit the SWCC data and incorporated into the MEPDG to model the behavior of unsaturated subgrade soils.

The EICM also requires input information of unsaturated soil properties (ψ and volumetric water content, θ_w) to predict variations of M_R with ψ and moisture content. Level 1 design requires direct measurement of pairs of ψ and θ_w for fitting the entire SWCC. Level 2 requires the measurement of index properties (plasticity index (I_P), percent passing No. 200 sieve (P_{200}), and the effective grainsize corresponding to 60 percent passing by weight (D_{60})) to estimate the Fredlund and Xing (1994) model parameters to predict the SWCC. In Level 3, the SWCC may be estimated via correlation with soil gradation, classification, or other index properties.

2.4 Advances in pavement design in North America

Prior to the early 1920's, pavement design was solely based on experience or correlations with past performance. The same pavement thickness was typically used for highway sections even though widely different soils were encountered (Huang 2004). As experience was gained over time, more rational and feasible design methods were developed. The Public Roads (PR) soil classification system was the first step towards the evolution of modern pavement design methods.

The first version of the PR classification system was published in 1929. This method grouped various subgrade soils as uniform or non-uniform. Uniform soils ranged from index A-1 to A-8 and non-uniform from index B-1 to B-3. In 1945, the PR classification system was modified by the Highway Research Board (HRB), in which subgrade soils were grouped into 7 categories (A-1) to (A-7) with indexes to differentiate soils within each group. The classification was applied to estimate subbase quality and total pavement thickness.

The second major event to consider in the evolution of pavements was the adoption of empirical methods such as California Bearing Ratio (*CBR*). After World War II, the US Army Corps of Engineers (USACE) developed a pavement design procedure for airfield pavements, which was then adopted for design of public roads. This procedure made use of the *CBR*-value which was developed by O.J. Porter for the California highway department to estimate the thickness of pavements. The *CBR* can be defined as the force required to achieve a pre-defined amount of penetration into a subgrade soil expressed as a percentage of the force required to obtain the same penetration in a standard crushed stone (Stephens 1990).

Another noteworthy advancement in pavement design practice was the development of the three major road tests conducted by the HRB. Between 1940 and 1960, the HRB conducted three road tests under controlled conditions to develop empirical relationships between axle loads and pavement performance for different structural designs. The three road tests conducted were: Maryland road test, Western Association of State Highway Officials (WASHO) road test and AASHO road tests. The AASHO road test proved to be one of the important pavement research projects. Based on the information obtained from the AASHO road test, American Association of State Highway and Transportation Officials (AASHTO) developed empirical structural design tools for designing flexible and rigid pavement structures (Kim et al. 2011). This led to the publication of *AASHO Interim Guide for the Design of Flexible Pavement Structures* (AASHTO 1961), and highlighted a major milestone in pavement engineering discipline as it was the first guide to consider serviceability and performance in the design of pavements.

The AASHTO-1961 guide was improved with updates published in 1972 and 1986, and a major change in 1993. In 1986, M_R replaced *CBR,* and *R*-value and it is considered as the main property that sufficiently describes the resilient behavior of pavement materials (Christopher et al. 2006). The design guide was renamed in 1993 as *AASHTO Guide for Design of Pavement Structures* (AASHTO 1993) and has since been extensively used by many agencies in North America till recent. The AASHTO-1993 design guide was exercised globally because of its straightforward design method. However, this design method is purely empirical, shedding lights on the need for revision of the guide.

2.4.1 Implementation of MEPDG for design of pavements in North America

In 1996, AASHTO Joint Task Force on Pavements (JTFP) in cooperation with the National Cooperative Highway Research Program (NCHRP) and Federal Highway Administration (FHWA) funded a research program to develop an improved design guide that exceeds the limitations of the AASHTO-1993 guide. As part of this effort, the JTFP sponsored a workshop to develop a framework for the improvement of AASHTO-1993 design guide, and based on the conclusions of this meeting, the NCHRP project 1-37A, *Development of the 2002 Guide for Design of New and Rehabilitated Pavement Structures: Phase II*, was awarded in 1998 to the ERES Consultants Division of Applied Research Associates, Inc (Kim et al. 2011).

In 2004, the product of the NCHRP project 1-37A was made available to the public as the Guide for Mechanistic-Empirical Design of New and Rehabilitated Pavement Structures (ARA Inc. ERES Division 2004). A revised version of the MEPDG along with an application software DARWin-ME was issued by AASHTO in 2008, under name: *Mechanistic Empirical Pavement Design Guide: A manual of practice* (AASHTO 2008). The software was given the name DARWin-ME to differentiate it from the computer version of the AASHTO-1993 design guide called DARWin (design, analysis, and rehabilitation for Windows) (Kim et al. 2011). DARWin-ME has been commercially available since the year 2011. Currently, the MEPDG Software is presently developed under the name of AASHTOWare® Pavement ME Design software (AASHTOWare®), which was released in February 2013.

The AASHTOWare® software requires a calibration to improve the accuracy of the software prediction models. The calibration correctly adjusts the prediction models to consider region specific conditions; it includes characterization of pavement materials, subgrade properties, traffic data, and hourly climatic data (i.e., temperature, precipitation, solar radiation, cloud cover, and wind speed) for specific regions. A list of the progress made so far towards implementation of MEPDG is summarised in Table 2-1. It should be noted that the *Guide for the Local Calibration of the Mechanistic-Empirical Pavement Design Guide* (AASHTO 2010) was a milestone for the calibration as it provides a systematic summary of the local calibration procedures (Zhong 2017).

The MEPDG is widely used by several North American transportation agencies. Currently, the MEPDG is gradually being implemented in Canada, with MTO taking lead as one of the transportation agencies. So far, three revisions have been developed summarising efforts made towards calibrating the AASHTOWare® software for Ontario conditions: the first in November 2012 and two subsequent editions in May 2016, April 2019. These interim documents entailed customized default parameters for Ontario conditions when using AASHTOWare® software.

Table 2-1 Progress of the implementation of MEPDG (from Zhong 2017)

Author	Publication Year	Title	Report/ Project Number
NCHRP	2004	Guide for Mechanistic-Empirical Design of New and Rehabilitated Pavement Structures	Project 01-37A
NCHRP	2005	Traffic Data Collection, Analysis, and Forecasting for Mechanistic Pavement Design	Project 01-39, Report 538
NCHRP	2006	Independent Review of the Mechanistic-Empirical Pavement Design Guide and Software	Project 01-40A, Digest 307
NCHRP	2006	Changes to the Mechanistic-Empirical Pavement Design Guide Software Through Version 0.900	Project 01-40D, Digest 308
AASHTO	2008	Mechanistic-Empirical Pavement Design Guide: A Manual of Practice	AASHTO 2008
NCHRP	2009	Local Calibration Guidance for the Recommended Guide for Mechanistic-Empirical Pavement Design of New and Rehabilitated Pavement Structures	Project 01-40B
NCHRP	2010	Models for Predicting Reflection Cracking of Hot-Mix Asphalt Overlays	Project 01-41, Report 669
AASHTO	2010	Guide for the Local Calibration of the Mechanistic-Empirical Pavement Design Guide	AASHTO 2010
FHWA	2010	Local calibration of the MEPDG using pavement management	DTFH61-07-R-00143
NCHRP	2011	Sensitivity Evaluation of MEPDG Performance Prediction	Project 1-47
AASHTO	2011	Software Help System DARWin-ME Mechanistic-Empirical Pavement Design Software	AASHTO 2011
AASHTO	2013	AASHTOWare Pavement ME Design User™ Manual	AASHTO 2013

Author	Publication Year	Title	Report/ Project Number
NCHRP	2013	Guide for Conducting Forensic Investigations of Highway Pavements	Project 01-49, Report 474
NCHRP	2014	Implementation of the AASHTO Mechanistic-Empirical Pavement Design Guide and Software: A Synthesis of Highway Practice	Project 20-05, Report 457
NCHRP	2015	Consideration of Preservation in Pavement Design and Analysis Procedures	Project 01-48, Report 810

2.5 Mechanical properties of pavement materials

Pavements can be subjected to certain loading cycles without appreciable damage due to accumulation of permanent strains. A key design requirement for rational design of pavement materials is its resistance to permanent deformation and ability to remain in the elastic domain under loading. Therefore, the strength and stiffness or resistance to permanent deformation becomes the most important mechanical properties for describing the rational behavior of pavement materials.

2.5.1 Strength - California Bearing Ratio (*CBR*)

CBR is an index that compares penetration resistance of laboratory-compacted soil material to that of a durable, well-graded, crushed rock material (Keaton 2018). The test was devised by the California Division of Highways in or about 1929 for the original purpose of comparing base and subbase course materials and only later for the evaluation of cohesive soils and subgrades (Wooltorton 1958). The *CBR* is measured from the force corresponding to the driving of a cylindrical punch (with a diameter equal to 49.6 mm) into the sample at the constant rate of 1.27 mm/min (Andrianatrehina et al. 2018). The forces for two conventional displacements (2.5 and 5.08 mm) are compared to the equivalent crushed-rock standard stress values of 13.4 kN for the 2.54 mm penetration and 20.1 kN for the 5.08 mm penetration.

2.5.2 Stiffness - Resilient Modulus (M_R)

The term resilient modulus, M_R was initially introduced by Seed et al. (1962) for characterizing the elastic response of subgrade soil. Under repeated load tests, it is observed that as the number of loading cycles increases, the energy dissipated during a given loading cycle decreases. This is evidenced by a decrease in stress-strain hysteresis and is accompanied by an increase in the secant moduli. After several loading cycles, the M_R becomes nearly constant, and the response can be assumed to be approximately elastic. This steady value of M_R is defined as M_R and is assumed to occur after about 200 cycles of loading (Drumm et al. 1990). It is defined as the ratio of the repeatedly applied load stress to the recoverable strain determined after repeated loading.

$$\boldsymbol{M_R = \frac{\sigma_d}{\varepsilon_r}} \qquad \textbf{[2-1]}$$

where $\sigma_d = \sigma_1 - \sigma_3$ is the maximum applied deviatoric stress; ε_r: resilient (recoverable) strain. Eqn. [2-2] is suggested by the MEPDG for describing the stress dependent nature of M_R.

$$\boldsymbol{M_R = k_1 p_a \left(\frac{\theta_b}{p_a}\right)^{k_2} \left(\frac{\tau_{oct}}{p_a} + 1\right)^{k_3}} \qquad \textbf{[2-2]}$$

where $\theta_b = 3\sigma_c + \sigma_d$ is the bulk stress; τ_{oct} is the octahedral shear stress; k_1, k_2, and k_3 are model parameters; p_a is the atmospheric pressure. τ_{oct} = $0.471\sigma_d$ for conventional triaxial tests. Sukumaran et al. (2004) opined that there is an apparent wide variation in the M_R value that can be obtained using the *CBR* which depends on many factors.

2.5.3 Correlations between *CBR* and M_R

There are numerous publications in the literature that propose empirical relationships to estimate the *CBR* from M_R. These relationships are usually expressed in the form:

$$\boldsymbol{M_R(MPa) = \mathrm{A} \times CBR^B} \qquad \textbf{[2-3]}$$

where *A* and *B* are fitting parameters. *A* and *B* depends on the nature of the material and moisture conditions (Dione et al. 2014; Gansonré et al. 2021). Sukumaran et al. (2004) opined that there is an apparent wide variation in the M_R value that can be obtained using the *CBR* which depends on many factors. Some of the more popular equations used by several transportation agencies are summarized in Table 2-2. Vanapalli and Han (2017) proposed Eqn. [2-4] based on the results of 8 subgrade soils from Ontario, with a regression acceptance value of 98%. This relationship suggests good correlations and is valid for determination M_R determination from *CBR* for Ontario subgrade soils. The correlation is however valid only for optimum moisture conditions.

$$\boldsymbol{M_R(MPa) = 19(CBR)^{0.65}} \qquad \textbf{[2-4]}$$

There are several correlations published in the literature that provides relationship between *CBR* and M_R. The earlier studies show that *CBR* and M_R produce poor correlations. A common conclusion drawn was that *CBR* is a measure of shear strength, which is not necessarily expected to correlate with a measure of stiffness or M_R (Drumm et al. 1990; Sukumaran et al. 2004; Dione et al. 2014). Another important point is that the M_R is not a simple function of *CBR* but depends on the soil type and the level of the applied deviatoric stress (Lotfi et al. 1988; Brown and Selig 1991; Erlingsson 2007).

Table 2-2 Values for A and B used by some transportation agencies (from Erlingsson 2007)

A	B	Author(s)	Agency
10	1	Heukelom and Klomp (1962)	AASHTO
37	0.71	Green and Hall (1975)	USACE
18	0.64	Lister and Powell (1987)	MEPDG
21	0.65	Ayres (1997)	CISR

2.6 Relationship between *CBR, M_R*, and properties of unsaturated soils

The *CBR* and M_R are two material properties commonly accepted as an indicator of the strength of pavement materials. These properties are both largely dependent on molding moisture content, density (soil structure or fabric), and method of compaction (Han and Vanapalli 2016b; Gansonré et al. 2021). The *CBR* tests are simpler and inexpensive in comparison to the M_R tests. Due to this reason, several investigators in recent years have modified conventional *CBR* tests to interpret the results taking account of the influence of ψ. Some of these researchers proposed relationships between M_R and *CBR* exploiting the strong link with ψ. In summary, the combined effect of ψ and moisture content provide more reliable correlation for estimating M_R from *CBR*. There are numerous publications available in the literature that propose relationships to estimate or predict M_R from ψ, or *CBR* from ψ, which are discussed in later sections. However, only a few of these studies provide relationships or methods to predict M_R from *CBR* considering the influence of ψ.

2.6.1 *CBR*-ψ correlations

Franco and Lee (1987) noted that variations in the *CBR* test results are largely explained by the molding water content, density, and method of compaction. Each of these intrinsic properties can have an influence on ψ which describes the stress state of the soil. For the interpretation of the moisture dependence of the *CBR* test, it is recommended to perform the test in soaked and unsoaked conditions (Loach 1987; Ikechukwu et al. 2018; Gansonré et al. 2021). Various research publications (Ampadu 2007; Toll 2015) propose rational concepts for interpretation of *CBR* test results using principles of unsaturated soil mechanics. However, these studies do not provide correlations for determination of *CBR* from ψ or vice versa. Loach (1987) derived Eqn. [2-5] from experiments performed on three fine-grained soils from UK over the ψ range of 0 to 100 kPa.

$$\log CBR = 0.019\,\psi - 0.417 \qquad [2\text{-}5]$$

Ampadu (2007) derived Eqn. [2-6] based on *CBR* tests performed on specimens wetted or dried from optimum moisture condition. This experiment was carried out on a fine-grained soil for ψ values between 0 and 10^5 kPa.

$$CBR_u = CBR_s \times \left(\frac{\psi}{\psi_b}\right)^n \qquad [2\text{-}6]$$

where CBR_u is the *CBR*-value under unsoaked or unsaturated conditions; CBR_s is *CBR*-value under soaked or saturated conditions; ψ_b is the ψ at air entry value; n is a constant which depends on ψ and soil structure. Ampadu (2007) reported n value as 1.4 for soils compacted at lower dry densities, 0.5 for higher dry densities, and constant for ψ values up to 15,000 kPa. Ikechukwu et al. (2018) suggested n values of 0.18 to 0.33 for soils with relatively high fines content.

2.6.2 M_R-ψ correlations

The relationship between M_R and ψ exhibit highly non-linear characteristic behavior due to the influence of several factors which include soil type, soil fabric or structure, applied stress level, compaction effort, and hysteresis (Vanapalli and Han 2014). Numerous approaches are available in the literature to predict the M_R variation with respect to ψ. Comprehensive list and summary of these approaches is presented in Ghayoomi et al. (2020). Han and Vanapalli (2016b) categorized these approaches into three groups based on the different methods used to take account of ψ. The first method was categorized as empirical relationships, which are usually developed based on extensive experimental data using regression analysis. For instance Ba et al. (2013) proposed Eqn. [2-7] based on the experimental data on four granular materials from Senegal.

$$\frac{\boldsymbol{M_R}}{\boldsymbol{M_{ROPT}}} = \mathbf{0.385 + 0.267}\ \boldsymbol{log(\psi)} \qquad \textbf{[2-7]}$$

The second group of correlations were classified as constitutive models which incorporate ψ into applied shearing or confining stresses. These correlations are usually based on Bishop's effective stress concept for unsaturated soils or micromechanics theory and thermodynamic laws (Vanapalli and Han 2014). An example is Eqn. [2-8] proposed by Liang et al. (2008) which was derived for two fine-grained subgrade soils over the ψ range of 150 to 380 kPa.

$$\boldsymbol{M_R = k_1\left(\frac{\theta_b + \chi\psi}{p_a}\right)^{k_2}\left(1 + \frac{\tau_{oct}}{p_a}\right)^{k_3}} \qquad \textbf{[2-8]}$$

χ is the effective stress parameter; P_a is the atmospheric pressure. Liang et al. (2008) suggested estimating the χ values in Eqn. [2-9] using the empirical equation proposed by Khalili and Khabbaz (1998):

$$\boldsymbol{M_R = \begin{cases} \left(\dfrac{\psi}{\psi_b}\right)^{-0.55} & \textit{when}\ \psi \geq \psi_b \\ 1 & \textit{when}\ \psi \leq \psi_b \end{cases}} \qquad \textbf{[2-9]}$$

where ψ_b is the air-entry ψ value. The third set of correlations were grouped as constitutive models that use stress state variable approach either consider the independent contribution of the ψ to the M_R or treat ψ as one of the stress tensors. For example, Gupta et al. 2007 considered the independent contribution of the ψ and proposed Eqn. [2-10]. This correlation was derived for fine-grained subgrade soils from Minnesota, over the ψ range of 10-10,000 kPa.

$$\boldsymbol{M_R = k_1 p_a\left(\frac{\theta_b}{p_a}\right)^{k_2}\left(1 + \frac{\tau_{oct}}{p_a}\right)^{k_3} + k_{us}p_a\Theta^{\kappa}(\psi)} \qquad \textbf{[2-10]}$$

where $\Theta = \theta/\theta_s$ is the normalized volumetric water content; κ and k_{us} are model parameters. Empirical relationships are easy to perform and are inexpensive for use in practice. For example, the application of Eqn. [2-7] only requires the soil parameter M_R or M_{Ropt} which can be measured from conventional triaxial tests. These empirical relationships define one unique relationship between the M_R and ψ regardless of other influencing factors such as the soil type, stress state, soil structure or fabric. These relationships provide acceptable predictions of the variation of the M_R with respect to the ψ for some soils. However, extending these empirical relationships to other soil types may not yield satisfactory predictions (Han and Vanapalli 2014). Successful extension of these relationships also requires high quality testing data, as the predictions of some empirical relationships are extremely sensitive to the testing data . Han and Vanapalli (2015) proposed Eqn. [2-11], a normalized model that can be used to predict the variation of the M_R with moisture and ψ. This model is formed using values of M_R and soil physical states at saturated condition (M_{Rsat}) and optimum moisture content condition (M_{Ropt}, ψ_{opt} and w_{opt}) and a model parameter ξ.

$$\frac{M_R - M_{Rsat}}{M_{Ropt} - M_{Rsat}} = \frac{\psi}{\psi_{opt}}\left(\frac{w}{w_{opt}}\right)^{\xi} = \frac{\psi}{\psi_{opt}}\left(\frac{S}{S_{opt}}\right)^{\xi} \qquad \text{[2-11]}$$

For using this model, the moisture content corresponding to the ψ can be estimated using the SWCC for predicting M_R–ψ relationships, and the ψ corresponding to the moisture content can also be estimated using the SWCC for predicting M_R–moisture content relationships; According to Han and Vanapalli (2015) a constant ξ value of 1.0 and 2.0 for coarse and fine grained soils respectively.

2.6.3 *CBR-M_R-ψ* relationships

Loach (1987) was the first to develop correlation between *CBR* and M_R taking account the effect of ψ. In this study, Eqn. [2-12] was proposed based on several tests performed on three fine-grained soils from UK over the ψ range of 0 to 100 kPa.

$$M_R = \frac{\sigma_d}{A}\left[\frac{(\log(CBR) - D)}{C \times \sigma_d}\right]^B \times 10^{-3} \qquad \text{[2-12]}$$

where *A, B*, *C* and *D* are regression coefficients; σ_d is the deviatoric stress; Ikechukwu et al. (2018) proposed Eqn. [2-13] based on three subgrade soils between 0 to 10^5 kPa. In this publication, attempt was made to validate Eqn. [2-6] proposed by Ampadu (2007).

$$M_R = 43.46 + 0.8581CBR_u \qquad \text{[2-13]}$$

2.7 Soil Water Characteristic Curve (SWCC)

The behavior of unsaturated pavement materials is highly dependent on the magnitude of suction, which in turn is influenced by the water content (volumetric, θ_w or gravimetric, w). Suction is defined as the potential pressure difference between the soil pore-air and pore-water which can also be expressed free energy state of soil water (Fredlund and Rahardjo 1993). Suction (i.e., total suction, ψ_T) is composed of matric suction (ψ) and osmotic suction (ψ_π). ψ occurs due to adsorptive and capillary forces existing in the interface of air and water, or air, water, and soil, whereas ψ_π arises from dissolved salts contained in the soil water.

The soil water characteristic curve (SWCC) is a constitutive relationship between water content (θ_w or w) or degree of saturation (*S*) and suction (ψ_T, ψ or ψ_π). The first SWCCs were obtained by Edgar Buckingham in 1907 for six different soils varying from sand to clay (Al-Hashemi 2018). The SWCC provides a conceptual framework for understanding the hydro-mechanical behavior of unsaturated soils. There are three soil parameters that can be identified from the SWCC, namely, the air entry suction value (ψ_b), pore-size distribution index (λ), and the residual suction (ψ_r) which corresponds to the residual water content ($\theta_r, S_r\ or\ w_r$) on the SWCC. The ψ_b is a measure of the maximum pore size in a soil, hence ψ_b is the suction value that must be exceeded before air recedes into the soil pores. It designates the point at which the soil begins to truly behave as an unsaturated soil. In other words, it is the point beyond which the soil properties are no longer constants but rather, take on the form of nonlinear functions of soil suction (Fredlund 2021). ψ_b is also referred to as the displacement pressure in petroleum engineering or the bubbling pressure in ceramics engineering. The intersection points between the straight sloping and the saturation ordinate (i.e., *S* = 100 %, as shown on Figure 2-5) defines the ψ_b.

The residual water content is defined as the water content at which a large suction change is required to remove additional water from the soil (Fredlund and Xing 1994). The residual water content, which corresponds to the residual suction can be considered as the point at which the liquid phase becomes discontinuous and isolated with thin films of water surrounding the soil and air (Vanapalli et al. 1998). Suction values are measured as negative pore-water pressures and can range from 0 to -10^6 kPa. Therefore, a logarithmic scale is most suitable for plotting laboratory results (Fredlund 2006).

The SWCC can be divided into three zones: namely, the boundary effect, transition, and residual zones. A conceptual schematic of a typical SWCC with the different zones of desaturation is shown in Figure 2-5. In the boundary effect zone, soil pores are saturated with capillary water, and possibly contain air in the form of occluded bubbles. As the SWCC approaches the transition zone, air begins to enter the largest pores subsequently draining the capillary water. In the transition zone, both the air phase and water phase are continuous; however, liquid phase flow and capillary effect tends to decrease with increasing suction. The residual zone is a point where the suction exceeds the residual state and the amount of capillary water and contribution of ψ becomes negligible.

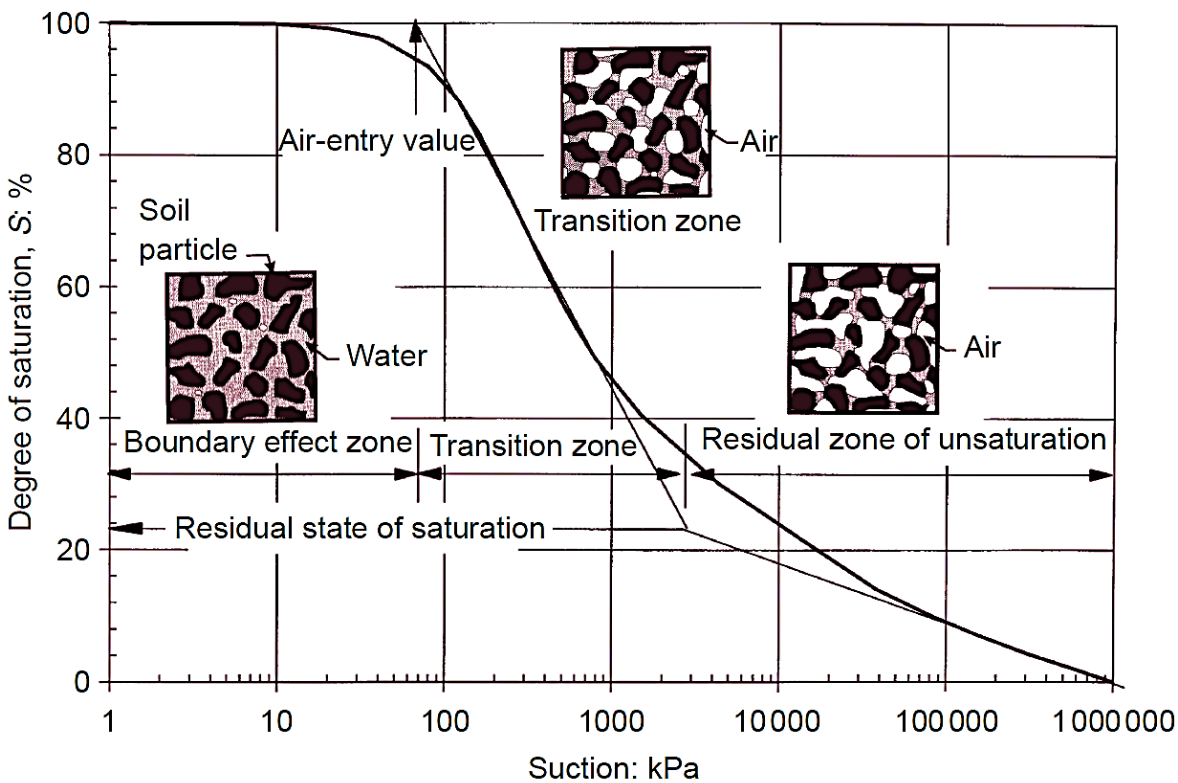

Figure 2-5 Typical soil-water characteristic curve showing zones of desaturation (from Vanapalli et al. 1999)

In the residual zone, water contained in the soil pores exist in vapour form, and the air phase is continuous. Consequently, the water phase becomes discontinuous as the water phase retreats to the micro-pores and the rate of the desaturation of water becomes remarkably slower. This characteristic can be recognised from the flattened part of the SWCC at higher suction values. Generally, ψ_π plays a dominant role in the residual zone while ψ is prevalent in the boundary effect zone.

2.7.1 Methods for measuring soil suction

The drying SWCC can be expressed as a relationship by plotting the measurements of the negative pore-water pressure and corresponding water content at several points during the saturation or desaturation of a soil specimen. There are numerous techniques that provide reliable measurements of the ψ and water content values at low suction range. However, measuring ψ_π and water content values in the residual zone (i.e., at high suction range) can prove expensive and time-consuming. The techniques for measuring suction can be grouped into two categories: namely, direct, and indirect methods. The direct methods are used for measuring the ψ component of the negative pore-water pressure through separation of the air and water phase. This can be accomplished with the use of a ceramic disc or ceramic cup. The ψ component can be measured directly as it is dependent on the tortuosity of the capillary water, while ψ_π can be measured indirectly as it is contingent on the continuity of the air phase. It is important to note that the maximum ψ value that can be measured using direct method is limited by the ψ_b of the ceramic disc or ceramic cup. The direct methods for measuring ψ include axis-translation technique, tensiometer and suction probe. Indirect methods can be used to measure ψ_T, ψ and ψ_π. The techniques for indirect measurement ψ include: in-contact filter paper technique, thermal conductivity sensors (TCS), time domain reflectometry (TDR) and electrical conductivity sensors. Indirect measurement of ψ_π mainly include squeezing technique and saturation extract method. Indirect methods to measure ψ_T include: psychrometer technique, relative humidity sensor, chilled-mirror hygrometer technique and non-contact filter paper method. Detailed explanations on these methods are summarized in Caicedo (2019). The experimental studies on unsaturated soils are time consuming and costly. Due to this reason, the SWCC is mostly estimated using closed-form, empirical models.

2.7.2 Equations to best-fit the SWCC

There are several closed-form, empirical equations proposed in literature to best-fit the SWCC. A list of the commonly used equations is summarized in Table 2-3. The equations can be divided into categories of two and three parameter equations and can be best fit to laboratory data using a least squares regression analysis. Each of the proposed equations has one variable that bears a relationship to ψ_b of the soil and the second variable that is related to the rate at which the soil desaturates (Fredlund 2006). The SWCC is used in the MEPDG to account for the unsaturated behavior of the pavement materials. Eqn. [2-14], proposed by Fredlund and Xing (1994) is used to fit the SWCC data and incorporated into the MEPDG to model the behavior of unsaturated subgrade soils.

$$\boldsymbol{\theta_w = C(\psi) \times \left[\frac{\theta_{sat}}{\left[ln \left[\exp(1) + \left(\frac{\psi}{a_f} \right)^{b_f} \right] \right]^{c_f}} \right]} \quad \textbf{[2-14]}$$

where

$$\boldsymbol{C(\psi) = 1 - \frac{ln\left[1 + \frac{\psi}{\psi_r}\right]}{ln\left[1 + \frac{10^6}{\psi_r}\right]}} \quad \textbf{[2-15]}$$

where θ_{sat} is the saturated volumetric water content or porosity; ψ is the matric suction (in kPa); a_f, b_f, and c_f are model parameters; ψ_r is the residual suction (in kPa). a_f is a parameter which is primarily a function ψ_b of the soil, b_f is a parameter which is primarily a function of the rate of water extraction from the soil, once ψ_b has been exceeded, c_f is a parameter which is primarily a function of residual water content, and $C(\psi)$ is a correction factor which is primarily a function of the suction at which residual water content occurs. For a better fit of the SWCC at high suction range, some of these equations use the normalized volumetric water content as shown in Eqn. [2-16].

$$\boldsymbol{\Theta_n = \frac{\theta - \theta_r}{\theta_{sat} - \theta_r} = \frac{w - w_r}{w_{sat} - w_r}} \quad \textbf{[2-16]}$$

where Θ_n is the normalized water content; θ_r and w_r are the is the residual volumetric and gravimetric water content respectively; θ_{sat} and w_{sat} are the volumetric and gravimetric water content at saturation, respectively. Using the normalized water content provides better estimation of ψ_b and ψ_r for soils that undergo volume change during drying (e.g., highly plastic clays).

Table 2-3 Equations proposed to best-fit the SWCC

Author	Equation	Eqn. N°	Parameter
Gardner (1956)	$\Theta_n = \frac{1}{1 + a_g \psi^{b_g}}$	**[2-17]**	a_g, b_g

Brooks and Corey (1964)	$\Theta_n = 1 \text{ for } \psi \leq \psi_b$ $\Theta_n = \left(\frac{\psi}{\psi_b}\right)^{-\lambda_{bc}} \text{for } \psi > \psi_b$	**[2-18]**	ψ_b, λ_{bc}
Brutsaert (1967)	$\Theta_n = \frac{1}{1+\left(\frac{\psi}{a_b}\right)^{b_b}}$	**[2-19]**	a_b, b_b
Van Genuchten (1980)	$\Theta_n = \frac{1}{\left[1+\left(\frac{\psi}{a_v}\right)^{b_v}\right]^{c_v}}$	**[2-20]**	a_v, b_v, c_v
McKee and Bumb (1987)	$\Theta_n = \frac{1}{1+exp\left(\frac{\psi - a_m}{b_m}\right)}$	**[2-21]**	a_m, b_m
a_g, a_b, a_v, a_m are soil parameters which is primarily a function of the air entry value of the soil; b_g, b_b, b_v, b_m are parameter which is primarily a function of the rate of water extraction from the soil, once the air entry value has been exceeded; c_v is a parameter which is primarily a function of residual water content; λ_{bc} is the pore-size distribution index.			

The Fredlund and Xing (1994) SWCC model parameters (a_f, b_f, and c_f) for best-fitting the SWCC can be derived from soil index properties such as the plasticity index (I_P), percent passing No. 200 sieve (P_{200}), and the effective grainsize corresponding to 60 percent passing by weight (D_{60}). Generally, soils can be divided into fine grained (i.e., $I_P > 0$) and coarse-grained ($I_P = 0$). The fitting parameters for fine grained soils can be correlated to the product P_{200} and I_P. While for granular soils, the fitting parameters for the SWCC can be related to the effective grainsize corresponding to 60 percent passing by weight (i.e., D_{60}) obtained from the grain-size distribution curve. For example, Perera et al. (2005) proposed Eqns. [2-22] to [2-24] for estimating model parameters (a_f, b_f, and c_f) for the SWCC of fine grained soils (i.e., $I_P > 0$) using the product of P_{200} and I_P:

$$\boldsymbol{a_f = 0.00364(P_{200}I_p)^{3.35} + 4P_{200}I_p + 11} \quad \textbf{[2-22]}$$

$$\boldsymbol{b_f = 0.0514(P_{200}I_p)^{0.465} + 0.5} \quad \textbf{[2-23]}$$

$$\boldsymbol{c_f = b_f\left(-2.313(P_{200}I_p)^{0.14} + 5\right)} \quad \textbf{[2-24]}$$

$$\psi_r = a_f 32.44 e^{0.0186 P_{200} I_p}$$ **[2-25]**

For granular soils (i.e., $I_P = 0$), the water retention curve was related to the diameter D_{60} obtained from the grain-size distribution curve. The set of correlations proposed by Perera et al. (2005) for soils with $I_P = 0$ are:

$$a_f = 0.8627 D_{60}^{-0.751}$$ **[2-26]**

$$b_f = 0.1772 \ln(D_{60}) + 0.7734$$ **[2-27]**

$$c_f = 7.5$$ **[2-28]**

$$\psi_r = \frac{a_f}{D_{60} + 9.7e^{-4}}$$ **[2-29]**

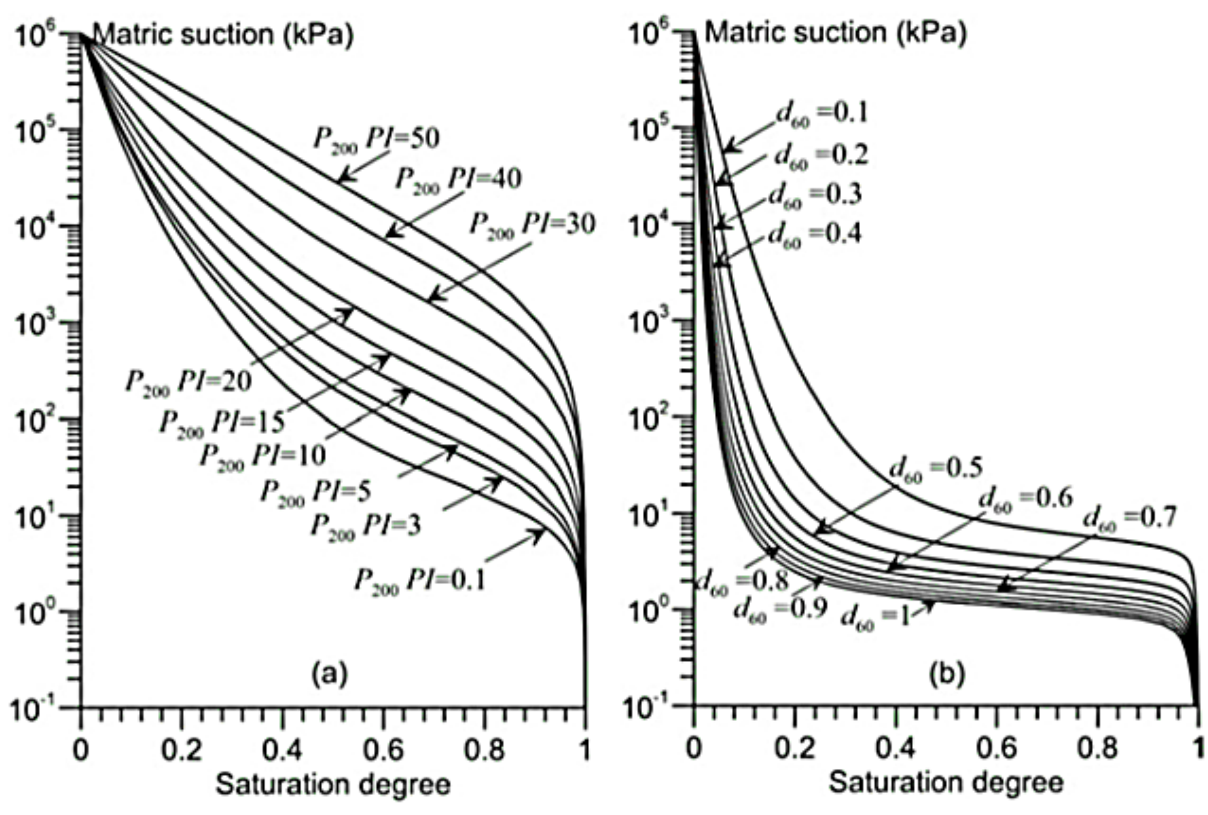

Figure 2-6 SWCC obtained using the set of correlations proposed by Perera et al. (2005) for (a) fine grained materials , and (b) coarse grained materials (from Caicedo 2019)

Figure 2-6 shows the water retention curves obtained by Perera et al. (2005) using the Fredlund and Xing (1994) equation for materials having different properties which are represented either by the product $P_{200}I_P$ or the diameter size D_{60}. There are several equations available in literature for the SWCC; however, the Fredlund and Xing (1994) and Van Genuchten (1980) equations are most widely used. One of key advantages of using the Van Genuchten (1980) equation is that it can be used to obtain unsaturated hydraulic conductivity by using a methodology based on the SWCC model parameters (Caicedo 2019).

2.8 Summary

The MEPDG is a mechanistic-empirical method for the design of pavements. This design guide is widely used in the United States and is presently under review for implementation in Canada. The mechanistic component of the MEPDG incorporates engineering principles and succinct characterization of all factors that can possibly affect pavement reliability and performance. While the empirical component relates to the use of empirical models developed from experimental data. The MEPDG considers the unsaturated behavior of pavements through the integration of EICM into the software, and the EICM in turn uses the SWCC to estimate the unsaturated behavior of the pavement materials. The *CBR* and M_R are two commonly accepted methods for characterizing strength of pavement materials and are moisture dependent properties. For this reason, *CBR*-M_R relationships should be interpreted considering both saturated and unsaturated principles. The SWCC can be used as a tool to provide a framework for understanding unsaturated behavior and to predict the unsaturated properties of pavement materials.

CHAPTER 3

RESEARCH BACKGROUND AND METHODOLOGY

3.1 Introduction

The AASHTOWare® software requires the material properties of pavement construction materials (i.e., asphalt, concrete, engineered fill, and subgrade soils) as input information taking account influence of the environmental factors (such as temperature and moisture changes) of the region for which the pavement is to be designed and constructed. In other words, the mechanical properties of these materials need to be measured taking account the typical temperature and moisture content variations that occur in the specific region. Some of these properties include the M_R that is either measured or estimated as well as the matric suction, ψ and water content of the subgrade soils in the pavement. The MEPDG hierarchical approach allows the use of relatively inexpensive methods to characterize subgrade strength for the AASHTOWare® design input parameters. For example, Level 1 design is recommended for important pavement projects that are expected to perform with relatively no risks (i.e., stringent design recommendations to cater high intensity traffic load and achieve best possible performance of the pavement throughout the various seasons of the year), and Levels 2 and 3 design is recommended for projects with lower budgets and some allowable or low risk. The Level 2 design recommends the estimation of M_R from other material properties such as the *CBR*, UCS, or *R*-value. The *CBR* is a method commonly used in practice today to characterize the strength of pavement and geo-materials, and as such would prove advantageous for use in Level 2 design. The current study aims to characterize Ontario subgrade soils for Level 2 design using the AASHTOWare® software and suggests the determination of M_R from *CBR*. It is important to note that the Level 1 subgrade characterization which is based on direct determination of M_R was completed in the study previously carried out by Vanapalli and Han (2017). This chapter contains the methodology used in execution of the key research objectives as well as a discussion on some of the significant studies in literature that inspired the experimental techniques used for this study. Also, methods that involve measurement of the *CBR* and properties of unsaturated soils are also discussed.

3.2 Methodology

The Level 1 subgrade characterization (which is denoted as "M_R testing" throughout this manuscript) have previously been completed and is summarized in Vanapalli and Han (2017). For the study, six natural subgrade soil samples were collected from various locations in Ontario (one soil each from Kincardine, Sudbury, Kingston, Ottawa and two soils from Toronto), and all soils were sampled at shallow depths of approximately 3 m, which is the typical depth of natural soil excavated for pavement construction. Figure 3-1 shows a topographical map of the locations at which the soils used for this study were obtained.

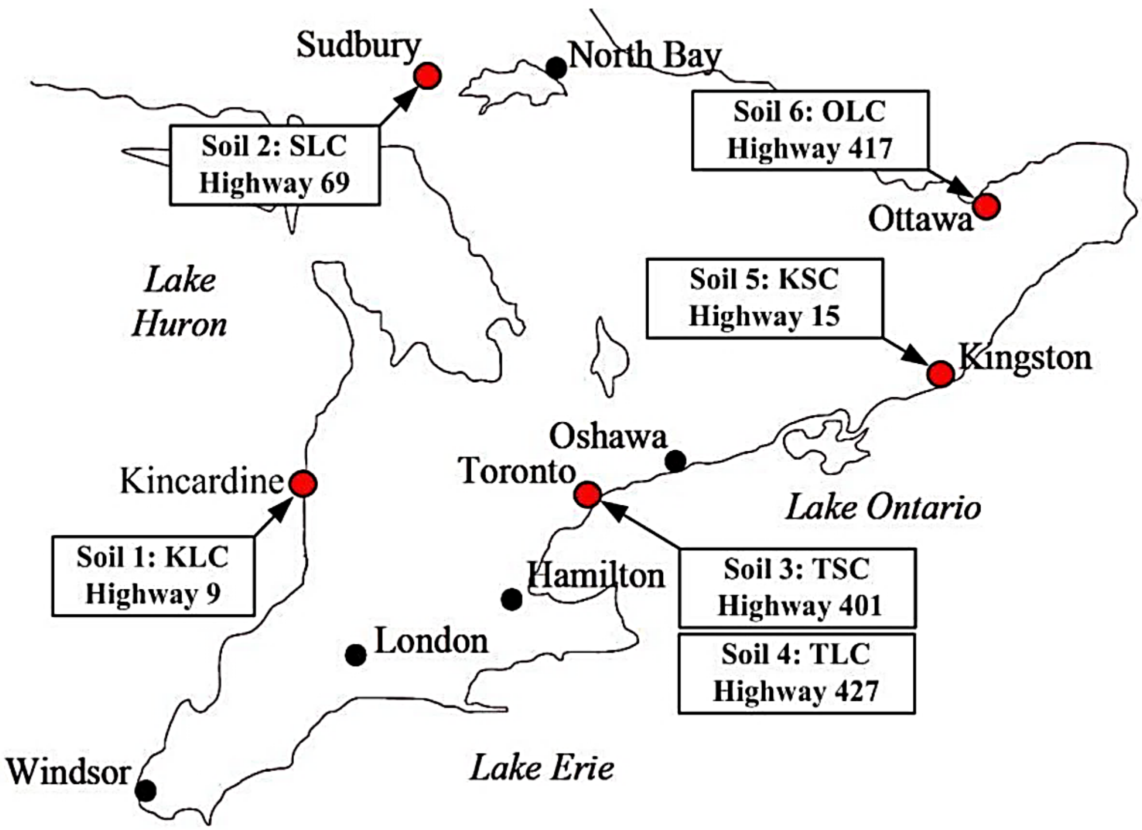

Figure 3-1 Locations of six Ontario subgrade soils used for Level 1 M_R testing (from Vanapalli and Han 2017)

Pavement subgrade soils and embankments are typically compacted to a percentage of the maximum dry density ($\rho_{d,max}$) that corresponds to the optimum moisture content (w_{opt}) measured from the proctor tests following standard practice, ASTM D698-12 (ASTM 2012a) or ASTM D1557-12 (ASTM 2012b), and the moisture in these material tends to increase or decrease with moisture influx or efflux as explained in Chapter 1. The M_R of the subgrade soils which is moisture dependent tends to vary with its fluctuations. Due to this reason, the experimental program for Level 1 M_R testing was carried out to determine the M_R of Ontario subgrade soils under the influence of moisture content (and ψ). In the previous study carried out by Vanapalli and Han (2017) for Level 1 M_R testing, test specimens were initially prepared at w_{opt} and wetted or dried prior to M_R testing. The specimens were prepared to have the same density and water content that corresponds to the $\rho_{d,max}$ and w_{opt} measured from the standard proctor tests.

For the current study, *CBR* tests are proposed to be performed on several specimens that are prepared from same soils used in Level 1 M_R testing. These soils are compacted at w_{opt} condition (i.e., using the $\rho_{d,max}$ and w_{opt} measured from the standard proctor tests), with the aim to replicate a similar soil fabric to the specimens prepared in the previous study. The compacted specimens are then either tested at w_{opt} condition, saturated, wetted, or dried to achieve similar moisture content measured by Vanapalli and Han (2017), after which the *CBR* tests are to be performed. The ψ values corresponding to the moisture content of the tested *CBR* specimens will also be determined.

In this study, 5 out of the 6 soils discussed were used for the present study. Also, not all of the soils used were tested for *CBR* considering wetting and drying conditions. The two soils from Toronto, Toronto lean clay (TLC) and Toronto silty clay (TSC) were tested for *CBR* considering wetting, drying, saturated and w_{opt} condition. While the remainder soils (i.e., Kingston silty clay (KSC), Ottawa Leda clay (OLC) and Kincardine lean clay (KLC)) were only tested under saturated and w_{opt} conditions. The initial plan for this study was to perform extensive testing on all soils (i.e., considering wetting, drying, saturation and w_{opt} condition). However, due to the restrictions imposed on the laboratory and research facility at the university due to the pandemic, all planned experimentations could not be accomplished.

The research objective is well defined; however, the major challenge was associated with the development of a suitable method to incorporate wetting and drying of specimens into the standard *CBR* test procedure, as well as developing reliable techniques to measure ψ and soil moisture content of the specimens during the wetting and drying process. Such a technique is required to develop reliable relationships between the M_R and the *CBR* test results, which is the key objective of the research study.

3.3 Methods used for similar studies in the literature

The process of wetting, drying or saturating specimens prior to experimental testing are complex and time consuming. As such, use of the proper instrumentation is necessary for obtaining reproducible experimental results. There are some studies in the literature that propose techniques to measure ψ and moisture content of specimens tested for M_R and *CBR*. For example, Lusher (2004) carried out experiments on four Missouri aggregates to develop relationships for predicting the M_R from *CBR*. For the study, *CBR* and M_R tests were performed on compacted specimens with similar initial water content and compaction effort conditions such that they are identical, having similar soil structure. Tests were also carried out on soaked and unsoaked specimens.

Ampadu (2007) performed *CBR* tests on decomposed granite (sandy clay) to determine the variation of *CBR* with water content and ψ. In the study, specimens prepared using three different compaction efforts were subjected to soaking or drying for varying periods of time, after which *CBR* and specimen moisture content were determined. Another set of specimens compacted at two different densities were used to measure the SWCC using the filter paper technique ASTM D5298-10 (ASTM 2010). The SWCC of other specimens were extrapolated from the difference in densities between the tested *CBR* specimens and the SWCC specimens. Furthermore, a linear relationship was assumed for the SWCC in regions drier than the air entry value. The ψ information was derived from the corresponding water content of the SWCC and related to the *CBR* test results for identical conditions. In the study, the variation of *CBR* with respect to ψ was plotted as a log–log relationship.

Purwana (2013) performed a rigorous study that involved direct measurement of ψ from *CBR* test specimens with the use of tensiometers. The apparatus used comprised of a *CBR* mold retrofitted with tensiometers to allow for ψ measurements as shown in Figure 3-2. The experiments were performed on compacted specimens containing various proportions of sand-kaolin clay mixtures with clay fractions ranging from 0 % (pure sand) to 20 %. The *CBR* tests were performed on the compacted sand-kaolin specimens in soaked and unsoaked conditions. Another set of specimens for each sand-kaolin portion was subjected to various periods of drying. The results suggest that the *CBR* versus ψ forms a bi-linear curve.

The experimental findings from Purwana (2013) suggest that the *CBR* of compacted sand-kaolin clay mixtures are influenced by the combined effect of kaolin clay and water content. However, the results were only for suction values of less than 70 kPa, which is the range of ψ that can be measured using the tensiometer. The results suggest that for clean sand, the *CBR* values increase for ψ up to about 7 kPa, but then fell as ψ increased to 40 kPa. However, for mixtures containing 5 % or 10 % of kaolin clay, *CBR* values continued to increase with increasing ψ, up to their measurement limit of 70 kPa.

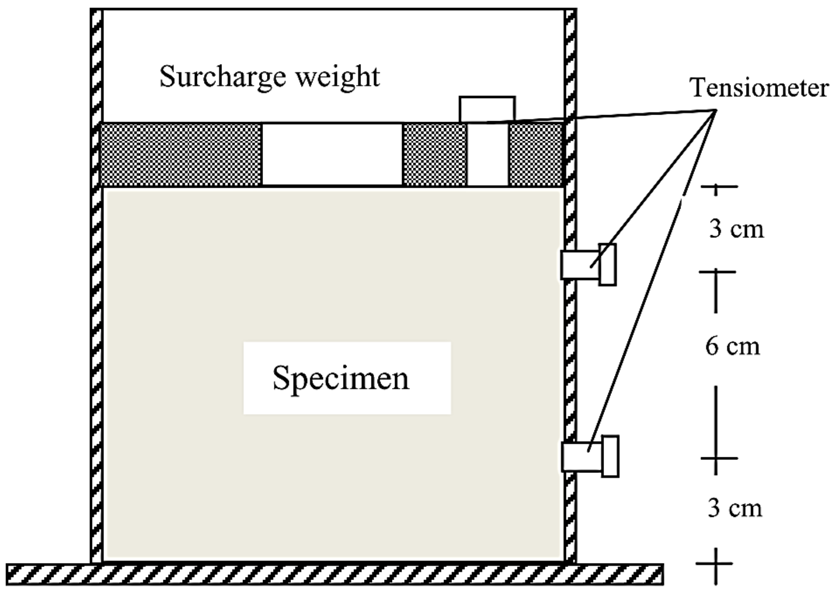

Figure 3-2 Set-up for measuring ψ of *CBR* test specimens using tensiometers (from Purwana 2013)

Toll (2015) performed *CBR* tests on lateritic gravel to investigate the effect of water content and ψ on *CBR*. In the study, 28 series of standard *CBR* tests were performed on samples compacted for a range of water contents, using three different compaction levels. A further set of 9 *CBR* tests were carried out using a specially designed *CBR* apparatus shown in Figure 3-3, which allows for measurement of ψ in the *CBR* sample with the use of a ceramic plate. The first six *CBR* tests were carried out on unsoaked samples, statically compacted at a range of water contents and to different densities. In the final three tests, samples were soaked to observe the changes in ψ. Measurements of confining stress were also made in the latter three tests.

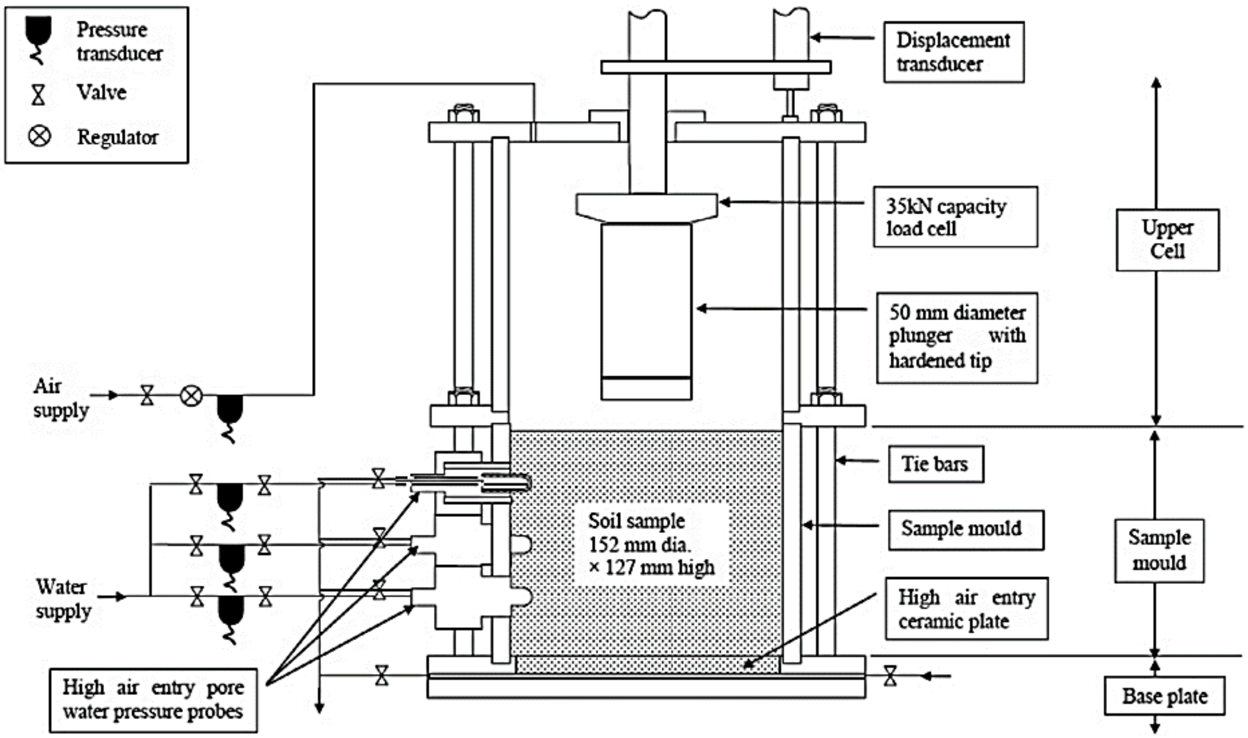

Figure 3-3 The *CBR* apparatus for ψ measurement using a ceramic plate (from Toll 2015)

Mirzaii and Negahban (2016) carried out a series of *CBR* and filter paper tests on a 60:40 sand-kaolin mixture compacted at different densities. The aim of the study was to determine the influence of initial dry density, moisture content, degree of saturation, and ψ on the *CBR* along drying and wetting paths. The study involved replicating specimens with identical soil fabric, after which the samples are subjected to varying periods of drying. Figure 3-4 shows the set-up used for the drying *CBR* tests, which is consistent with the experimental drying set-up described in the next Chapter.

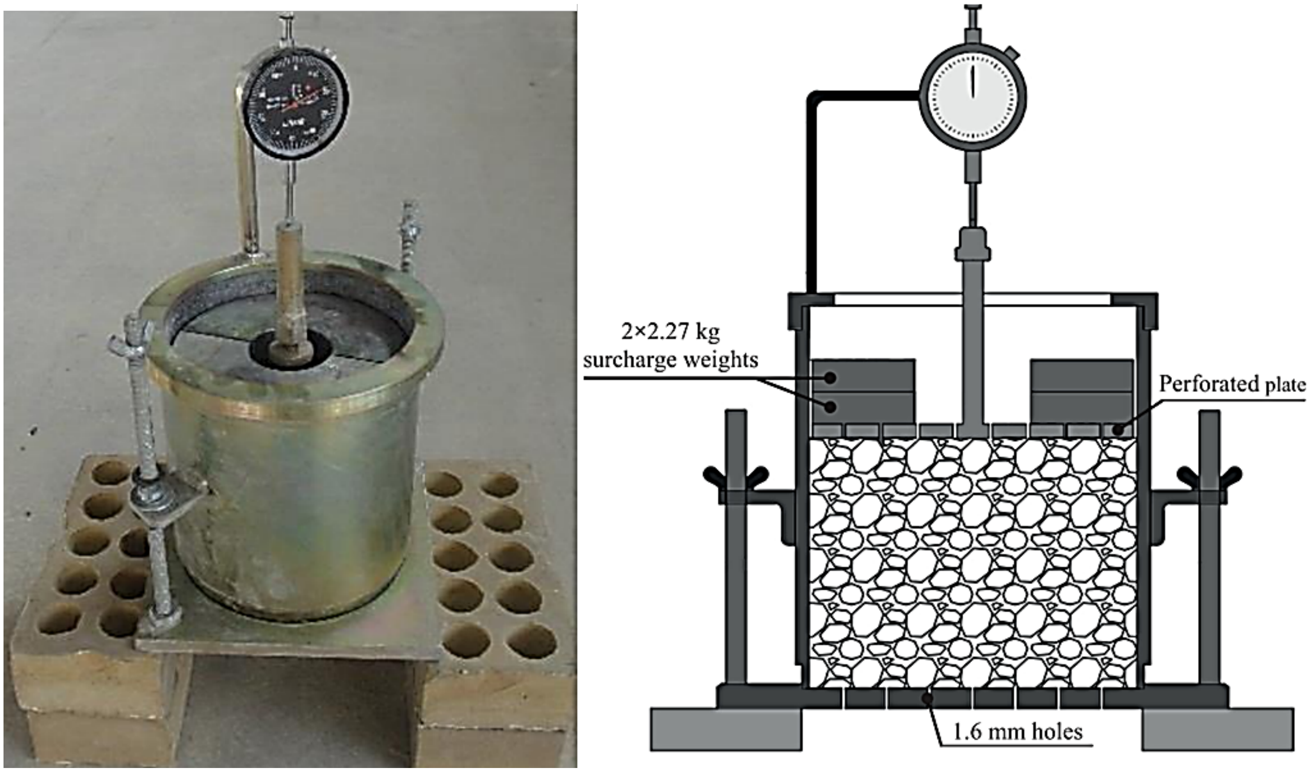

Figure 3-4 Set-up for drying *CBR* test specimens prior to penetration testing (from Mirzaii and Negahban 2016)

3.4 Instrumentation used for *ψ* and moisture content measurement

The instrumentation proposed for solving the challenges of measuring soil moisture and *ψ* during the wetting and drying process is presented in Figure 3-5. The instrumentation involves drilling of orifices into the standard *CBR* mold to allow for moisture content and *ψ* measurements during the wetting and drying process. The moisture content can be measured using the EC-5 sensors while the *ψ* can be measured using the MPS-6 or TEROS-21 sensors. The MPS-6 sensors are similar in shape and orientation; however, the TEROS-21 sensor is a more recent version. The MPS-6, TEROS-21 and EC-5 instruments are dielectric sensors produced by Decagon® Devices. These sensors determine the water content (in the case of EC-5) and matric potential (in the case of MPS-6 or TEROS-21) of a medium by measuring its dielectric permittivity. These sensors have dielectric measurement frequency of 70 MHz and an output requirement of RS232 (TTL) with 3.6-volt levels or SDI-12 communication protocol. Also, the sensors can be connected to any data acquisition system capable of 3.6 to 15 V excitation and serial or SDI-12 communication. The dielectric constant is a measure of a material's insulating capabilities; it is equal to the ratio of the electrostatic capacity of condenser plates separated by the given material to that of the same condenser with a vacuum between the plates (Scullion and Saarenketo 1997). Dielectric sensors do not measure water content; however, they provide information about the bulk dielectric permittivity of a soil. Therefore, the accuracy of the sensors is affected by the precision with which the sensor can determine the bulk dielectric constant, and by the validity of the relationship between the bulk dielectric constant and soil water content.

The MPS-6 and TEROS-21 sensors are comprised of two ceramic disks sandwiched over a circuit board. The ψ_b of the sandwiched ceramic disc is approximately - 8 kPa. However, the ceramic disc must have access to air for the large pores to begin draining and the response of the sensor to change. The MPS-6 and TEROS-21 sensors are similar and capable of measuring ψ with reasonable accuracy. However, the TEROS-21 sensors provide improved readings and can measure matric potential in the range of 9 to 10^5 kPa with 0.1 kPa resolution and an accuracy of +/- 10 % of sensor reading.

The EC-5 sensors have two prongs as shown in Figure 3-5. This instrument can determine the volumetric water content (θ_w) by measuring the dielectric constant of the media using capacitance and frequency domain technology. The gravimetric water content is commonly used in geotechnical engineering practice; as such, gathering data in terms of gravimetric water content would prove to be more beneficial for engineering applications. The relationship between the volumetric and gravimetric water content is described as follows:

$$\boldsymbol{w = \frac{\rho_w}{\rho_d}\theta_w} \quad \textbf{[3-1]}$$

It is important to note that dielectric sensors provide erroneous readings for soils with saturation extracts electrical conductivity greater than 10 dS/m. Saturation extract describes the salinity of a soil. It is the salt concentration in water extracted from a saturated soil. In other words, these instruments should not be used for measuring water content of matric potential of saline soils. Fluctuations in temperature can also affect the capacitance readings for the dielectric sensors. Hence the experiments are to be carried out in a temperature-controlled environment. The calibration curves used for the EC-5 sensors are detailed in Ren (2020).

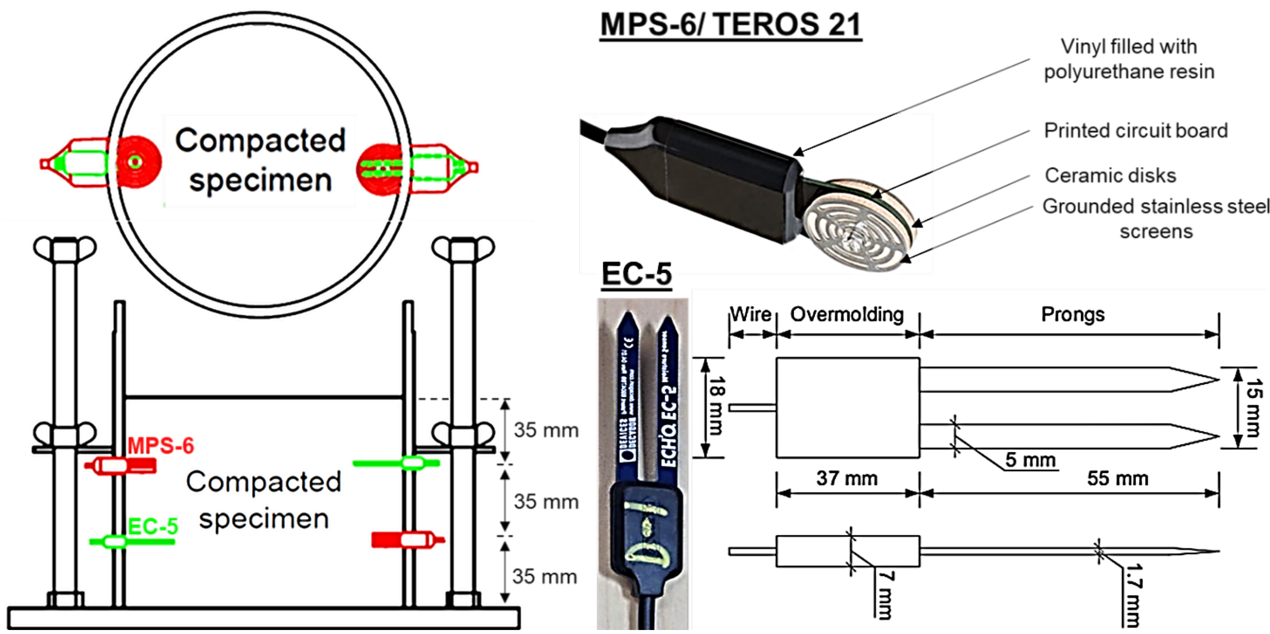

Figure 3-5 Instrumentation proposed to measure ψ and water content for the present study

3.5 Summary

In summary, the experimental studies undertaken in the present research study were based in part following the methodology described in Mirzaii and Neghban (2016). The method used to replicate the soil fabric was executed following Lusher (2004). The saturation procedure was performed following standard practice method ASTM D1883-16 (ASTM 2016). The method used for measuring of ψ is as per Purwana (2013) for direct measurement of ψ and Ampadu (2007) for indirect measurement of ψ. The wetting process was consistent with that used by Vanapalli and Han (2017). More detailed explanations on these methods and procedures used for the wetting and drying tests are discussed in the next chapter.

CHAPTER 4
EXPERIMENTAL PROGRAM

4.1 Introduction

This chapter describes the experimental program which include: the grainsize analysis, Atterberg limits, *CBR* tests and matric suction (ψ) measurements using dielectric sensors and filter paper technique. The grainsize analysis and Atterberg limit tests were performed to ensure that the soils used for this study were the same as that for the previous study (Level 1 M_R testing) that was performed by Vanapalli and Han (2017). The *CBR* tests and ψ measurements were carried out on several specimens that were initially compacted to the predetermined maximum dry density that corresponds to the optimum water content, w_{opt} measured from the standard proctor test (ASTM 2012a). The test specimens were grouped into 4 categories ((i) water content greater than w_{opt}, (ii) water content less than w_{opt}, (iii) saturated, and (iv) water content equal to w_{opt}) depending on whether the specimen had to be wetted, dried, saturated, or tested at w_{opt} condition, respectively. During the wetting and drying process, the specimen moisture contents were monitored using EC-5 sensors, and the ψ measurements were obtained using MPS-6 and TEROS-21 sensors. The sequential procedure for testing involved: soil-water mixing, specimen compaction, wetting, drying or saturation along with measurement of water content and ψ, and *CBR* tests; except in the case of the specimens tested at water content equal to w_{opt}, where the *CBR* tests are performed without the specimens being subjected to wetting, drying or saturation, and the filter paper technique was used to measure the ψ. The ψ measurements attained using the filter paper technique provides a means to verify the reliability and verification of the MPS-6 and TEROS-21 sensors used for measuring the ψ of specimens tested for *CBR* at water content greater w_{opt} and water content less than w_{opt}.

4.2 Material selection

Five out of six of the soils discussed in Chapter 3 were selected for use in the present study; two of these soils, Toronto lean clay (TLC) and Toronto silty clay (TSC) are from the Toronto region, and the remainder three, Kincardine lean clay (KLC), Kingston silty clay (KSC) and Ottawa Leda clay (OLC) are from Kincardine, Kingston, and Ottawa regions respectively. The sixth soil, Sudbury lean clay (SLC) was not tested because insufficient quantity was available for testing.

As discussed in the earlier chapter, due to the restrictions imposed on the research and laboratory facilities because of the COVID-19 pandemic, the complete scope of the experimental program was not completed as planned. Two soils from Toronto, TLC and TSC were tested extensively (i.e., considering wetting, drying, saturation and w_{opt} condition). The remainder soils (i.e., Kingston silty clay (KSC), Ottawa Leda clay (OLC) and Kincardine lean clay (KLC)) were only tested under saturated and w_{opt} condition. The index properties of these soils were previously determined by Vanapalli and Han (2017) and are summarized in Table 4-1.

Table 4-1 Physical properties of 5 Ontario subgrade soils used in this study

	Soil 1 - KLC	**Soil 3 - TSC**	**Soil 4 - TLC**	**Soil 6 - KSC**	**Soil 7 - OLC**
w_L (%)	31	20	25	22	48
w_p (%)	21	14	13	15	22
I_p (%)	10	6	12	7	26
AASHTO	A-4	A-4	A-6	A-4	A-6
USCS	CL	CL-ML	CL	CL-ML	CL
w_{opt} (%)	20.3	13.5	12.2	12.0	23.0
w_{sat} (%)	24.41	14.93	13.79	-	25.52
$\rho_{d,max}$ (kg/m^3)	1631	1915	1962	1935	1616
G_S	2.71	2.68	2.69	2.65	2.75
Sand (%)	15	3	31	35	20
Silt (%)	60	81	50	51	48
Clay (%)	25	16	19	14	32
Activity	0.40	0.38	0.63	0.50	0.88

Note: $\boldsymbol{w_L}$ = liquid limit; $\boldsymbol{w_P}$ = plastic limit; $\boldsymbol{I_p}$ = plasticity index; $\boldsymbol{w_{opt}}$ = optimum water content; $\boldsymbol{\rho_{d,max}}$ = maximum dry density; $\boldsymbol{G_s}$ = specific gravity; **Activity** = $\frac{I_p}{Clay\ (\%)}$; AASHTO = American Association of State Highway and Transportation Officials soil classification system (AASHTO M145-08, AASHTO 2008b); USCS = Unified Soil Classification System (ASTM D2487-17, ASTM 2017a).

4.3 Soil-water mixing

Once the soil properties were verified for their consistency with those used for the earlier study for the earlier study performed by Vanapalli and Han (2017), each soil was air-dried and grinded separately using a grinding machine, and a rubber or wooden head mallet to break down larger soil clods, when necessary. Each soil was then carefully sieved through N$^{o.}$ 10 (2 mm) ASTM standard sieve to reduce the likelihood of larger particles forming during the mixing process. The sieved soils were mixed at optimum water content corresponding to that measured from the standard proctor tests, ASTM D698-12 (ASTM 2012a). The required water content was achieved using water spilled from spray bottles, which was carefully mixed with the soil using a large tray and a pair of spatulas. This procedure was completed in as little time as possible to minimise moisture loss that is usually experienced during mixing periods. Based on trial tests, a little more moisture was used to mix the soil to account for water loss that typically occurs due to evaporation.

After mixing, the soil-water mixture was sieved through the 2.0 mm sieve to ensure uniform grainsize and reduce time required to attain an even moisture distribution in the sample bag; the mixed soil was then sealed in large plastic bags and stored in a Styrofoam container for 24 hours for moisture equilibration, after which the soil the bag is then mixed again. The soil moisture content in bag was checked 48 hours after the initial time of mixing using the oven dry procedure ASTM D2216-19 (ASTM 2019), and either water or soil was added to the mixed soil as necessary to achieve the required compaction water content if it was not equal to the target w_{opt} value. The procedure was repeated until the soil moisture content was within ± 0.1 % of the target w_{opt} value.

4.4 Specimen preparation

The specimens that were prepared can be classified into four different groups (water content greater than w_{opt}, water content less than w_{opt}, saturated, and water content equal to w_{opt}). Based on the initial water within the specimen, appropriate tests were performed by wetting, drying, saturating, or testing at w_{opt} condition. The specimens grouped as water content greater than w_{opt} simulate natural field conditions, while specimens that were saturated and tested simulate the most adverse conditions in the field. The specimens to be tested at water content greater than w_{opt} are subjected to wetting to mimic a situation where the subgrade soil experiences water content increase due to rainfall or other forms of water influx. Finally, the specimens tested at water content drier than optimum were intended to replicate a situation where the subgrade soil undergoes reduction in water content due to evaporation. The compaction procedure for the specimens tested for *CBR* at water content equal to w_{opt} and at saturated conditions are analogous. The same procedures were used for specimens that are wetted and dried to achieve water content wetter than w_{opt} and water content drier than w_{opt} scenarios, respectively. Detailed explanations on these procedures are presented in Figure 4-5 and Figure 4-6.

Prior to compaction of the soil-water mixture, a spacer disk is placed at the base plate, with a filter paper of the same dimension directly above it. The volume of the *CBR* mold was then determined based on its actual internal dimensions, and the mold was then divided into three equal parts, which was achieved by marking depths on the interior circumference of the mold as shown in Figure 4-1. The amount of soil-water mixture required for compaction is determined considering the volume of the mold and the bulk density that was measured from the relationship between the maximum dry density and corresponding w_{opt} for each soil presented in Table 4-1. The quantity of soil-water mixture calculated was then divided into three equal masses and compacted in three lifts that have corresponding thickness to the lengthwise divisions marked on the interior of the *CBR* mold. The standard proctor rammer was used to deliver target compaction efforts at approximately 300 mm from the surface of the specimen as specified in ASTM D698-12 (ASTM 2012a). Also, a 50-mm diameter metal plunger was used to distribute the soil evenly to a near horizontal surface prior to compacting each layer. After compaction, the water content of the specimen was verified using the oven dry procedure. Following the compaction, the specimens to be tested at w_{opt}

condition were stored in a commercial cooler with inner Styrofoam lining for 48 hours to achieve uniform water content distribution within the *CBR* mold.

The bulk density was measured from the mass of soil and the corresponding volume of mold filled with soil to verify the dry density of compacted *CBR* specimen. The bulk density is determined from Eqn. [4-1].

$$\rho_{bulk} = \frac{Mass\ of\ compacted\ specimen\ and\ CBR\ mold\ -\ Mass\ of\ CBR\ mold}{Volume\ of\ CBR\ mold} \quad [4\text{-}1]$$

The $\rho_{d,max}$ of the compacted *CBR* specimen is calculated from Eqn. [4-2].

$$\rho_d = \frac{\rho_{bulk}}{1+w} \quad [4\text{-}2]$$

The void ratio, e is calculated using Eqn. [4-3].

$$e = \frac{G_s\rho_w}{\rho_d} - 1 \quad [4\text{-}3]$$

The degree of saturation was calculated using Eqns. [4-4], [4-5] or [4-6].

$$S = \frac{wG_S}{e} \quad [4\text{-}4]$$

$$S = \frac{w}{w_{sat}} \quad [4\text{-}5]$$

$$S = \frac{V_w}{V_v} = \frac{\theta_w}{n} \quad [4\text{-}6]$$

where porosity, n can be calculated from Eqn. [4-7].

$$n = \frac{e}{1+e} = 1 - \frac{\rho_d}{G_S\rho_w} \quad [4\text{-}7]$$

The EC-5 moisture sensors measure the volumetric water content. The gravimetric water content was determined using Eqn. [4-8].

$$w = \frac{\rho_w}{\rho_d}\theta_w \quad [4\text{-}8]$$

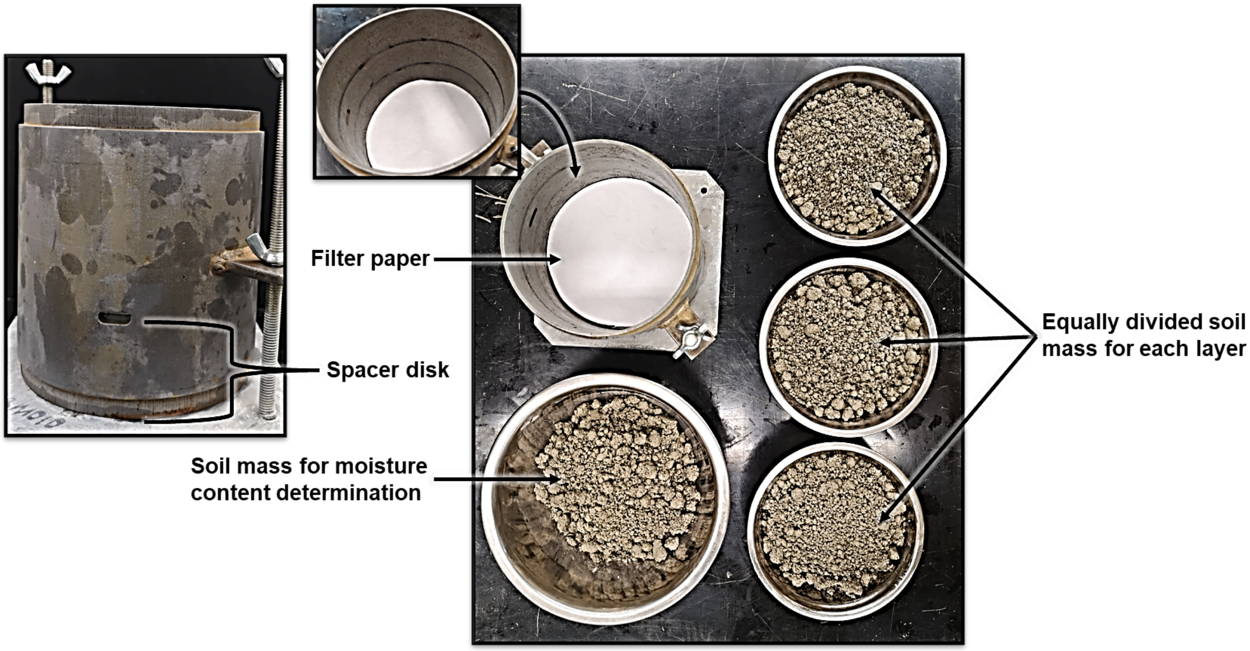

Figure 4-1 Illustration of compaction procedure for specimens tested in saturated and w_{opt} condition

4.4.1 Specimens tested at water content equal to w_{opt}

Prior to testing the specimens that were prepared at w_{opt} condition, two EC-5 sensors were inserted into the orifices that were drilled on the *CBR* mold to measure the water content. Following the penetration tests, soil samples from the penetrated surface were collected to determine the moisture content in the vicinity of the failure area. A cylindrical soil specimen with a diameter of 60 mm was extruded using a load press. A length of 30 mm was cut from the specimen and used for determination of ψ, while the remainder soil specimen was used for moisture content determination. The measured moisture content was used for checking the reliability of the EC-5 sensors results for measuring moisture variations during the wetting and drying tests. After the *CBR* test was completed, a soil specimen was extruded using a load press and extrusion device shown in Figure 4-8. The extruded sample was used to determine the ψ following ASTM D5298-10 (ASTM 2010) while the remainder soil was used for moisture content determination.

4.4.2 Saturated specimens

The procedure used for preparing the specimens that were to be tested under saturated conditions are similar to that used for preparing the specimens tested at water content equal to w_{opt}, except that after compaction, the specimen was loaded with a 4.5 kg surcharge and submerged into a container with water for four days. The weight and height of the specimen before and after soaking was recorded to calculate the amount of water imbibed from soaking. An illustration of the set-up used for saturation of the specimens are shown in Figure 4-2.

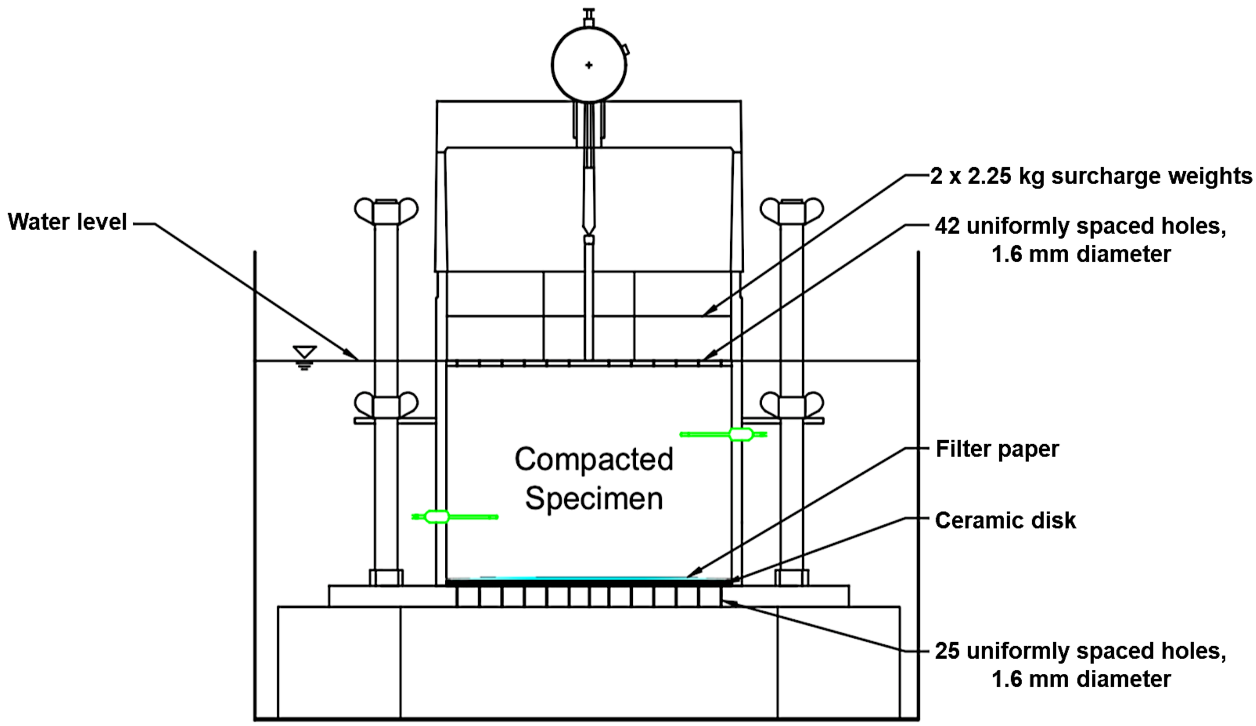

Figure 4-2 Set-up for saturation of specimens

A ceramic disk was placed at the bottom of the specimen to imbibe moisture to alleviate soil peeling or segregation of the soil particles. After soaking, the swell was measured, and the sample was allowed to drain excess water for 15 minutes, after which the *CBR* test was performed. Following this, the soil contained in the entire *CBR* mold was subjected to oven drying to determine the moisture content, while the degree of saturation was back calculated from the mass-volume relationship. In addition, EC-5 sensors were used to measure the saturated water content of the specimen. The soil suction ψ of the specimens saturated can be assumed equal zero. Due to this reason, ψ of the specimens soaked for four days were not measured. More comprehensive details of the *CBR* test procedure are detailed in a later section.

4.4.3 Specimens wetted to achieve water content greater than w_{opt}

The compaction procedure for specimens that required wetting is same as that used for specimens tested at w_{opt}, except that MPS-6 or TEROS-21 sensors are inserted into orifices on the mold during compaction to allow for measurements of ψ. After compaction, the specimen is wetted by covering both ends of the *CBR* mold with a damped filter paper and wrapping the *CBR* mold with plastic film to prevent moisture loss. The specimen is placed in an isothermal environment while the specimen moisture content and ψ was monitored using the EC-5 and MPS-6 sensors, respectively. During the wetting procedures, the specimen moisture and ψ was monitored at regular time intervals of 30 minutes to gather relevant data. An illustration of the set-up used for wetting the specimens is shown in Figure 4-3.

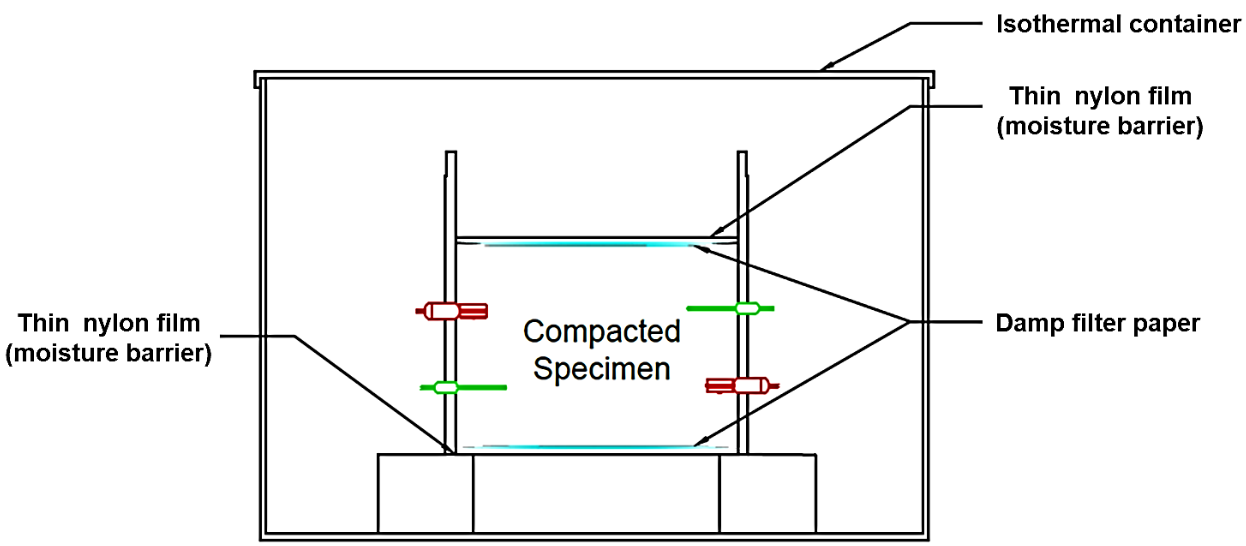

Figure 4-3 Set-up for wetting of specimens

4.4.4 Specimens dried to achieve water content less than w_{opt}

The specimens to be tested at water content less than w_{opt} were prepared in a similar manner as described for the specimens wetted to achieve water content greater than w_{opt}. However, instead of wetting, the specimens were left to have a contact with the free air so that some of the pore-water evaporates. During this period, the EC-5 and MPS-6 (or TEROS-21) were used to monitor the water content and ψ of the specimens. When the desired water content was achieved, air drying was discontinued. Prior to *CBR* penetration, the specimen was covered with a plastic sheet to avoid further evaporation. An illustration of the experimental set-up used for drying of the specimens is shown in Figure 4-4.

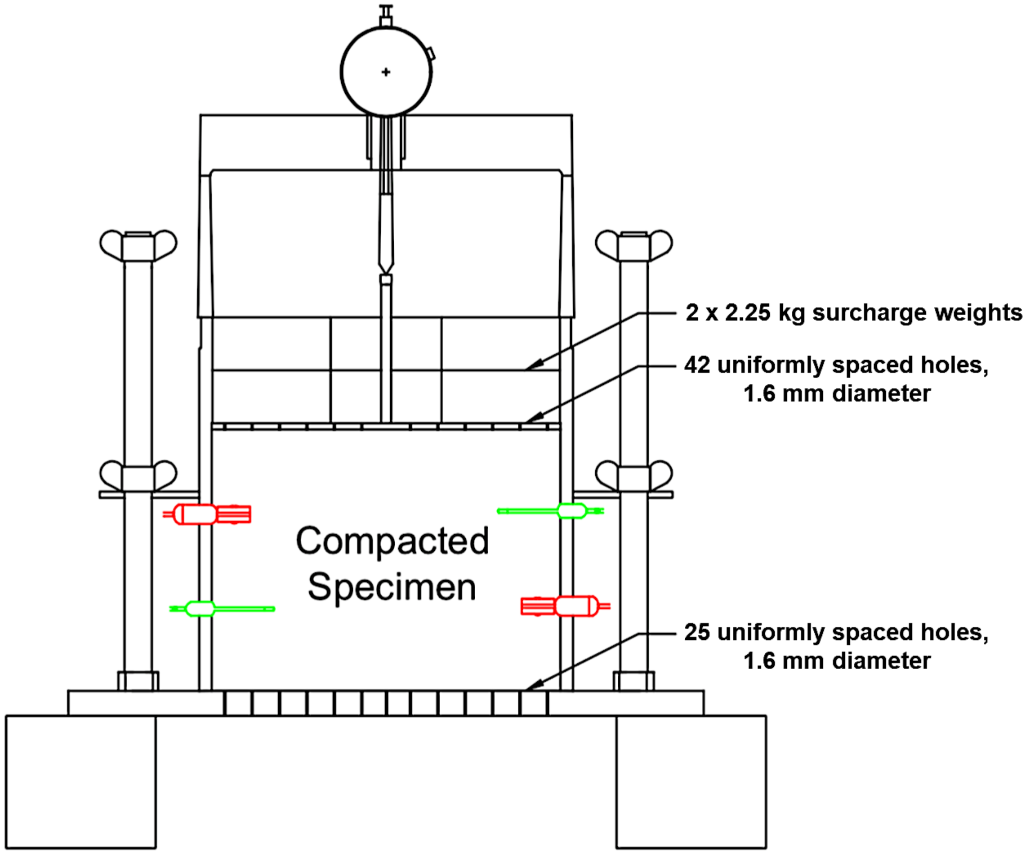

Figure 4-4 Set-up for drying of specimens

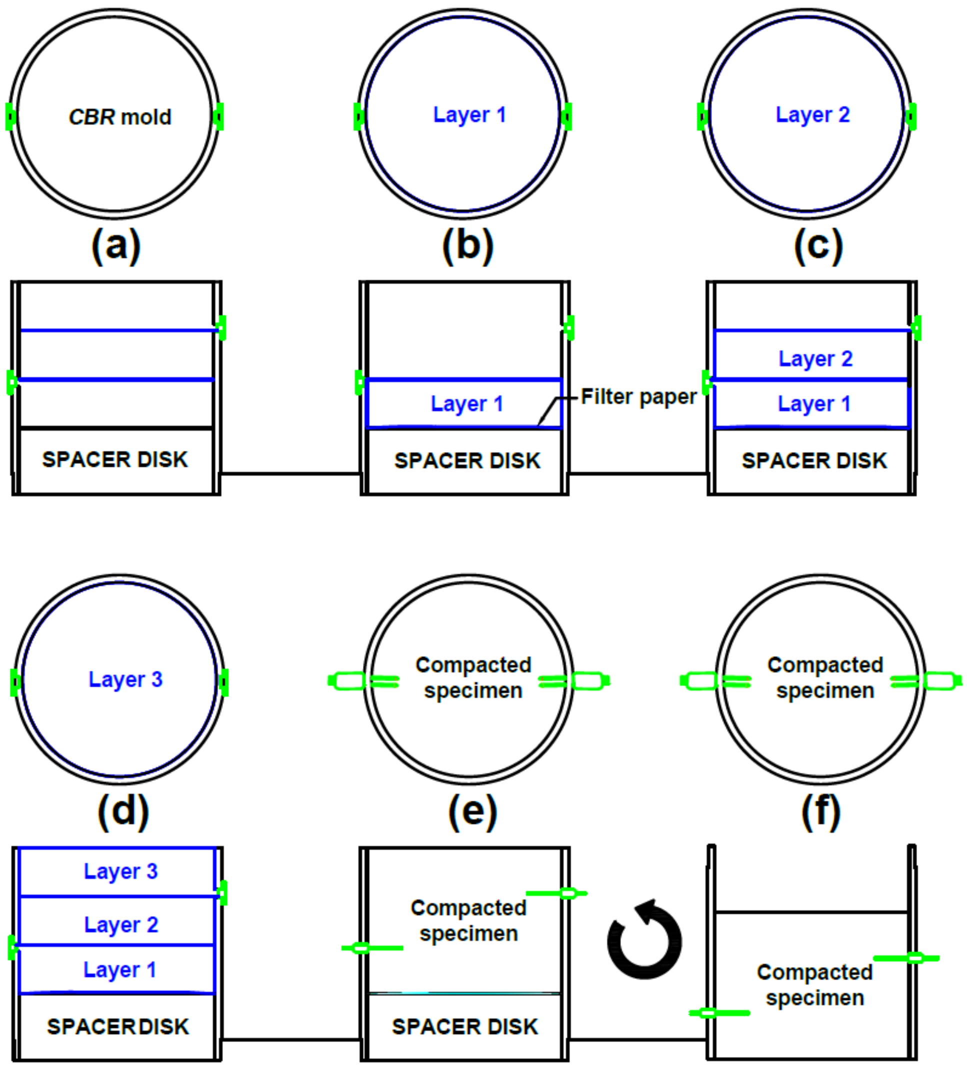

Preliminary Calculation:

Determine the mass of soil required for each layer using equation: $m = \rho_d(1+w_{opt})/3v$.

(a) Divide the height of the *CBR* mold into three equal parts (one for each mass calculated above).

(b) Place filter paper above spacer disk and compact layer 1.

(c) Compact layer 2.

(d) Compact layer 3.

(e) Insert the EC-5 moisture sensors into top and bottom orifices.

(f) Invert the *CBR* mold, remove spacer disk and filter paper.

Figure 4-5 Compaction procedure for preparation of specimens tested under saturated and as-compacted state

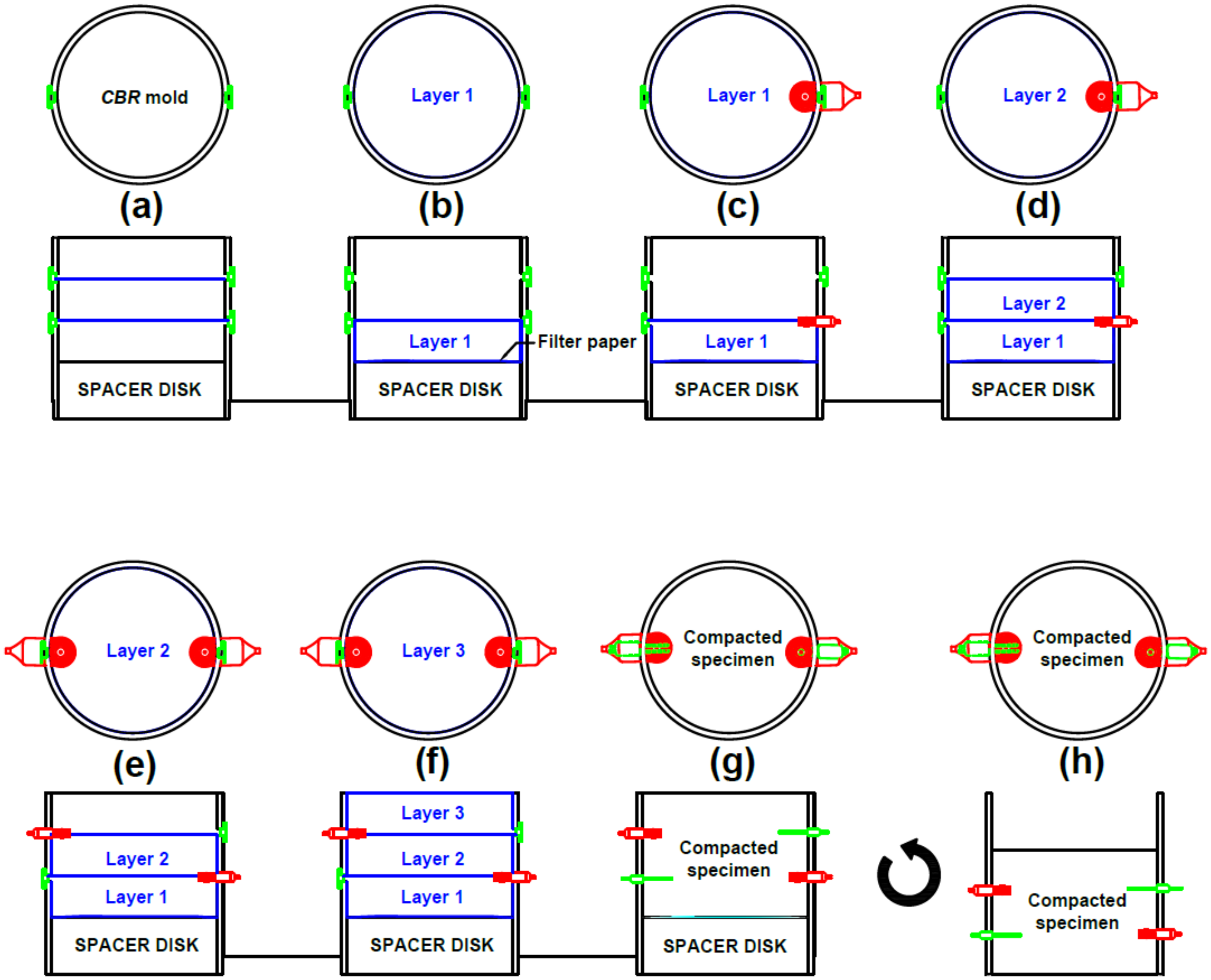

<u>Preliminary calculation</u>:
Determine the mass of soil required for each layer using equation:
$m = \rho_d(1+w_{opt})/3v$.

(a) Divide the height of the *CBR* mold into three equal parts (one for each mass calculated).

(b) Place the filter paper above the spacer disk and compact layer 1.

(c) Insert the MPS-6 water potential sensor into the bottom orifice.

(d) Compact layer 2.

(e) Insert the MPS-6 water potential sensor into the top orifice.

(f) Compact layer 3.

(g) Insert the EC-5 moisture sensors into top and bottom orifices.

(h) Invert the *CBR* mold, remove the spacer disk and filter paper.

Figure 4-6 Compaction procedure for preparation of specimens tested under drying and wetting conditions

4.5 *CBR*-tests

The *CBR* test was performed in accordance with ASTM D1883-16 (ASTM 2016). The main apparatus used in this test were a set of conventional *CBR* devices (compacted mold, a surcharge weight, and loading machine). The *CBR* test was performed by penetrating a 49.6 mm in diameter of piston into the specimen. A loading machine with a penetration rate of 1.27 mm/s was set for a penetration period of 15 minutes. 4.5 kg surcharge weights were used to simulate pavement load. A 50 kN loadcell with an accuracy of 40 N was used as a load indicating mechanism, while a 20 mm LVDT was used to measure the penetration. The data from the load cell and LVDT was collected from using a data acquisition system connected to a computer.

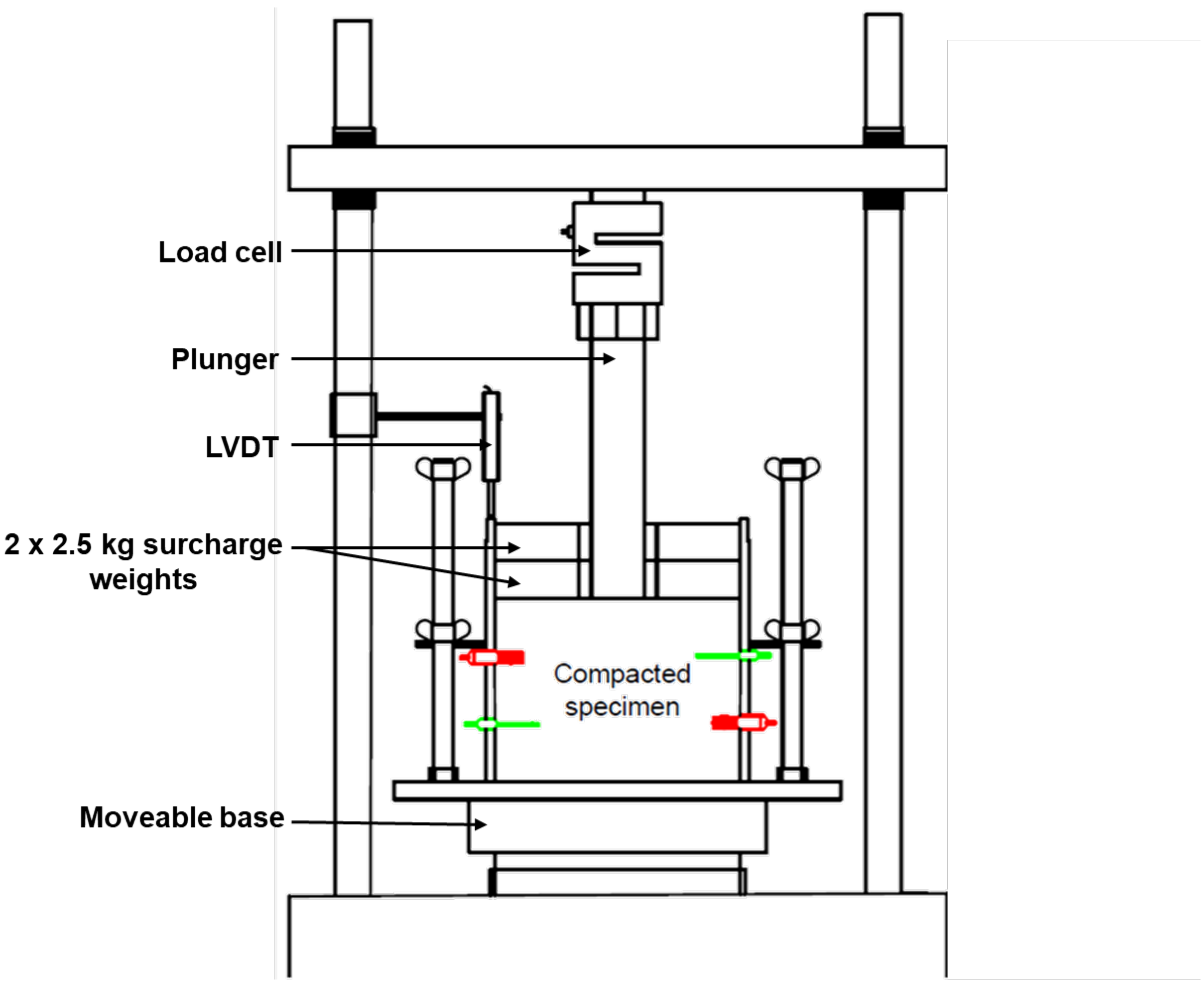

Figure 4-7 *CBR* equipment set-up

A seating load of 44 N is initially applied to the specimen to ensure sufficient contact between the piston surface and soil sample. The *CBR* (stress-penetration) curve was developed using the load corresponding to 0.64 mm, 1.3 mm, 1.9 mm, 2.5 mm, 3.18 mm, 3.8 mm, 4.45 mm, 5.1 mm, 7.6 mm, 10 mm, and 13 mm. The *CBR* value was determined from the stress-penetration curve for 2.54 mm and 5.08 mm penetrations. It was calculated by dividing the stresses corresponding to 2.54 mm and 5.08 mm penetration by standard stresses of 6.9 MPa and 10 MPa respectively. The maximum value was taken as the *CBR*-value. In most cases, the stress ratio at 2.54 mm was higher than that corresponding to 5.08 mm penetration. The *CBR* test was repeated in cases where the stress corresponding to 5.08 mm was the higher value. If the new results were determined to be analogous to the previous, the ratio at 5.08 mm was taken as the *CBR* value. The *CBR* experiment set-up is shown in Figure 4-7. After conducting the *CBR* tests, soil samples from the penetrated surface were collected so that soil moisture content in the vicinity of the failure area could be determined.

4.6 ψ measurement using filter paper technique

The ψ of all specimens tested for *CBR* at water content equal to w_{opt} was determined using the filter paper technique following standard practice ASTM D5298-10 (ASTM 2010). The main apparatus used for the filter paper test include: two digital scales with respective accuracies of 0.01 g and 0.0001 g, rubber gloves, Whatman No. 42 filter paper, two stainless steel containers and tweezers. The first stainless steel container was used to store the samples for the filter paper test during the equilibration period, and the second was used to measure the weight of the filter paper after equilibration. The scale with an accuracy of 0.0001 g was set-up specifically for weighing the filter paper, whilst the other one with an accuracy of 0.01 g, was prepared for weighing the extruded soil specimens. To obtain samples for the filter paper tests, a 63.5 mm diameter sampler similar in shape to a split spoon sampler typically used in geotechnical field investigations was used to extrude samples from the *CBR* mold as illustrated in Figure 4-8. The extruded samples were carefully trimmed to 30 mm height, and further split lengthwise into two equal halves allowing them to closely fit into the containers used for the filter paper test.

During the filter paper test, a filter paper of 60.0 mm diameter was sandwiched between two larger sized filter papers of 63.5 mm diameter and placed in between both halves of the specimen. The purpose of using larger filter papers was to protect the sandwiched paper so that particles from the specimen would not cling to the sandwiched filter paper. Before usage, the filter paper was oven dried at 105 °C for 24 hours and stored in the desiccator to maintain dryness. The filter paper was handled carefully (during storage, placing, and removing) by using rubber gloves and tweezers. As ψ is affected by temperature, and tends to decrease as temperature increases, the test was performed at a constant room temperature of 20 °C.

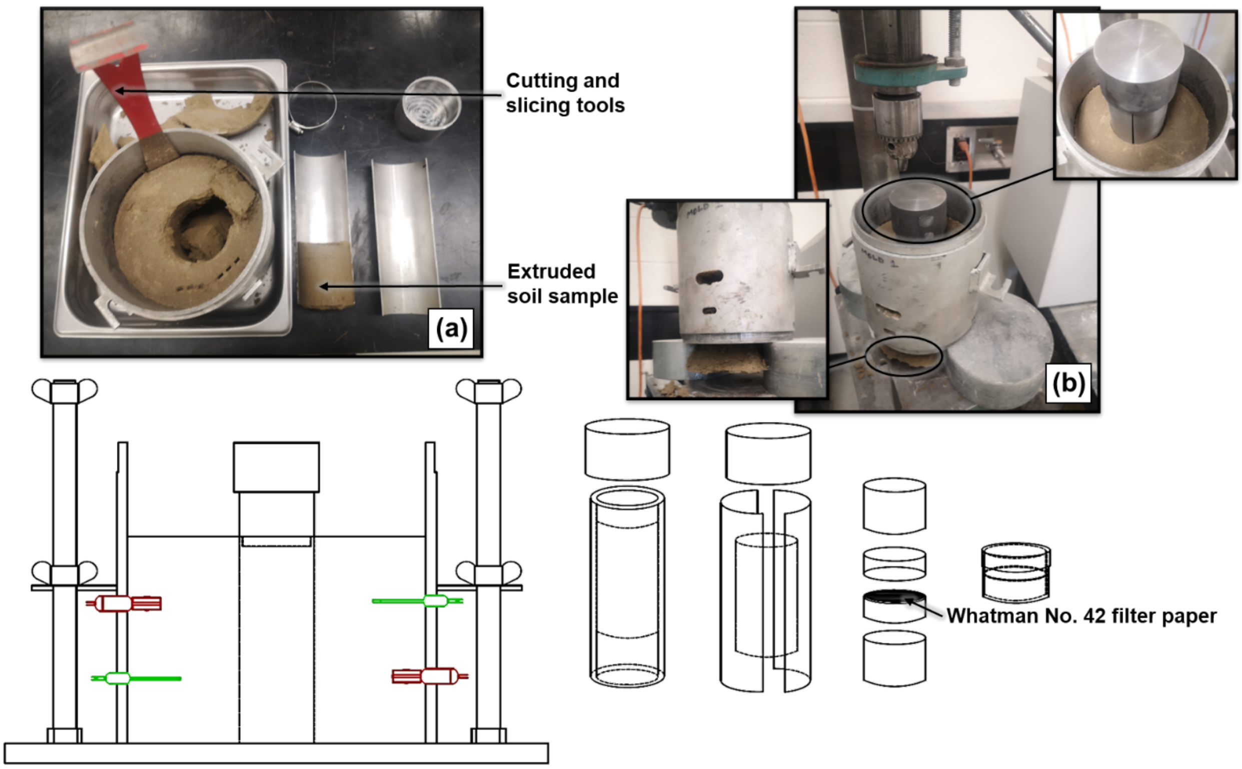

Figure 4-8 Specimen preparation for filter paper tests: (a) Soil extrusion and cutting tools; (b) Load press device

After splitting the specimen lengthwise into equal halves, the stainless steel container was then covered with a lid, sealed with electric tape and placed in a room for at least 7 days at a constant temperature for equilibration as suggested in standard practice method ASTM D5298-10 (ASTM 2010). After equilibration, the sandwiched filter paper was carefully taken out of the specimen and put into the second clean stainless-steel container, which was sealed immediately after placement of the filter paper. The weight of the stainless-steel container and the moist filter paper were then measured using 0.0001 g scale. This procedure was performed in as little time as possible to reduce amount of water that may evaporate, as this may affect the results. After this, the stainless-steel container was placed inside an oven with the lid half open to dry for a minimum of two hours, after which the filter paper was allowed to cool down, and the weight was recorded. It was vital to the filter paper water content calculation that the weight of the empty stainless-steel container before and after oven drying is known precisely. Once the filter paper water content was obtained, the specimen's ψ was then determined by using the calibration curve in accordance with ASTM D5298-10 (ASTM 2010).

4.7 Summary

In summary, the main laboratory work of this study constituted of performing soaked and unsoaked *CBR* tests using a specially designed modified *CBR* apparatus. The objective of this experimental program was to determine *CBR* values of saturated and unsaturated soil specimens using a new technique on several soils typically used as pavement subgrade materials from Ontario. To accomplish this, 5 subgrade soils (one each from Kingston, Kincardine, Ottawa, and two from Toronto) were tested for *CBR* under soaked and unsoaked conditions. The soils from Toronto, TLC and TSC were tested for *CBR* under wetting, drying, saturated and w_{opt} conditions, and the remainder soils (KLC, KSC, and OLC) were tested only under saturated and as-compacted state. Modification to conventional *CBR* apparatus include drilling orifices into the *CBR* mold so that ψ and water content can be measured. ψ measurement was performed either directly using MPS-6 sensors or indirectly using the filter paper method; and the water content measurements were made using EC-5 sensors.

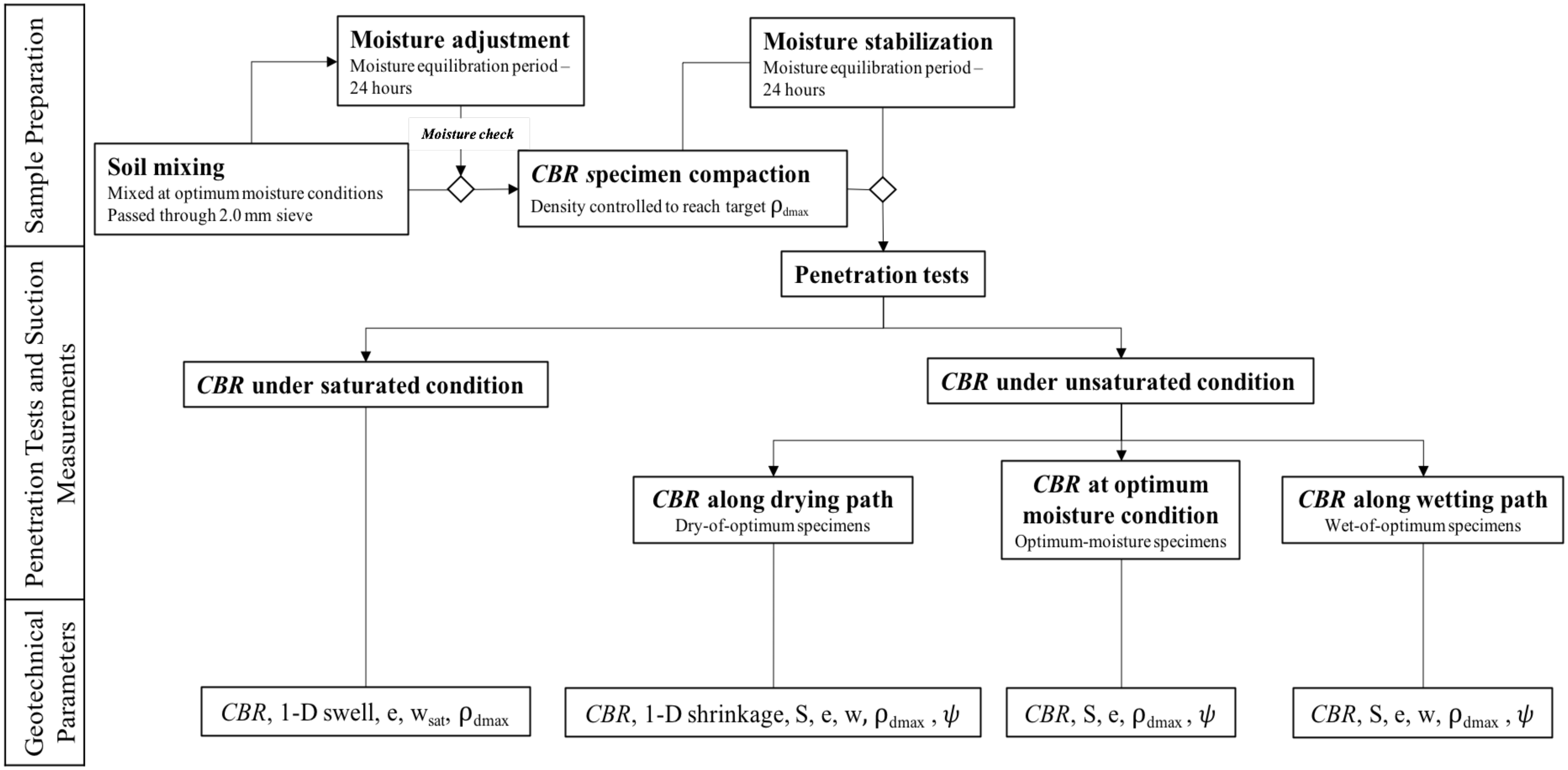

Figure 4-9 Testing program flow-chart summary

CHAPTER 5
RESULTS AND ANALYSES

5.1 Introduction

Three different approaches are used for determination or estimation of the M_R by the MEPDG that are referred as Level 1, Level 2, and Level 3 based on the cost and criticality of pavement transportation projects. 1. Level 1 design requires the direct measurement of M_R, while the Level 2 design requires the use of empirical relationships to estimate the M_R from *CBR* test results. More details of these approaches are summarized in Chapter. Rigorous laboratory tests were previously carried out to measure the M_R of typical Ontario subgrade soils for use in Level 1 design. The experimental findings and results of these investigations are summarized in Vanapalli and Han (2017). The key research objective of the present study is to develop empirical relationships to estimate the M_R from *CBR* test results for use in Level 2 design. For the present study, the *CBR* test is performed on the same soils that were used in the previous investigation carried out to measure the M_R for Level 1 design. Also, the specimens tested for *CBR* are prepared to have the same density and initial water content as that of the samples prepared in the previous study. The *CBR* values measured are compared with the M_R measured for Level 1 design, with aim develop reasonable correlations for predicting the M_R from *CBR*. This chapter includes a summary of the laboratory test results along with their analysis and discussion. The results of the index property tests are discussed first, followed by the *CBR* test results for experiments performed on compacted saturated specimens and other compacted specimens that were prepared at different initial water contents and subjected to gradual wetting and drying from their initial conditions. In addition, a comparison between the matric suction (ψ) values measured from the MPS-6/TEROS-21 sensors and filter paper tests is provided and discussed. Lastly, the relationship between the *CBR* and M_R and their relationships with ψ, volumetric water (θ_w), degree of saturation (S), and water content (w) are presented and discussed.

5.2 Soil index properties

The grainsize distribution and Atterberg limits tests were determined following standard practice methods of ASTM D7928-21 (ASTM 2021) and ASTM D4318-17 (ASTM 2017b), respectively.

For the grain-size distribution, hydrometer analysis was used to determine the percentage of fines (i.e., particles smaller than N$^{o.}$ 200 or 75 μm sieve), whilst the sieve analysis was used to determine the coarse-grained fractions (i.e., particles larger than 75 μm). The results from these experiments are presented in Table 5-1 alongside the data measured from the previous study carried out by Vanapalli and Han (2017). The experimental findings both bear similarities, and as such the soils were deemed verified to be the same as that used for the previous study. The grain-size charts for these soils are shown in Figure 5-1.

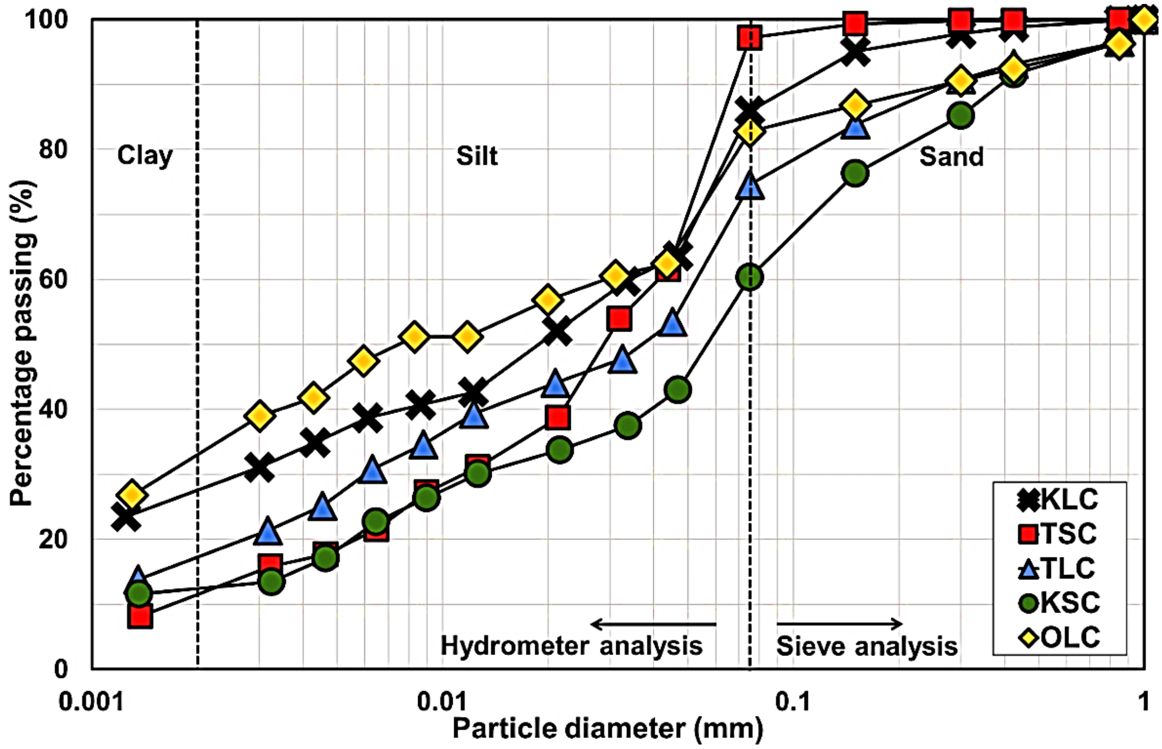

Figure 5-1 Grain-size charts for soils tested

Table 5-1 Soil index properties measured from current study in comparison to measurements from Vanapalli and Han (2017)

Soil	Sand (%)	Silt (%)	Clay (%)	w_L (%)	w_P (%)	I_P (%)
TLC[1]	25.4	58.1	16.5	23	15	9
TLC[2]	31	50	19	25	13	12
TSC[1]	2.8	86.4	10.8	17	13	4
TSC[2]	3	81	16	20	14	6
KLC[1]	14.1	59.5	26.4	34	20	14
KLC[2]	15	60	25	31	21	10
OLC[1]	17.2	51.0	31.8	47	19	28
OLC[2]	20	48	32	48	22	26
KSC[1]	39.7	48.1	12.2	26	16	10
KSC[2]	35	51	14	22	15	7

[1]Present study; [2]Vanapalli and Han (2017); w_L - Liquid limit; w_P - Plastic limit; I_P - Plasticity index.

5.3 Results for specimen wetting, drying, saturation and *CBR* tests

The experimental investigation carried out by Vanapalli and Han (2017) was focused towards determination of the M_R under varying water content conditions. The study involved the wetting, drying or saturation of specimens initially compacted at $\rho_{d,max}$ and corresponding w_{opt} summarized in Table 5-2 prior to performing the M_R tests for Level 1 design.

Table 5-2 Values for $\rho_{d,max}$, w_{opt} and w_{sat} measured from Vanapalli and Han (2017)

Soil	Kincardine Lean Clay (KLC)	Toronto Silty Clay (TSC)	Toronto Lean Clay (TLC)	Kingston Silty Clay (KSC)	Ottawa Leda Clay (OLC)
$\rho_{d,max}$ (kg/m^3)	1631	1915	1962	1935	1616
w_{opt} (%)	20.3	13.5	12.2	12.0	23.0
w_{sat} (%)	24.4	14.9	13.7	-	25.5

Table 5-3 Summary of compaction results and wetting-drying tests

Soil type	w_{target} (%)	$w_{attained}$ (%)	ρ_{target} (kg/m^3)	$\rho_{d,compaction}$ (kg/m^3)
Toronto Lean Clay specimens	-	14.83$^{(1)}$	1962	1954.87
	-	14.21	1962	1974.42
	13.25	13.28	1962	1963.32
	12.89	12.93	1962	1970.72
	12.20	12.22$^{(2)}$	1962	1968.94
	11.80	11.72	1962	1966.92
	-	10.13	1962	1966.32
	-	7.58	1962	1966.32
Toronto Silty Clay specimens	-	15.05$^{(1)}$	1915	1911.64
	14.65	14.68	1915	1939.93
	14.27	14.3	1915	1926.31
	13.48	13.52$^{(2)}$	1915	1917.23
	12.50	12.61	1915	1924.17
	-	11.89	1915	1929.15
	-	9.42	1915	1913.70
Kincardine Lean Clay specimens	-	23.28$^{(1)}$	1631	1644.12
	20.3	20.22$^{(2)}$	1631	1671.77
Kingston Silty Clay specimens	-	16.18$^{(1)}$	1935	1930.04
	12.0	12.19$^{(2)}$	1935	1962.85
Ottawa Leda Clay specimens	-	24.51$^{(1)}$	1616	1638.53
	23.0	23.10$^{(2)}$	1616	1666.04

w_{target} - water content measured by Vanapalli and Han (2017); $w_{attained}$ - water content attained from current study after wetting, drying or saturation tests; ρ_{target} - maximum dry density measured following ASTM D698-12 (ASTM 2012a); $\rho_{d,compaction}$ - dry density attained after compaction of specimens for current study; $^{(1)}$specimens at w_{sat}; $^{(2)}$specimens at w_{opt}.

For the current study, specimens were compacted at the same $\rho_{d,max}$ and w_{opt} state and either wetted, dried or saturated to achieve similar water contents measured by Vanapalli and Han (2017). The *CBR* tests were then performed after the target water content was achieved following the test procedures described in Chapter 4. The $\rho_{d,max}$ of the specimens prepared for the current study along the water content values after wetting, drying or saturation periods are summarized in Table 5-3. During the wetting and drying process, the water content and ψ of the specimens were monitored using EC-5 and MPS-6/ TEROS-21 sensors, respectively. Preliminary test results suggested that the data produced by these sensors were sensitive to temperature fluctuations. Due to this reason, the wetting and drying tests were performed in a room equipped with a thermostat to regulate the ambient temperature at 20 °C.

The primary research objective was to measure the *CBR* of the 5 soils listed in Table 5-2 considering wetting, drying, saturation and as-compacted state (w_{opt} condition). However, it was not possible to perform the complete study on all soils collected due to the restrictions imposed on the research and laboratory facilities as a result of the COVID-19 pandemic. The two soils from Toronto, Toronto lean clay (TLC) and Toronto silty clay (TSC) were both tested extensively (i.e., considering wetting, drying, saturation and w_{opt} condition). While the remainder soils (i.e., Kincardine lean clay (KLC), Ottawa Leda clay (OLC) and Kingston silty clay (KSC)) were tested under saturated and as-compacted state. A summary of the experiments carried out for each soil is shown in Table 5-4.

Table 5-4 Summary of experiments carried out for each soil

Soil	**Wetting and drying**	**Saturation test**	**w_{opt} conditions**
Toronto Lean Clay (TLC)	✓	✓	✓
Toronto Silty Clay (TSC)	✓	✓	✓
Kincardine Lean Clay (KLC)		✓	✓
Ottawa Leda Clay (OLC)		✓	✓
Kingston Silty Clay (KSC)		✓	✓

In total, 21 *CBR* tests were performed for the current study. Seven of these *CBR* tests were performed on TSC specimens (2 wetted, 3 dried, 1 saturated, and 1 as-compacted), and eight of these tests were performed on TLC (3 wetted, 3 dried, 1 saturated, and 1 as-compacted). While 6 *CBR* tests were performed on KLC, KSC and OLC specimens (1-saturated and 1-as compacted state for each).

Figure 5-2 and Figure 5-3 show the *CBR* curves with varying water contents for TLC and TSC soils, respectively. The *CBR* curves for the other soils are presented in the Appendix. The *CBR* as expected decreases with wetting (i.e., increasing water content) and increases drying conditions. It can be observed that for each penetration value, the load required to penetrate the specimen increases as the water content decreases, and vice versa. Also, Figure 5-2 and Figure 5-3 show that the lowest stress-penetration curve corresponds to the data measured for the soaked specimens. The soaked specimens represent the most adverse field condition (i.e., a state where the soil is saturated), while the wetted and dried samples simulate natural field conditions in which the subgrade soil is unsaturated and tend to undergo increase or decrease in water content.

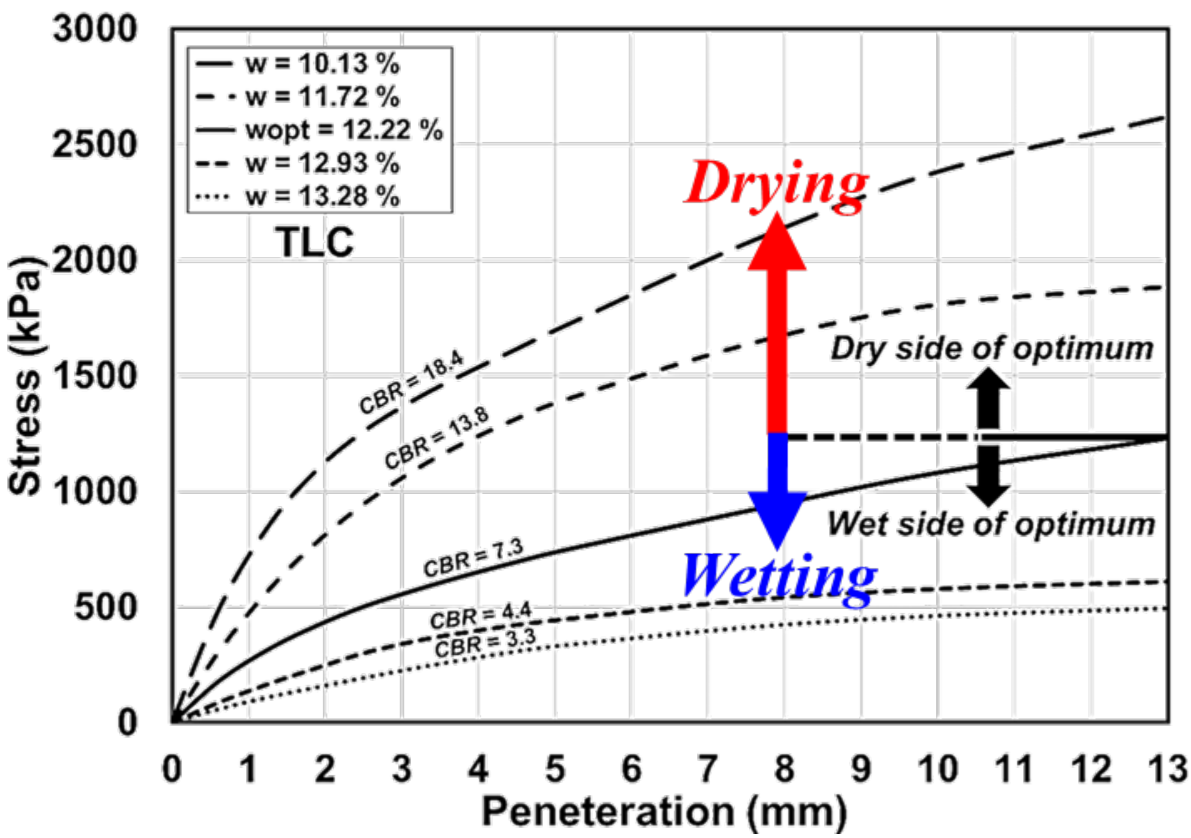

Figure 5-2 *CBR* curves for TLC specimens subjected to wetting and drying

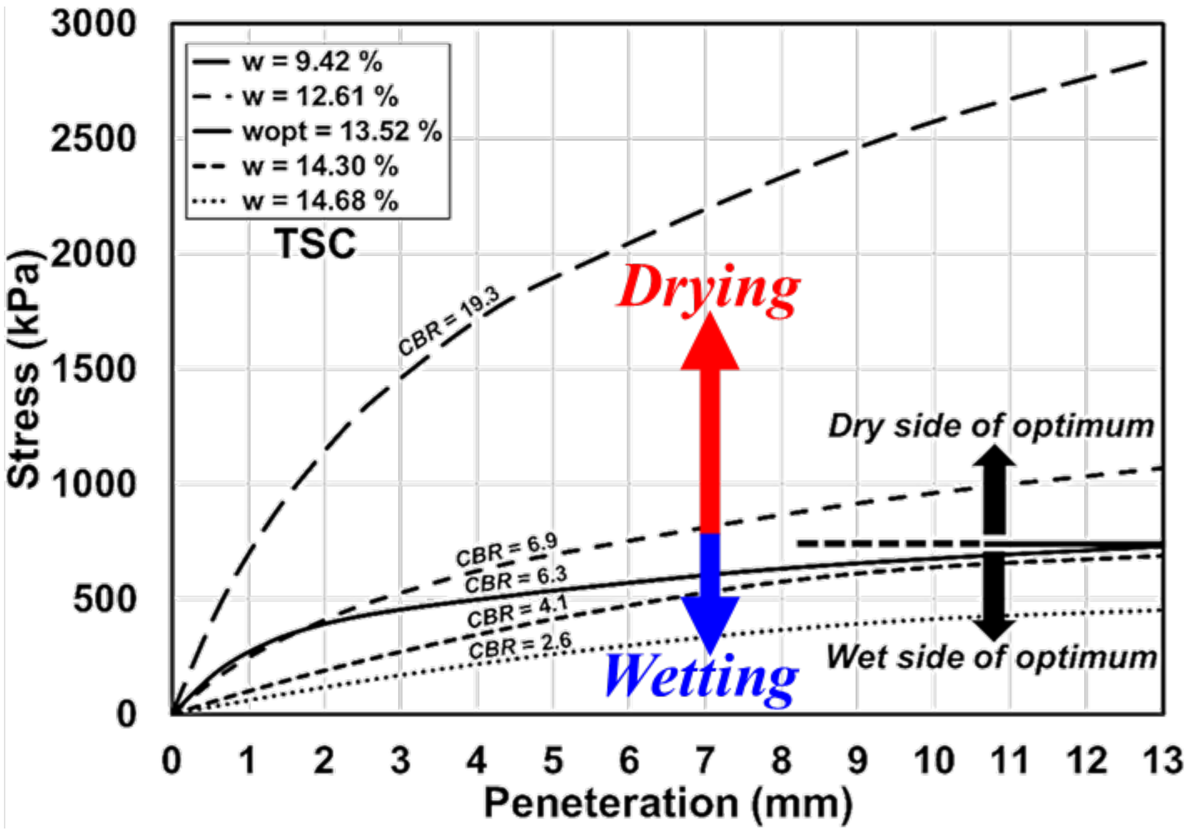

Figure 5-3 *CBR* curves for TSC specimens subjected to wetting and drying

The decrease in water content leads to an increase in the ψ. The degree of saturation in the soil increases with an increase in the water content and unsaturated state reaches a saturated state (S =100 %). For such a scenario, the pore-water pressure approaches the pore-air pressure and the ψ of the soil reaches a value equal zero. On the other hand, when the soil is unsaturated, the effect of ψ on the *CBR* becomes relevant as can be seen in Figure 5-4. This result may be explained as the decrease in water content due to drying causes an increase in the water tension amongst the soil particles causing the increase in ψ, and consequently, the *CBR* increases.

5.4 Relationship between the *CBR* and other properties of unsaturated soils

The variation of the *CBR* with ψ, gravimetric water content (w) and degree of saturation (S) for TLC and TSC are shown in Figure 5-4 to 5-6. The results show an increase in the *CBR* with decreasing water content and increasing ψ. Similar trends of results were reported by other investigators for various other fine-grained soils in the literature.

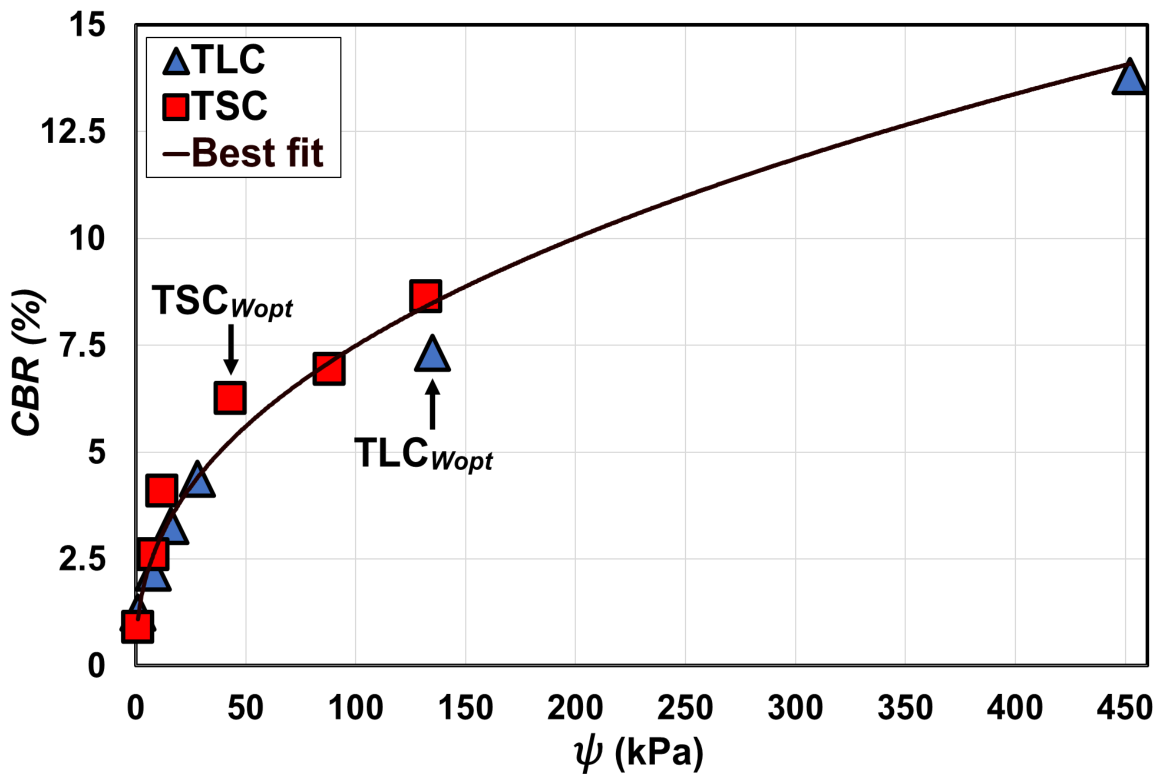

Figure 5-4 Relationship between *CBR* and matric suction for TLC and TSC

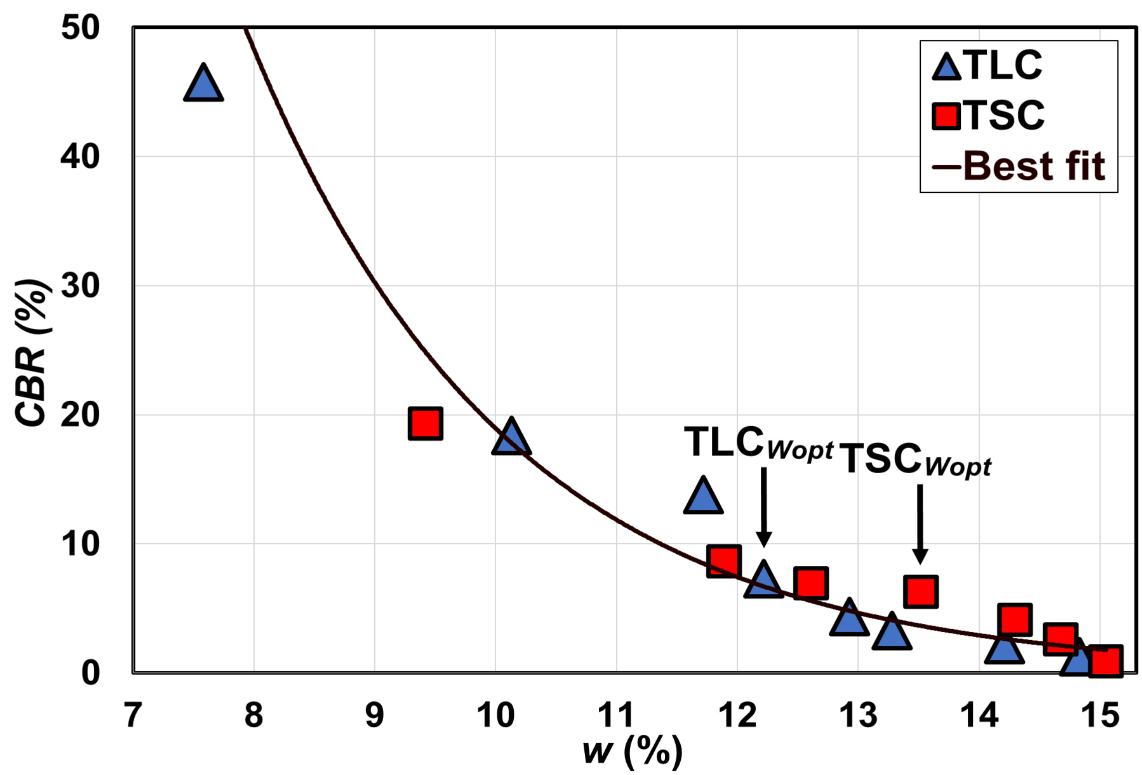

Figure 5-5 Relationship between *CBR* and gravimetric water content for TLC and TSC

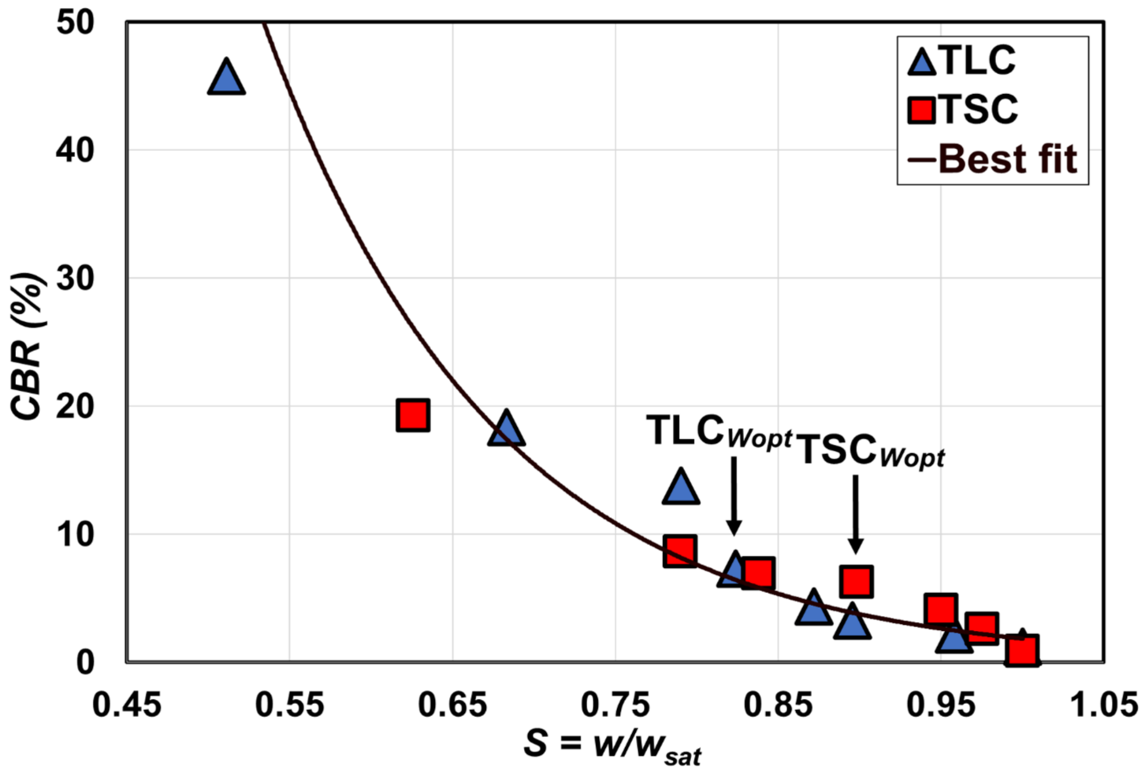

Figure 5-6 Relationship between *CBR* and degree of saturation for TLC and TSC

For example, Toll (2015) performed a series of *CBR* tests on lateritic gravel; the samples were compacted with different mechanical efforts and tested at varying water content. The results showed a reduction of *CBR*-value with increasing water content, as well as a rapid increase for values on the dry side of optimum. Ikechukwu et al. (2018) attributed this abrupt increase in *CBR* values to an increases in ψ that occurs during the drying process. Ampadu (2007) performed *CBR* tests on a subgrade soil compacted at three different densities and wetted or dried to different water contents. The *CBR* variation observed for a percent change in water content on the dry side of optimum was 3 to 7 times greater when compared for the same percent value on the wet of optimum. This similar trend can be observed from Figure 5-5 and 5-6, where the *CBR* is seen to increase slightly for every increment of water content, up to w_{opt}, and a significant increase rate in *CBR* occurs when the water content is less than w_{opt}. These results also shown good agreement with the results from the study by Purwana (2013). The results summarized in Figure 5-4 suggest a nonlinear relationship between *CBR* and ψ. This behavior is similar to experimental trends presented by Lachgueur et al. (2021). The non-linear behaviour can be attributed to the variation of the capillary water and its associated ψ changes which contributes to the changes in the skeleton constitutive stress and, therefore, the *CBR*. At relatively high degree of saturation conditions (i.e., close to saturation) ψ changes fully contributes to the constitutive stress of the soil skeleton, resulting in a significant increase in the *CBR* value. These results are consistent with the shear strength behavior in unsaturated soils in the boundary effect zone (e.g., Vanapalli et al. 1996).

The contribution of ψ reduces with a further ψ increase due to the drainage of capillary water from the soil pores, which results in a less significant increase in the *CBR* value. It should be noted that, apart from the ψ, the physicochemical inter-particle forces such as the Van der Waals and cementation forces also influence the *CBR* value. The physicochemical inter-particle forces are more prevalent in fine-grained soils and become dominant as the influence of ψ decreases with decreasing capillary water. The relationship between water content and ψ can be observed from Figure 5-4 and 5-5. It is evident from comparison of both curves that the ψ tends to decrease as water content increases and vice versa. This shows the unique relation between water content and ψ which is often described using the SWCC.

Some researchers (Purwana 2013; Mirzaii and Negahban 2016; Ikechukwu et al. 2018) suggest a bi-linear relationship between *CBR* and ψ. Purwana (2013) noted that the inflection point of the bi-linear curve occurs at some point between ψ_b and ψ_r. This bi-linear relationship can be observed from independent analysis of the *CBR*-ψ relationship for TLC and TSC, as shown in Figure 5-7 and 5-8, which is similar to the conclusions drawn by Purwana (2013). The ψ_b values were estimated from the SWCC of TLC and TSC summarised in Han and Vanapalli (2016a) and Ren (2020).

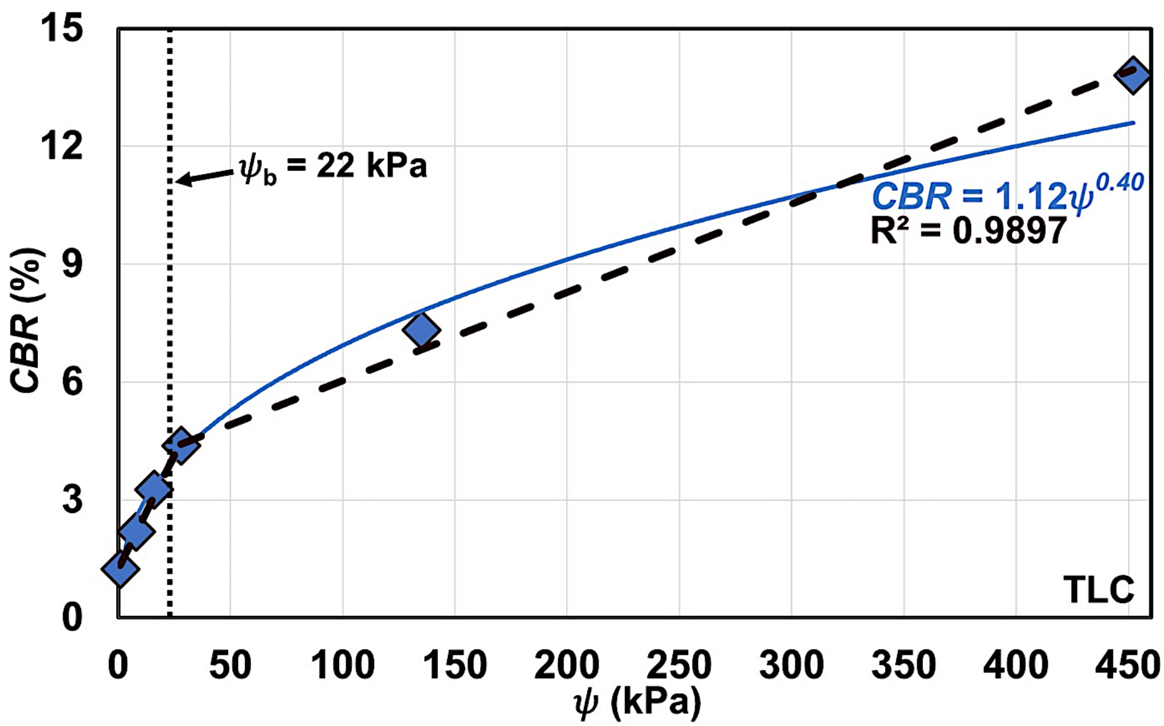

Figure 5-7 Relationship between *CBR* and matric suction for TLC

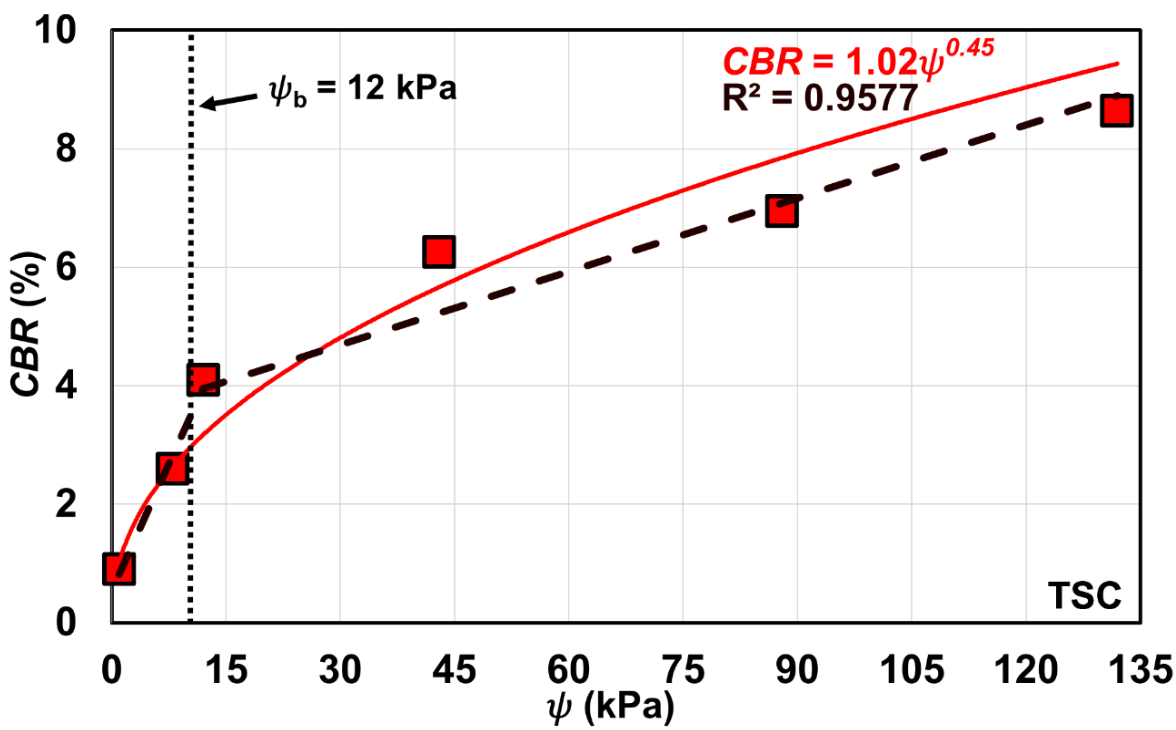

Figure 5-8 Relationship between *CBR* and matric suction for TSC

5.5 Relationship between the *CBR* and M_R

Figure 5-9 summarizes the relationship between *CBR* and M_R for TLC and TSC specimens subjected to wetting and drying. Eqns. [5-1] and [5-2] are proposed to determine M_R from *CBR* for TLC and TSC respectively. While Eqn. [5-3] shows the relationship derived for all soils tested.

$$M_R(MPa) = 18.98(CBR)^{0.68} \quad [5\text{-}1]$$

$$M_R(MPa) = 23.36(CBR)^{0.40} \quad [5\text{-}2]$$

$$M_R(MPa) = 15.03(CBR)^{0.76} \quad [5\text{-}3]$$

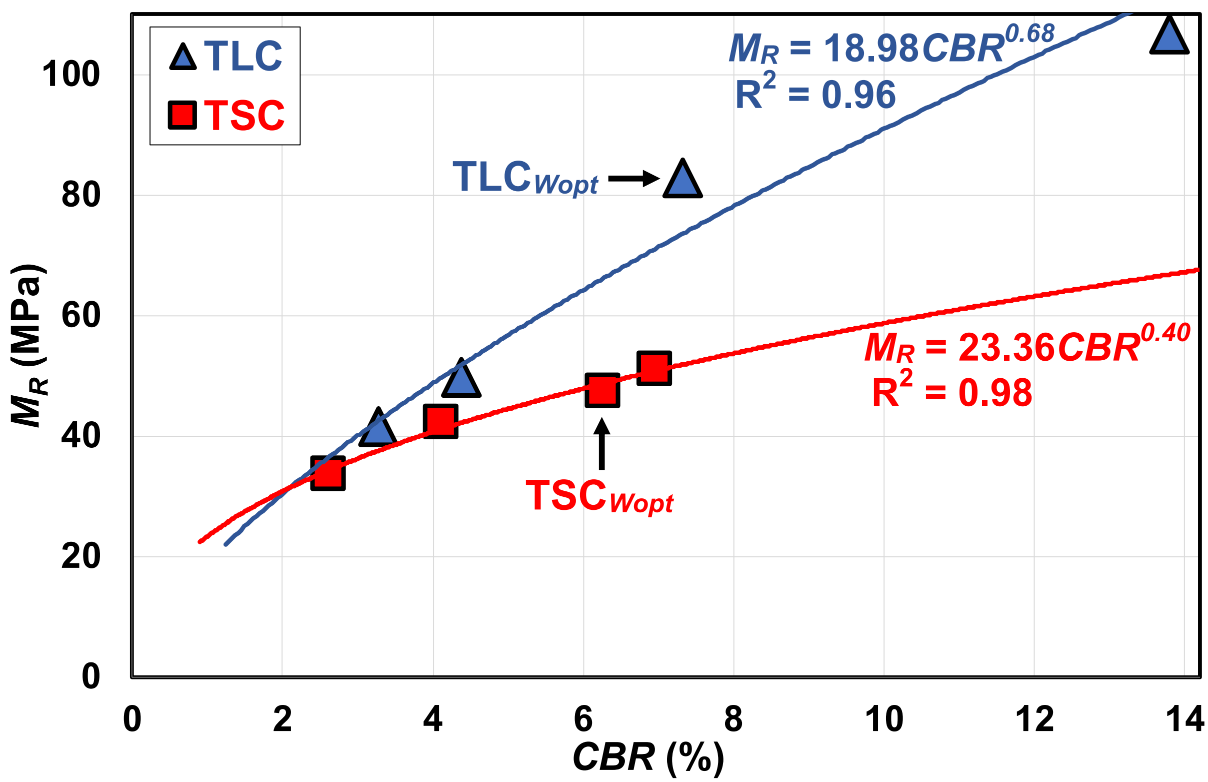

Figure 5-9 Relationship between *CBR* and M_R for TLC and TSC

Figure 5-10 shows a comparison of Eqn. [5-3] to other equations proposed in the literature to determine the M_R from *CBR* test results. The results show similar trends for *CBR* test results reported in the literature. The equation derived from the study conducted by Green and Hall (1975) show considerable deviation from the data presented by others. This may be as a result of the difference is test methods, soil type or regression model used. The M_R values used to develop the correlations in this study was measured using triaxial testing equipment, while Green and Hall

(1975) used the wave propagation method to carry out in situ measurements on pavement base, subbase, and subgrade materials. In addition, other researchers which include Heukelom and Klomp (1962), Lister and Powell (1987) and Vanapalli and Han (2017) carried out the tests on fine-grained soils.

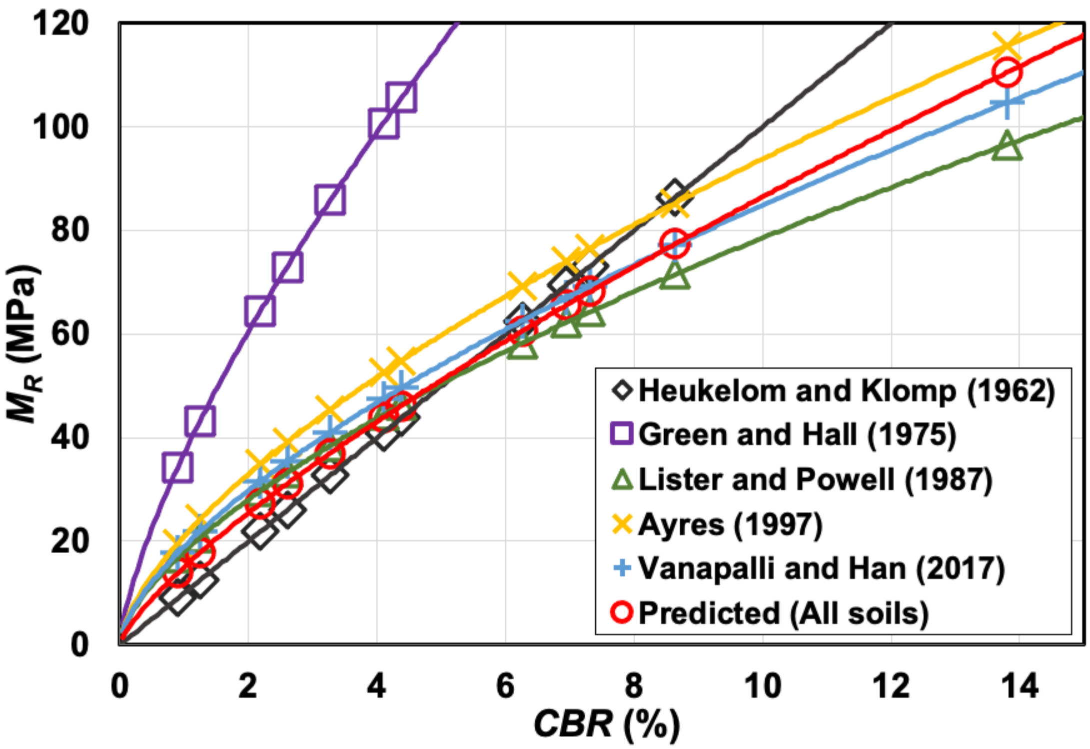

Figure 5-10 *CBR-M_R* relationship developed for all soils in comparison to other studies from the literature

5.6 Comparison between the ψ values measured using MPS-6/TER0S-21 sensors and filter paper tests

The filter paper tests method and MPS-6/TEROS-21 sensors were used to collect ψ measurements for the specimens tested at w_{opt} condition. Only the MPS-6/ TEROS-21 sensors were used to measure the ψ of specimens that were subjected to wetting and drying. Figure 5-11 shows a plot of the ψ values measured using filter paper and that measured from the MPS-6/ TEROS-21 sensors. It can be observed that the sensors provide more accurate readings at low ψ range, and the results show larger variations at high ψ range. This comparison provided a means by which the accuracy of the sensors can be verified.

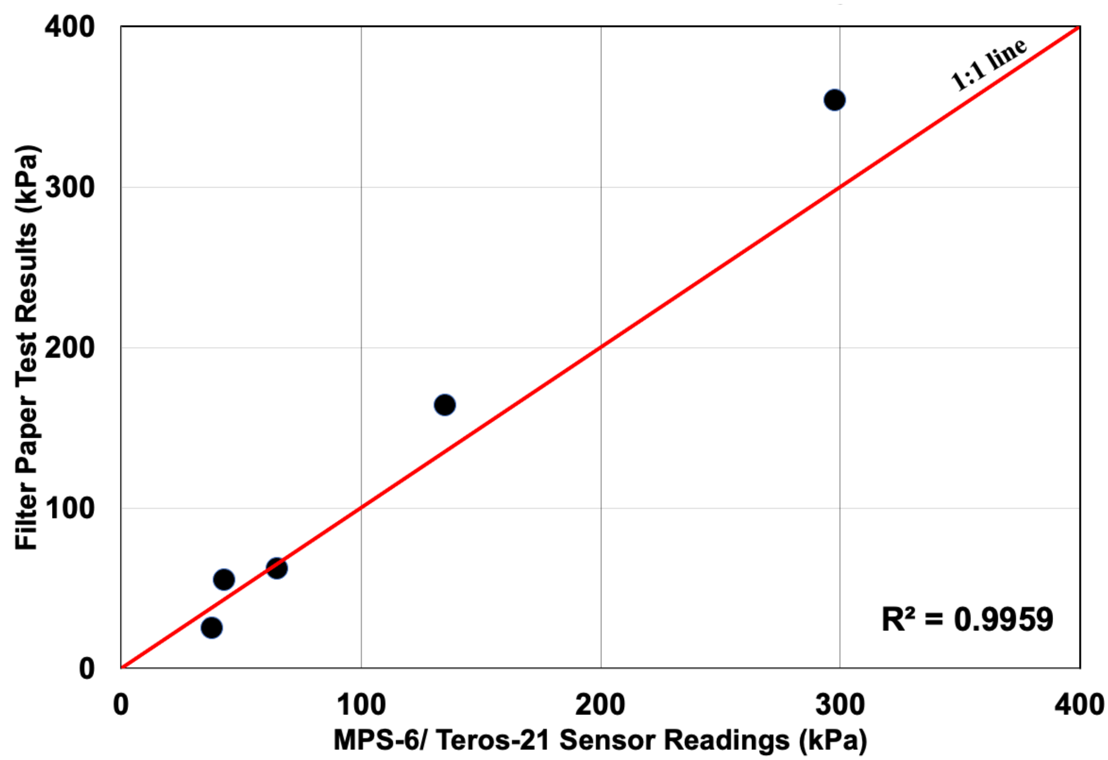

Figure 5-11 Comparison between ψ values measured from MPS-6/TEROS-21 sensors and filter paper tests

5.7 Comparison between measured and predicted M_R

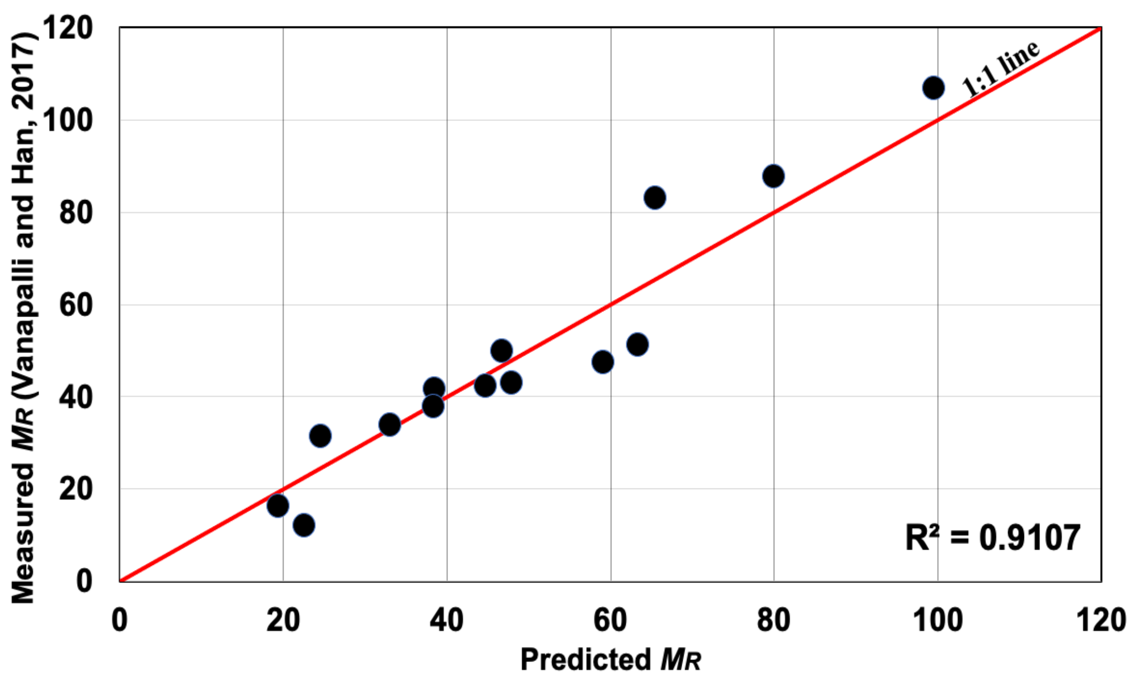

Figure 5-12 Comparison between measured and predicted values of M_R

Figure 5-12 shows a comparison between measured and predicted values of M_R along with the associated R^2 value. The measured values of M_R were obtained from the study completed by Vanapalli and Han (2017), while the predicted values were calculated by substituting the *CBR* measured from this study into Eqn. [5-3]. From Figure 5-12, it can be observed that most of the data points are situated near the unity line, and based on the distribution of the data points, an R^2 value of approximately 91 % was obtained.

5.8 Summary

An experimental program was conducted in the present research program with the objective to develop correlations between the M_R and *CBR* considering the influence of water content and ψ for use in the design of Level 2 pavements following the MEPDG. The experimental program was conducted on several Ontario subgrade soils for the measurement of *CBR* under soaked and unsoaked conditions and to understand the influence of water content and ψ following the wetting and drying paths on two soils: namely, Toronto lean clay (TLC) and Toronto silty clay (TSC). Modifications were introduced into the conventional *CBR* tests through continuous monitoring of water content and ψ using the EC-5 and MPS-6/ TEROS-21 sensors, respectively. In other words, the variation of *CBR* with respect to water content, degree of saturation and ψ were measured. These experimental results were interpreted with the M_R values measured from the previous study conducted by Vanapalli and Han (2017), and correlations were developed to estimate the M_R values from *CBR* tests. In addition to the two soils tested for *CBR* under varying water content conditions, three other soils were tested for *CBR* only at optimum water content and saturated conditions. Future research is proposed to develop valid correlations between *CBR* and M_R for these soils for different water content variations.

The *CBR* values measured from this study along with the M_R and corresponding water content measured from the previous study by Vanapalli and Han (2017) are summarized in Table 5-5. It can be observed that the w_{sat} values measured for both studies are slightly different. This is mainly due to differences in experimental methods and compaction procedures. Also, the specimens with density values slightly greater than the target compaction density yielded lower w_{sat} results and vice versa. This may be attributed to the effect compaction effort on the soil structure. The specimen in a denser state tends to have less voids and as such tends to yield a lower value for w_{sat}. The relationship between *CBR*, water content and ψ is also determined using regression analysis. From the results, it was observed that the *CBR* is strongly moisture dependent property and tends to increase with decrease in water content and vice versa.

The relationship between *CBR* and ψ was observed to be non-linear; however, for simplicity purposes it can also be considered a bi-linear model. The inflection point in this relationship was suggested to occur somewhere in the transition zone, which can be obtained from the information of the soil-water characteristic curve. In the low ψ range, (i.e., in the boundary effect zone where degree of saturation is close to saturation condition), there is a significant increase in the *CBR* is as ψ influence is predominant due to capillary effect. The contribution of ψ becomes less significant in the increase in the *CBR* value in the transition and residual zone due to the drainage of the capillary water from the soil pores. These results summarized in this study are consistent with published research in the literature for the mechanical properties of unsaturated soils (e.g., Vanapalli et al. 1996).

Table 5-5 Summary of experimental results for all soils tested

Soil type	w_{target} (%)	$w_{attained}$ (%)	$\rho_{d,compaction}$ (kg/m³)	*CBR* (%)	M_R (MPa)	*S*	ψ (kPa)
Toronto Lean Clay specimens	-	14.83(1)	1954.87	1.25	-	1.00	-
	-	14.21	1974.42	2.19	-	0.96	8
	13.25	13.28	1963.32	3.27	41.63	0.90	16
	12.89	12.93	1970.72	4.38	49.83	0.87	28
	12.20	12.22(2)	1968.94	7.32	82.93	0.82	135
	11.80	11.72	1966.92	13.80	106.80	0.79	452
	-	10.13	1966.32	18.40	-	0.68	-
	-	7.58	1966.32	45.79	-	0.51	-
Toronto Silty Clay specimens	-	15.05(1)	1911.64	0.90	-	1.00	-
	14.65	14.68	1939.93	2.60	33.76	0.98	8
	14.27	14.3	1926.31	4.10	42.41	0.95	12
	13.48	13.52(2)	1917.23	6.26	47.49	0.90	43
	12.50	12.61	1924.17	6.95	51.16	0.84	88
	-	11.89	1929.15	8.64	-	0.79	132
	-	9.42	1913.70	19.29	-	0.63	183
Kincardine Lean Clay specimens	-	23.28(1)	1644.12	1.45	12.12	1.00	-
	20.3	20.22(2)	1671.77	3.25	37.90	0.89	65
Kingston Silty Clay specimens	-	16.18(1)	1930.04	1.65	31.39	1	-
	12.0	12.19(2)	1962.85	4.55	42.98	0.75	38
Ottawa Leda Clay specimens	-	24.51(1)	1638.53	1.15	16.25	1	-
	23.0	23.01(2)	1666.04	9.91	87.73	0.94	298

(1) specimens tested at w_{sat}; **(2)** specimens tested at w_{opt}; M_R - resilient modulus measured by Vanapalli and Han (2017).

CHAPTER 6

CONCLUSIONS AND RECOMMENDATIONS

Pavements are usually situated at depths well above the ground water table where the soil is typically in an unsaturated state. Consequently, the effect of ψ, which is a key stress state variable that influences unsaturated soil behavior should be incorporated in the rational design and analyses of pavements. The *CBR* and M_R are the most common tests used in practice for estimation of subgrade strength. The *CBR* is relatively inexpensive in comparison to the M_R. Due to this reason, it is usually used to estimate M_R in practice. The primary objective of this thesis was to develop correlations between *CBR* and M_R that takes into account the influence of water content and ψ. The experimental procedure primarily involved performing *CBR* tests on compacted specimens that have been subjected to wetting and drying. A modified *CBR* apparatus was used to measure the water content and ψ of the specimens during the wetting and drying process. ψ measurement was obtained using MPS-6 sensors, while the water content was measured using EC-5 sensors. This chapter provides a summary of the key findings from this study along with some recommendations for future research.

6.1 Key findings

The data measured from this study was used to develop relationships between the *CBR* and ψ for two subgrade soils from Toronto: namely, Toronto lean clay (TLC) and Toronto silty clay (TSC). The relationship between *CBR* and M_R for the same soils were also determined. The *CBR*-M_R correlations developed are summarized in Chapter 5. The key findings from the study are summarized as follows:

1. The variation of *CBR* with water content was analyzed and it was observed that there is an inverse relationship between *CBR* and water content. The results discussed in Chapter 5 show that as the water content increases, the *CBR* tends to decrease and vice versa.
2. A nonlinear relationship between *CBR* and ψ was observed from the results of the wetting-drying tests. An increase in ψ (i.e., decrease in water content) was seen to cause in an increase in *CBR*.

3. Further analysis of the results from the wetting-drying tests shows a bi-linear relationship between *CBR* and ψ. The inflection point on the bi-linear curve was noted to occur when the soil dries past the ψ_b point.
4. Eqn. [6-1] and Eqn. [6-2] was developed from the two Toronto soils tested extensively for this study. Eqn. [6-1] was developed based on the *CBR* values measured for TLC soil, while Eqn. [6-2] was developed for TSC soil. These equations can prove useful for estimating the M_R from *CBR* for design of pavements in Ontario.

$$M_R(MPa) = 18.98(CBR)^{0.68} \quad \textbf{[6-1]}$$

$$M_R(MPa) = 23.36(CBR)^{0.40} \quad \textbf{[6-2]}$$

6.2 Application in practice

The MEPDG is being implemented gradually in Canada, with Ontario being one of the first provinces to work in this direction by gathering the necessary information required to develop guidelines for its region. Soon, other Canadian provinces will make attempts to implement the guide for the design of pavements. Some of these provinces may also undertake studies, such as the one described in this thesis. For such scenarios, the procedures used in this study may be extended for use. For instance, the Modified *CBR* equipment fabricated for this study, under careful supervision can be fabricated for other studies that require measurement of *CBR* and unsaturated soil properties. Detailed description of the modified *CBR* apparatus and sensors used are summarized in Chapters 3 and 4 of this thesis document. Also, the data measured may prove advantageous for estimating the *CBR* or M_R of Ontario subgrade soils or other subgrade soils with similar soil properties.

6.3 Future research and experimental studies

One of the key purposes of developing a method such as MEPDG is to incorporate the effect of environmental factors (i.e., wetting-drying and freezing-thawing) for pavement design and analysis. For this reason, the approach used for the estimation of M_R should take into consideration the wetting-drying and freezing-thawing behavior of pavement materials. The hierarchical scheme proposed in the MEPDG classifies the approach used for determination of the M_R for pavement materials into three levels (Level 1, Level 2, and Level 3). Level 1 requires direct measurement of

M_R from elaborate testing equipment, Level 2 requires the estimation of M_R from other material properties such as *CBR*, and Level 3 requires the approximation of M_R from material classification and index properties. The overall goal for Level 1 was accomplished in the study carried out by Vanapalli and Han (2017) and Ren (2020) in which all six subgrade soils collected (i.e., TLC, TSC, KLC, KSC, SLC and OLC) were measured under wetting-drying and freezing-thawing conditions. To accomplish the overall goal for Level 2, experimentation needs to be carried out to measure the *CBR* under wetting-drying and freezing-thawing conditions. The *CBR* results from this study are useful for the determination of M_R for Level 2 for the two soils from Toronto under wetting-drying conditions.

The primary focus of the present study was to measure the CBR under wetting, drying, saturation and w_{opt} conditions for the six soils collected for this study. However, due to the nationwide lockdown and restrictions imposed because of the COVID-19 pandemic, the experiments completed for this study was to some extent limited. Due to this reason, only the 2 soils from Toronto, TLC and TSC were extensively tested (i.e., considering wetting, drying, saturation and w_{opt} conditions). The remainder soils (KLC, KSC and OLC) were only tested for *CBR* under saturated and w_{opt} conditions. The soil from Sudbury, Sudbury lean clay (SLC) was not used as there was insufficient quantity available for testing. Future research is proposed to develop valid correlations between *CBR* and M_R for the soils that were not tested under wetting and drying conditions. To meet the overall goal for Level 2, the following criteria still needs to be met:

1. Further research and laboratory studies to measure the *CBR*, water content and ψ of KLC, KSC, and OLC under wetting-drying conditions.
2. Experimentation to measure the *CBR* of all soils (i.e., TLC, TSC, KLC, KSC, SLC and OLC) under freezing-thawing conditions.

To accomplish the overall goal for characterizing the subgrade strength for the Level 3 design, further experiments need to be carried out to determine the relationship between M_R and soil index properties for the soils collected.

REFERENCES

Al-Hashemi, H.M.B. 2018. Estimation of SWCC for unsaturated soils and its application to design of shallow foundations. *In* World Congress on Civil, Structural, and Environmental Engineering.

Alao, O.O. 2014. Current trends in design and construction of concrete roads. *In* Structural Concrete Properties and Practice. Capetown, South Africa. p. 6.

American Association of State Highway and Transportation Officials (AASHTO). 1961. AASHO interim guide for the design of flexible pavement structures. American Association of State Highway Officials, Washington.

American Association of State Highway and Transportation Officials (AASHTO). 1993. AASHTO® guide for design of pavement structures. American Association of State Highway and Transportation Officials, Washington D.C., USA.

American Association of State Highway and Transportation Officials (AASHTO). 2008a. Mechanistic-Empirical pavement design guide: a manual of practice. *In* July 2008. American Association of State Highway and Transportation Officials.

American Association of State Highway and Transportation Officials (AASHTO). 2008b. AASHTO M145-91 Classification of soils and soil-aggregrate mixtures for highway construction purposes.

American Association of State Highway and Transportation Officials (AASHTO). 2010. Guide for the Local Calibration of the Mechanistic-Empirical Pavement Design Guide.

American Society for Testing and Materials (ASTM). 2010. ASTM D5298-10 Standard test method for measurement of soil potential (suction) using filter paper. ASTM International, West Conshohocken, USA.

American Society for Testing and Materials (ASTM). 2012a. ASTM D698-12 Standard test methods for laboratory compaction characteristics of soil using standard effort (12,400 ft-lbf/ft3 (600 kN-m/m3)). ASTM International, West Conshohocken, USA.

American Society for Testing and Materials (ASTM). 2012b. ASTM D1557-12 Standard test methods for laboratory compaction characteristics of soil using modified effort (56,000 ft-lbf/ft3 (2,700 kN-m/m3)). ASTM International, West Conshohocken, USA.

American Society for Testing and Materials (ASTM). 2016. ASTM D1883-16 Standard test method for California Bearing Ratio (CBR) of laboratory-compacted soils. West Conshohocken, USA.

American Society for Testing and Materials (ASTM). 2017a. ASTM D2487 Standard practice for classification of soils for engineering purposes (Unified Soil Classification System). American Society for Testing and Materials (ASTM), West Conshohocken, USA.

American Society for Testing and Materials (ASTM). 2017b. ASTM D4318-17 Standard test methods for liquid limit, plastic limit, and plasticity index of soils. ASTM International, West Conshohocken, USA.

American Society for Testing and Materials (ASTM). 2019. ASTM D2216-19 Standard test method for laboratory determination of water (moisture) content of soil and rock by mass. ASTM International, West Conshohocken, USA.

American Society for Testing and Materials (ASTM). 2021. ASTM D7928-21 Standard test method for particle-size distribution (gradation) of fine-grained soils using the sedimentation (hydrometer) analysis. ASTM International, West Conshohocken, USA.

Ampadu, S.I.K. 2007. A laboratory investigation into the effect of water content on the CBR of a subgrade soil. *In* Experimental Unsaturated Soil Mechanics. *Edited by* T. Sanchz. Springer Berlin Heidelberg, Berlin, Heidelberg. pp. 137–144.

Andrianatrehina, S.R., Taibi, S., and Boutonnier, L. 2018. Bearing capacity, small-strain stiffness and air permeability of non-standard compacted soils related to suction. European Journal of Environmental and Civil Engineering, **22**(11): 1399–1415. Taylor & Francis. doi:10.1080/19648189.2016.1262287.

ARA Inc. ERES Division. 2004. Guide for Mechanistic - Empirical design of new and rehabilitated pavement structures. *In* Transportation Research Board. Washington, D. C.

Asphalt Institute. 1991. Thickness design - asphalt pavements for highways and streets (manual series no. 1). *In* Ninth. p. 98.

Ayres, M. 1997. Development of a rational probabilistic approach for flexible pavement analysis.

University of Maryland.

Ba, M., Nokkaew, K., Fall, M., and Tinjum, J.M. 2013. Effect of matric suction on Resilient Modulus of compacted aggregate base courses. Geotechnical and Geological Engineering, **31**(5): 1497–1510. doi:10.1007/s10706-013-9674-y.

Brooks, R.H., and Corey, A.T. 1964. Hydraulic properties of porous media and their relation to drainage design. Transactions ofthe ASAE, **7**(1): 26–28.

Brown, S.F., and Selig, E.T. 1991. The design of pavement and rail track foundations. *In* Cyclic loading of soils: from theory to design. *Edited by* M.P. O'Reilly and S.F. Brown. New York.

Brutsaert, W. 1967. Some methods of calculating unsaturated permeability. Transactions of the ASAE, **10**(3): 400–404.

Caicedo, B. 2019. Geotechnics of roads. *In* 1st edition. Taylor & Francis Group, Leiden, Netherlands.

Canadian Strategic Highway Research Program (C-SHRP). 2002. Pavement structural design practices across Canada. Canadian Strategic Highway Research Program (C-SHRP), Ottawa, Canada.

Cekerevac, C., Baltzer, S., Charlier, R., Chazallon, C., Erlingsson, S., Gajewska, B., Hornych, P., Kraszewski, C., and Pavsic, P. 2009. Water influence on mechanical behaviour of pavements: experimental investigation. *In* Water in Road Structures. *Edited by* A. Dawson. Springer Netherlands, Dordrecht. pp. 217–242.

Christopher, B.R., Schwartz, C.W., and Boudreau, R. 2006. Geotechnical aspects of pavements. Woodbury, MN.

Coelho, N.F.C. 2016. Calibration of MEPDG performance models for flexible pavement distresses to local conditions of Ontario. University of Texas Arlington, USA.

Dione, A., Fall, M., Berthaud, Y., Benboudjema, F., and Michou, A. 2014. Implementation of Resilient Modulus - CBR relationship in Mechanistic-Empirical (M-E) Pavement Design. Revue du CAMES, **1**(January): 65–71.

Drumm, E.C., Boateng-Poku, Y., and Johnson Pierce, T. 1990. Estimation of subgrade Resilient Modulus from standard tests. Journal of Geotechnical Engineering, **116**(5): 354–354.

doi:10.1061/(ASCE)0733-9410(1992)118:2(354.2).

Erlingsson, S. 2007. On forecasting the Resilient Modulus from the CBR value of granular bases. Road Materials and Pavement Design, **8**(4): 783–797. doi:10.1080/14680629.2007.9690099.

Flintsch, G.W., Diefenderfer, B.K., and Nunez, O. 2013. Composite pavement systems: synthesis of design and construction practices. Virginia, USA.

Franco, C.A., and Lee, W.K. 1987. Improved California Bearing Ratio test procedure. Transportation Research Record, (1119): 91–97.

Fredlund, D.G. 2006. Unsaturated soil mechanics in engineering practice. Journal of Geotechnical and Geoenvironmental Engineering, **132**(3): 286–321. John Wiley & Sons, Inc., Hoboken, NJ, USA. doi:10.1061/(ASCE)1090-0241(2006)132:3(286).

Fredlund, D.G. 2021. Myths and misconceptions related to unsaturated soil mechanics. Soils and Rocks: An International Journal of Geotechnical and Geoenvironmental Engineering, **44**(3): 1–21.

Fredlund, D.G., and Rahardjo, H. 1993. Soil mechanics for unsaturated soils. John Wiley & Sons, Inc.

Fredlund, D.G., and Xing, A. 1994. Equations for the soil-water characteristic curve. Canadian Geotechnical Journal, **31**(4): 521–532. doi:10.1139/t94-061.

Fredlund, D.G., Xing, A., Fredlund, M.D., and Barbour, S.L. 1995. The relationship of the unsaturated soil shear strength to the soil-water characteristic curve. Canadian Geotechnical Journal, **33**(3): 440–448. doi:10.1139/t96-065.

Gansonré, Y., Breul, P., Bacconnet, C., Benz, M., and Gourvès, R. 2021. Estimation of lateritic soils elastic modulus from CBR index for pavement engineering in Burkina Faso. International Journal of Pavement Research and Technology, **14**(3): 348–356. doi:10.1007/s42947-020-0118-9.

Gardner, W.R. 1956. Calculation of capillary conductivity from pressure plate outflow data. Soil Science Society ofAmerica Journal, **20**(3): 317–320.

Garilli, E., Autelitano, F., and Giuliani, F. 2017. A study for the understanding of the Roman pavement design criteria. Journal of Cultural Heritage, **25**: 87–93. Elsevier Masson SAS.

doi:10.1016/j.culher.2017.01.002.

Van Genuchten, M.T. 1980. A closed-form equation for predicting the hydraulic conductivity of unsaturated soils. Soil science society of America journal, **44**(5): 892–898.

Ghayoomi, M., Dave, E., and Mousavi, S. 2020. Mechanistic load restriction decision platform for pavement systems prone to moisture variations. Minnesota, USA.

Green, J.L., and Hall, J.W. 1975. Nondestructive vibratory testing of airport pavements. Washington, DC.

Gupta, S., Ranaivoson, A., Edil, T.B., Benson, C.H., and Sawangsuriya, A. 2007. Pavement design using unsaturated soil technology. *In* Minnesota Department of Transportation, Research Services Section. Minnesota, USA.

Hall, K.T. 2000. State of the Art and Practice in Rigid Pavement Design. Transportation in the New Millennium,: 7.

Han, Z. 2016. Modelling stiffness and shear strength of compacted subgrade soils. University of Ottawa, Canada.

Han, Z., and Vanapalli, S.K. 2014. Prediction of the variation of the Resilient Modulus with respect to the soil suction for three granular materials using three methods. *In* Pavement Materials, Structures, and Performance. American Society of Civil Engineers, Reston, VA. pp. 414–423.

Han, Z., and Vanapalli, S.K. 2015. Model for predicting Resilient Modulus of unsaturated subgrade soil using Soil-Water Characteristic Curve. Canadian Geotechnical Journal, **52**(10): 1605–1619. doi:10.1139/cgj-2014-0339.

Han, Z., and Vanapalli, S.K. 2016a. Relationship between Resilient Modulus and suction for compacted subgrade soils. Engineering Geology, **211**: 85–97. Elsevier B.V. doi:10.1016/j.enggeo.2016.06.020.

Han, Z., and Vanapalli, S.K. 2016b. State-of-the-art: prediction of Resilient Modulus of unsaturated subgrade soils. International Journal of Geomechanics, **16**(4): 04015104. doi:10.1061/(ASCE)GM.1943-5622.0000631.

Heukelom, W., and Klomp, A.J.G. 1962. Dynamic testing as a means of controlling pavements during and after construction. International Conference on the Structural Design of Asphalt Pavements,: 495–510. Michigan, Ann Arbor.

Holt, A., Sullivan, S., and Hein, D.K. 2011. Life cycle cost analysis of municipal pavements in Southern and eastern Ontario. *In* 2011 Conference and Exhibition of the Transportation Association of Canada - Transportation Successes: Let's Build on Them, TAC/ATC 2011. Transportation Association of Canada, Alberta, Canada. p. 22.

Huang, Y. 2004. Pavement analysis and design. *In* Second. Pearson Education, New Jersey, USA.

Ikechukwu, A.F., Hassan, M.M., and Moubarak, A. 2018a. Evaluation of subgrade Resilient Modulus from unsaturated CBR test. *In* Novel Issues on Unsaturated Soil Mechanics and Rock Engineering Proceedings of the 2nd GeoMEast International Congress and Exhibition on Sustainable Civil Infrastructures, Egypt 2018. *Edited by* L.R. Hoyos and J.S. McCartney. Springer Nature Switzerland, Cham, Switzerland. pp. 61–81.

Ikechukwu, A.F., Hassan, M.M., and Moubarak, A. 2018b. Characterization of hydro-mechanical effects of suction and clay minerals on Resilient Modulus, Mr. *In* Novel Issues on Unsaturated Soil Mechanics and Rock Engineering Proceedings of the 2nd GeoMEast International Congress and Exhibition on Sustainable Civil Infrastructures, Egypt 2018. *Edited by* L.R. Hoyos and J.S. McCartney. Springer Nature Switzerland, Cham, Switzerland. pp. 37–59.

Keaton, J.R. 2018. California Bearing Ratio. *In* Encyclopedia of Engineering Geology. *Edited by* P.T. Bobrowsky and M. Brian. Springer International. pp. 97–98.

Khalili, N., and Khabbaz, M.H. 1998. A unique relationship for χ for the determination of the shear strength of unsaturated soils. Géotechnique, **48**(5): 681–687. doi:10.1680/geot.1998.48.5.681.

Kim, Y.R., Jadoun, F.M., Hou, T., and Naresh, M. 2011. Local calibration of the MEPDG for flexible pavement design. North Carolina, USA.

Kodikara, J., Islam, T., and Sountharajah, A. 2018. Review of soil compaction: History and recent developments. Transportation Geotechnics, **17**(September): 24–34. Elsevier. doi:10.1016/j.trgeo.2018.09.006.

Lachgueur, K., Abou-Bekr, N., Taibi, S., and Fleureau, J.-M. 2021. Effects of compaction and suction on the hydromechanical properties of a dam core clay. Transportation Geotechnics, **27**(November 2020): 100498. Elsevier Ltd. doi:10.1016/j.trgeo.2020.100498.

Li, Q., Xiao, D.X., Wang, K.C.P., Hall, K.D., and Qiu, Y. 2011. Mechanistic-Empirical Pavement Design Guide (MEPDG): a bird's-eye view. Journal of Modern Transportation, **19**(2): 114–133. doi:10.1007/BF03325749.

Liang, R.Y., Rabab'ah, S., and Khasawneh, M.A. 2008. Predicting moisture-dependent Resilient Modulus of cohesive soils using soil suction concept. Journal of Transportation Engineering, **134**(1): 34–40. doi:10.1061/(ASCE)0733-947X(2008)134:1(34).

Lister, N.W., and Powell, W.D. 1987. Design practice for bituminous pavements in the United Kingdom. *In* Proceeding of 6th International Conference of Structural Design of Asphalt Pavement. Ann Arbor, MI. pp. 220–231.

Loach, S.C. 1987. Repeated loading of fine grained soils for pavement design. University of Nottingham.

Lotfi, H.A., Schwartz, C.W., and Witczak, M.W. 1988. Compaction specification for the control of pavement subgrade rutting. Transportation Research Record, (1196): 108–115.

Lusher, S.M. 2004. Prediction of the Resilient Modulus of unbound granular base and subbase materials based on the California Bearing Ratio and other test data. University of Missouri-Rolla, USA.

Mallick, R.B., and El-Korchi, T. 2011. Pavement design: Principles and practice. *In* Pavement Engineering: Principles and Practice, 3rd edition. CRC Press, Florida, USA.

McKee, C.R., and Bumb, A.C. 1987. Flow-testing coalbed methane production wells in the presence of water and gas. SPE formation Evaluation, **2**(4): 599–608.

Ministry of Transportation Ontario (MTO). 2013. OPSS.PROV 1010: Material Specification for Aggregates - Base, Subbase.

Ministry of Transportation Ontario (MTO). 2016. OPSS.PROV 1151: Material Specification for Superpave and Stone Mastic Asphalt Mixtures.

Mirzaii, A., and Negahban, M. 2016. California Bearing Ratio of an unsaturated deformable pavement material along drying and wetting paths. Road Materials and Pavement Design,

17(1): 261–269. doi:10.1080/14680629.2015.1067247.

Myer, K. 2011. Handbook of transportation engineering. *In* Second. The McGraw-Hill Companies Inc., New York, USA.

Papagiannakis, A.T., and Masad, E.A. 2012. Pavement design and materials. John Wiley & Sons, Inc., Hoboken, NJ, USA.

Pearson, D. 2011. Pavements and their Management. *In* Deterioration and Maintenance of Pavements. ICE Publishing, London, UK. pp. 1–12.

Perera, Y.Y., Zapata, C.E., Houston, W.N., and Houston, S.L. 2005. Prediction of the soil-water characteristic curve based on grain-size-distribution and index properties. *In* Advances in Pavement Engineering. American Society of Civil Engineers, Reston, VA. pp. 1–12.

Purwana, Y.M. 2013. Experimental study on unsaturated direct shear and California Bearing Ratio tests with suction monitoring on sand-kaolin clay mixtures. Curtin University.

Ren, J. 2020. Interpretation of the frozen soils behavior extending the mechanics of unsaturated soils. University of Ottawa.

Saha, J. 2011. Evaluation of the effects of Canadian climatic conditions on pavement performance using the Mechanistic Empirical Pavement Design Guide. : 207.

Salour, F. 2015. Moisture influence on structural behaviour of pavements. KTH, Royal Institute of Technology.

Scullion, T., and Saarenketo, T. 1997. Using suction and dielectric measurements as performance indicators for aggregate base materials. Transportation Research Record: Journal of the Transportation Research Board, **1577**(1): 37–44. doi:10.3141/1577-05.

Seed, H.B., Chan, C.K., and Lee, C.E. 1962. Resilience characteristics of subgrade soils and their relation to fatigue failures in asphalt pavements. *In* International Conference on the Structural Design of Asphalt Pavements. Ann Arbor, MI. pp. 77–113.

Seeds, S.B. 2000. Flexible pavement design summary of the state of the art. Transportation in the New Millenieum,: 7.

Stephens, D.J. 1990. Prediction of the California bearing ratio. Civil engineer in South Africa,

32(12): 523–527.

Sukumaran, B., Kyatham, V., Shah, A., and Sheth, D. 2004. Suitability of using California Bearing Ratio test to predict Resilient Modulus. *In* Federal Aviation Administration Technology.

Tillson, G.W., and Thomson, R.H. 1900. Street pavements and paving materials: a manual of city pavements. John Wiley and Sons, New York, USA.

Toll, D.G. 2015. California Bearing Ratio tests on a lateritic gravel from Kenya. Transportation Geotechnics, **5**: 59–67. Elsevier Ltd. doi:10.1016/j.trgeo.2015.09.004.

Vanapalli, S.K., Fredlund, D.G., and Pufahl, D.E. 1999. Influence of soil structure and stress history on the soil–water characteristics of a compacted till. Géotechnique, **51**(6): 573–576. doi:10.1680/geot.51.6.573.40456.

Vanapalli, S.K., and Han, Z. 2014. Application of the unsaturated soil mechanics in the design of pavements. *In* Proceedings of the 6th International Conference on Unsaturated Soils. pp. 1799–1805.

Vanapalli, S.K., and Han, Z. 2017. Characterization of the Mechanistic-Empirical Pavement Design Guide input parameters for the Resilient Modulus of Ontario subgrade soils. Ottawa, Canada.

Vanapalli, S.K., Sillers, S.W., and Fredlund, M.D. 1998. The meaning and relevance of residual state to unsaturated soils. Proceedings of the 51st Canadian Geotechnical Conference,: 1–8.

Vujičić, V.A., and He, J.H. 2004. On two fundamental statements of mechanics. International Journal of Nonlinear Sciences and Numerical Simulation, **5**(3): 283–286. doi:10.1515/IJNSNS.2004.5.3.283.

Winterkorn, H.F., and Fang, H.Y. 1972. Effect of temperature and moisture on the strength of soil-pavement systems. *In* Fritz Laboratory Reports. Bethlehem, Pennsylvania.

Wooltorton, F.L.D. 1958. Moisture content and the CBR method of design. Highways Research Board, (Special Report No.40): 268–297.

Yoder, E.J., and Witczak, M.W. 1975. Principles of pavement design. *In* Second Edi. John Wiley & Sons, Inc., Hoboken, NJ, USA.

Zhong, J. 2017. Rigid pavement: Ontario calibration of the Mechanistic-Empirical Pavement Design Guide prediction models. University of Waterloo, Waterloo, Canada.

APPENDIX

Appendix I

The discussions entailed in this section relates to Chapter 4. The methodology used for moisture content adjustment and monitoring is discussed as well as the equations used to determine the mass-volume characteristics of the tested specimens.

1. For cases where measured water content after mixing is greater than w_{opt}

In this case, soil was added to sample bags to reduce soil moisture to near optimum conditions. The amount of dry soil required was determined based on the measured moisture content and mass of soil sample being monitored. The mass of dry soil was calculated from the difference between measured dry soil contained in the sample bag and mass of dry soil at optimum moisture content; these computations were performed based on the measured mass of sample bag being monitored. The measured dry soil samples contained in the sample bag was determined from the measured moisture content and mass of sample bag.

$$m_t = m_w + m_s \qquad \text{[A-1]}$$

$$m_w = w\,(m_s) \qquad \text{[A-2]}$$

$$m_t = m_s + w(m_s) \qquad \text{[A-3]}$$

$$m_t = m_s(1 + w) \qquad \text{[A-4]}$$

$$m_s = \frac{m_t}{1 + w} \qquad \text{[A-5]}$$

$$m_{s,optimum\ moisture\ condition} = \frac{m_t}{1 + w_{opt}} \qquad \text{[A-6]}$$

$$m_{s,current\ moisture\ condition} = \frac{m_t}{1 + w_{current\ moisture\ condition}} \qquad \text{[A-7]}$$

$$Mass\ of\ soil\ added = m_{s,optimum\ moisture\ condition} - m_{s,current\ moisture\ condition} \qquad \text{[A-8]}$$

where m_t is the total mass of monitored specimen (g); m_w is the mass of water (g); m_s is the mass of soil solids in grams; $m_{s,optimum\ moisture\ condition}$ is the mass of soil at optimum moisture condition in grams; $m_{s,current\ moisture\ condition}$ is the calculated mass of monitored soil sample in grams; $w_{current\ moisture\ condition}$ is the measured moisture content of monitored soil sample; $w_{opt}$is the water content at optimum moisture.

2. For cases where measured water content after mixing is less than w_{opt}

When the measured moisture content was situated dry of optimum moisture conditions, water was added to sample bags to increase the soil moisture within tolerable range of 0.15 % of optimum moisture. The mass of water added was determined from the difference between the mass of water at optimum conditions and measured mass of water in the monitored sample bag.

$$m_w = m_t - m_s \tag{A-9}$$

$$m_w = m_t - \frac{m_t}{1 + w} \tag{A-10}$$

$$m_{w,optimum\ moisture\ condition} = m_t - \frac{m_t}{1 + w_{opt}} \tag{A-11}$$

$$m_{w,current\ moisture\ condition} = \frac{m_t}{1 + w_{current\ moisture\ condition}} \tag{A-12}$$

$$Mass\ of\ water\ added = m_{w,optimum\ moisture\ condition} - m_{w,current\ moisture\ condition} \tag{A-13}$$

where $m_{w,optimum\ moisture\ condition}$ the mass of water at optimum moisture condition in grams; $m_{w,current\ moisture\ condition}$is the calculated mass water in monitored soil sample in grams.

Appendix II

This section of the appendix contains a summary of the results discussed in Chapter 5.

Table A-1 Summary of experimental results for KLC

Soil 1 - Kincardine lean clay (KLC)		
Test condition	Saturated	Optimum water content
$S = w/w_{sat}$	1.00	0.89
e **(%)**	0.65	0.62
w **(%)**	23.28	20.22
$\rho_{d,compaction}$ **(kg/m^3)**	1644.12	1671.77
Swell (%)	0.22	-
***CBR*-value**	1.45	3.25
ψ **(kPa)**	-	298.00
M_R **(MPa)**	12.12	37.90

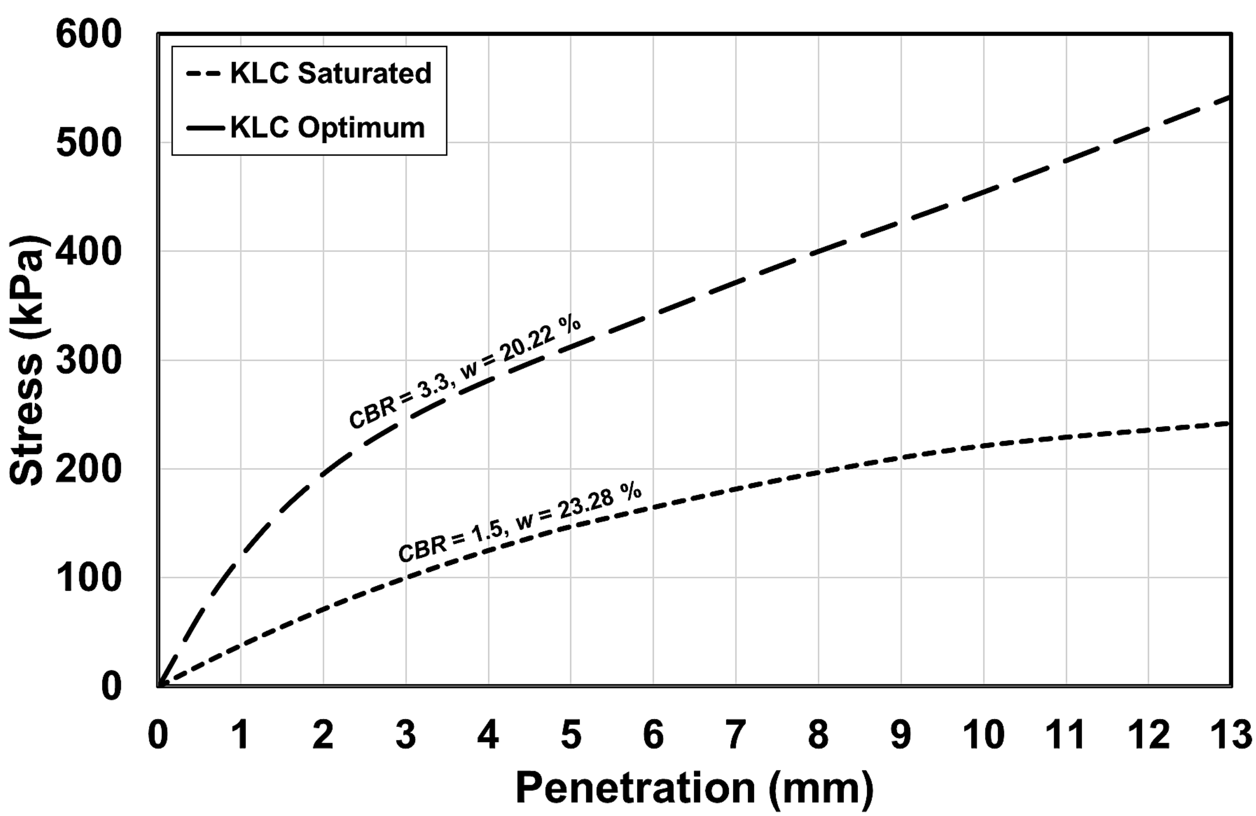

Figure A-1 *CBR* curves for KLC specimens

Table A-2 Summary of experimental results for KSC

Soil 6 - Kingston silty clay (KSC)		
Test condition	Saturated	Optimum water content
$S = w/w_{sat}$	1.00	0.92
e (%)	0.37	0.35
w (%)	16.18	12.19
$\rho_{d,compaction}$ (kg/m^3)	1930.04	1962.85
Swell (%)	0.14	-
***CBR*-value**	1.65	4.55
ψ (kPa)	-	298.00
M_R (MPa)	31.39	42.98

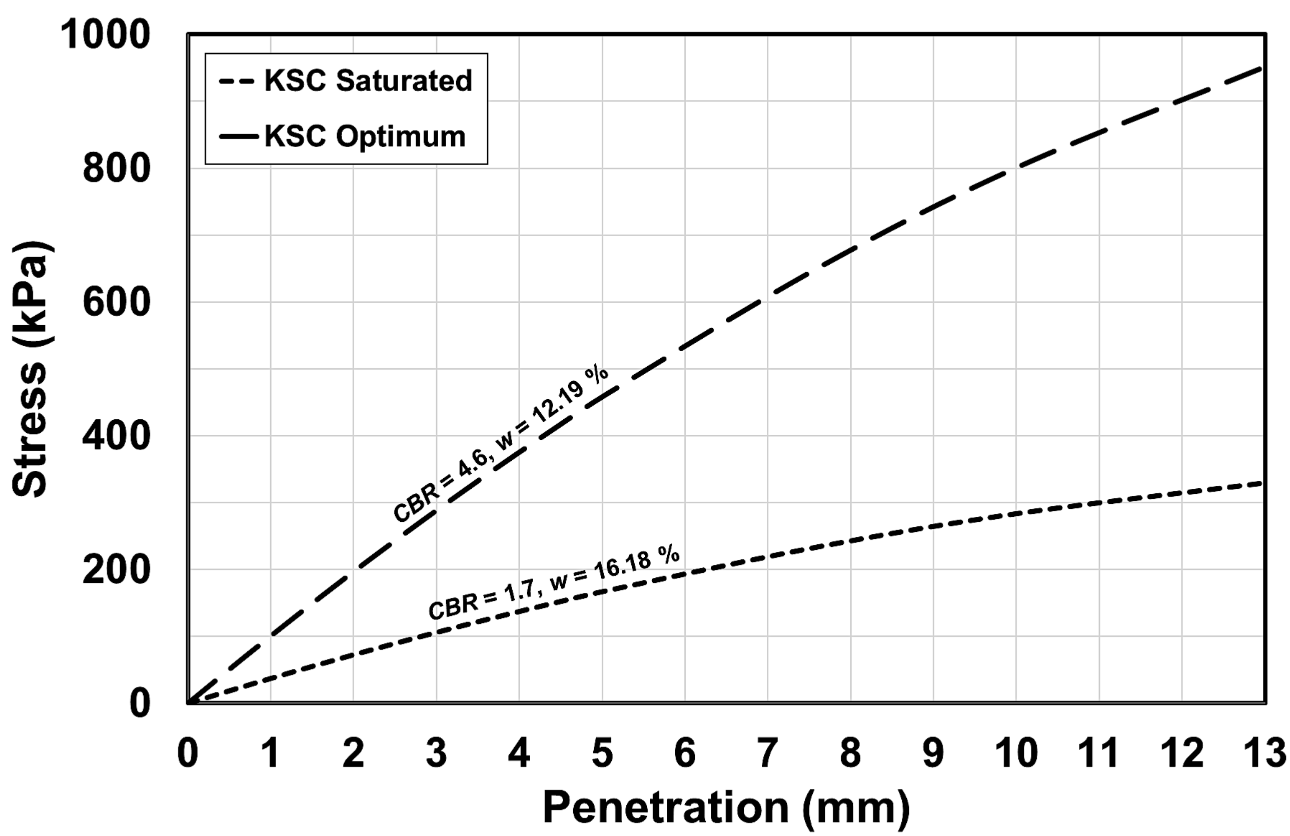

Figure A-2 *CBR* curves for KSC specimens

Table A-3 Summary of experimental results for OLC

Soil 7 - Ottawa Leda clay (OLC)		
Test condition	Saturated	Optimum water content
$S = w/w_{sat}$	1.00	0.94
e (%)	0.68	0.66
w (%)	24.51	23.01
$\rho_{d,compaction}$ (kg/m^3)	1638.53	1666.04
Swell (%)	0.12	-
***CBR*-value**	1.15	9.91
ψ (kPa)	-	298.00
M_R (MPa)	16.25	87.73

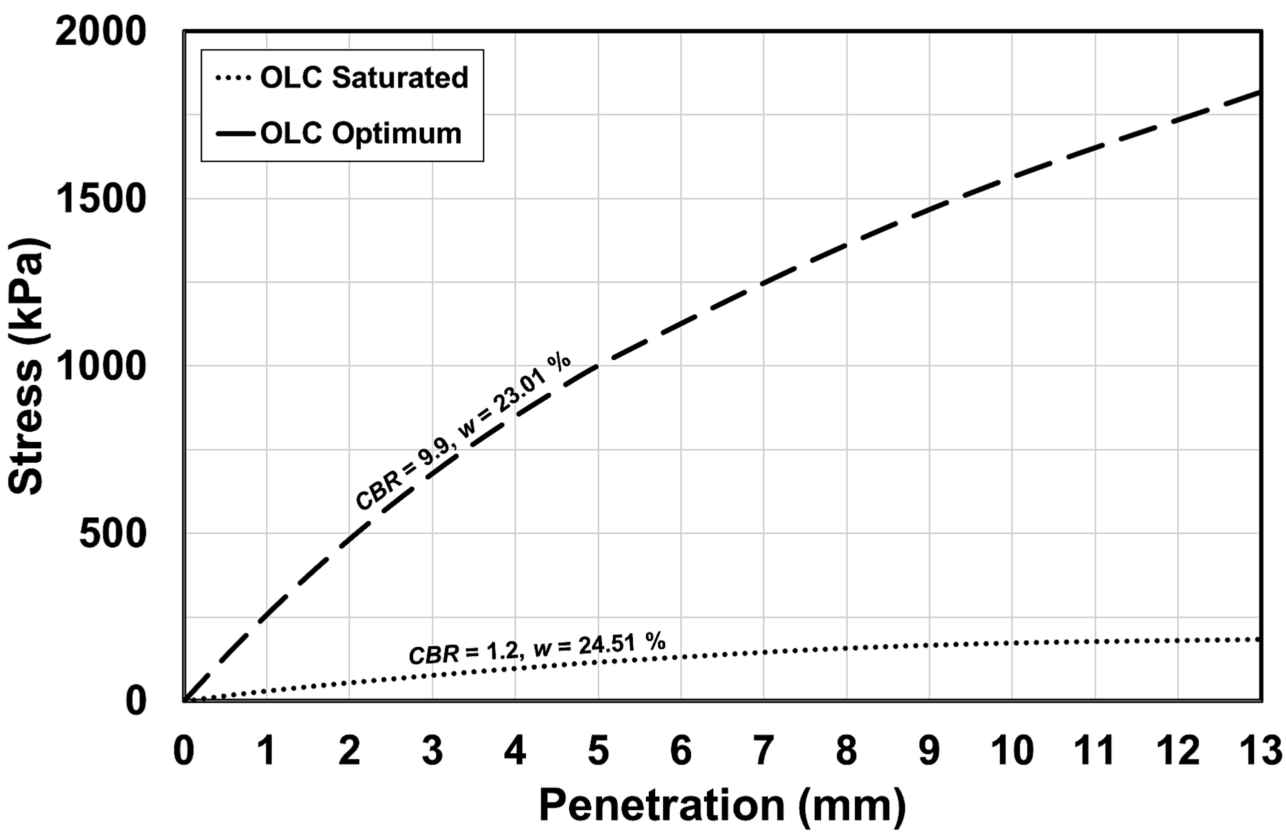

Figure A-3 *CBR* curves for OLC specimens